



מכון ויצמן למדע

WEIZMANN INSTITUTE OF SCIENCE

*Thesis for the degree
Doctor of Philosophy*

חבור לשם קבלת התואר
דוקטור לפילוסופיה

*By
Jason Friedman*

מאת
ג'ייסון פרידמן

*מאפייני האחיזה האנושית
Features of Human Grasping*

Regular Format

פורמט רגיל

*Advisor
Prof. Tamar Flash*

מנחה
פרופ' תמר פלש

May, 2007

איר, תשס"ז

Submitted to the Scientific Council of the
Weizmann Institute of Science
Rehovot, Israel

מוגש למועצה המדעית של
מכון ויצמן למדע
רחובות, ישראל

Abstract

Human grasping and object manipulation require the coordination and control of the contact points between the hand and the object, of the orientation, posture and impedance properties of the hand, and of the direction and magnitude of the forces applied by the fingers. The objective of this thesis was to understand some of the features of this complex system by developing models for the finger and the hand, and using these models to describe the behaviors observed during grasping. We have aimed to use these models to describe the kinematic and dynamic features of finger movements during grasping, and to suggest the goals of the nervous system in selecting grasps for actions.

A model has been described for the index finger, modeling it as a spring-damper-mass system, as well as taking into account the effect of Coriolis and centrifugal forces, and gravity. Some of the parameters of this model have been derived based on a geometric model of the finger, and were compared to the experimentally identified parameters, found in an experimental setup involving perturbing the entire finger with a “tendon” attached to an exoskeleton. Good agreement was generally found between the geometrically modeled and experimentally derived inertia ellipses. Additionally, it was found that using a full dynamic model of the finger sampled at many time points models the fingertip force during movement significantly better than a model of only the stiffness constructed from the total magnitude of the applied force and the perturbation.

The grasps selected for different tasks on an object were compared. The grasp Jacobian was constructed, as a function of the recorded posture, and allowed quantification of the force and velocity transmission capabilities of the grasp. Additionally, using a novel technique, the whole grasp stiffness was estimated. The differences between the grasps selected were compared in terms of these force and velocity transmission capabilities, and the stiffness. Despite the large amount of variation observed in the selected postures, the results show that some of these differences can be related to salient task

requirements.

This technique was extended by comparing the grasps selected for particular tasks to a large number of computer generated grasps, each of which have the same number of fingers grasp the same object in a feasible way. The force and velocity transmission capabilities and the stiffnesses were used for this comparison. A normalized compatibility score was computed to quantify the relative compatibility of the selected grasps compared to the compatibility scores of the computer generated grasps. Grasps with mean normalized compatibility scores significantly different from 0.5 were considered as candidates for quantities that may be optimized in the grasp selection process. Several of these quantities were related to requirements of the tasks.

The trajectory of the index finger was modeled during grasping movements. It was observed that the Cartesian arc length velocity profiles along the fingertip path are invariant when they are normalized with respect to time. The path of the fingertip was well modeled by two geometric models, one based on finding the best-fit logarithmic spiral to the movement, and the other one minimizing the integral of the weighted squared joint derivatives along the path. Similar predictions were also found by minimizing the integral of squared angular jerk. The predictive powers of these models was similar when the inertia of the finger was changed by adding a weight to the medial phalange, which was not the case for the minimum torque-change model. Thus, for the finger, it appears that the path and velocity profiles can be modeled independently.

Finally, two applications of this research have been presented. A telerobotics system based on recognizing the type of action was constructed. Also, the potential use of the grasping models described here in order to aid in the rehabilitation of grasping function was presented.

Contents

Acknowledgements	v
1 Introduction	1
1.1 Grasping	1
1.2 Thesis outline	3
2 Background	5
2.1 Structure of the hand	13
3 Hand impedance	17
3.1 Experimental estimation of fingertip impedance	17
3.1.1 Introduction	18
3.1.2 2D Dynamic equations of the index finger	20
3.1.3 Methods	25
3.1.4 Results	33
3.1.5 Discussion	38
3.2 Grasp stiffness estimation	41
4 Grasp selection	43
4.1 Introduction	44
4.2 Methods	45
4.3 Results	55
4.3.1 Cup	60
4.3.2 Wide jar	65
4.3.3 Spoon	66

4.3.4	General discussion	67
4.4	Optimal grasp selection	70
4.4.1	Methods	70
4.4.2	Results and Discussion	73
5	Trajectories of the fingers	81
5.1	Introduction	82
5.1.1	Logarithmic spirals for describing finger motion	83
5.1.2	Prediction of path from minimization of kinetic energy- like function	87
5.1.3	Time course of the movements	88
5.2	Methods	89
5.3	Results	94
5.3.1	Minimum jerk fit	96
5.3.2	Fit of the path	99
5.4	Discussion	106
6	Applications	111
6.1	Grasp recognition for telerobotics	111
6.2	Grasp prediction for use in rehabilitation	116
7	Summary and conclusions	119
7.1	Potential directions for future research	123
	Appendix A Glove Calibration	127
	Appendix B Grasp Jacobian	137
	Bibliography	147
	Publications based on Ph.D. research	161
	Independent collaboration	162

Acknowledgements

I would like to thank my supervisor Prof. Tamar Flash, for introducing me to the fascinating topic of human motor control, and for guiding my research for the past 7 years. With her amazing depth of knowledge in the field, she presented me with many interesting topics to examine, we had many thought provoking conversations, and she gave me useful advice on how to tackle the myriad of problems I encountered on the way. Her unwavering support during the more difficult times in this period was much appreciated.

I would also like to thank my other Ph.D. committee members, Prof. Moshe Shoham and Prof. Shimon Ullman, for their helpful comments and advice throughout my Ph.D. studies.

I would like to acknowledge the support for this research from the German-Israeli Project Cooperation (DIP) and by the Moross Laboratory.

My experimental work would not have been possible without the help of Eli Okon, who skillfully transformed my ideas into the many mechanical devices that I needed, and Oded Smikt for maintaining and fixing the many pieces of equipment that I used in the motor control laboratory.

I have greatly enjoyed studying at the Weizmann Institute, largely due to the people with whom I have shared the last few years. Armin Biess has been a constant support and help for all mathematical questions, big or small. It has been a pleasure to work, program, travel, and devise grand plans together with Lior Noy. I have also gained a lot from sharing ideas, Matlab programs and discussions with other current and former lab members, including Dario Liebermann, Sigal Berman, Assaf Dvorkin, Felix Polyakov, Avi Barliya, Ido Zelman, Uri Maoz and Maria Korman amongst others. It has also been enjoyable and rewarding collaborating long distance with Gideon Kowadlo.

Finally, I thank my wife Anatt for her support and for putting up with me throughout my research and during the preparation of the thesis, and my daughter Keshet for being particularly adorable, and always putting a smile on my face. I would also like to thank my family and Anatt's family for their support in many ways over the last few years.

Chapter 1

Introduction

The field of computational motor control seeks to understand how human movement is performed, primarily by examining the output of the system, namely, our movements. By presenting and evaluating models of how various motor systems may work, insights can be gained into the principles that the central nervous system (CNS) uses in planning multi-joint movements. Apart from gaining a deeper understanding of our own brains, this field of research can have practical implications for the understanding and treatment of movement disorders, in the construction of prosthetics, and in robotics.

1.1 Grasping

Human grasping is an ideal model system for studying human motor control. It is something that we perform all the time, albeit generally with little conscious thought, but it is highly complex in that we must constantly select from a very large range of possible hand configurations, which determine the hand's manipulation capabilities. The human hand has an amazing range of abilities, ranging from the fine accuracy needed to thread a needle to the large forces that can be applied by the hands to support the body in rock climbing. Grasping is also difficult to learn - it takes many years for children to be able to perform fine manipulation (for example, accurate drawing, or opening a child-proof bottle), long after they can walk and talk. The ability

to grasp is found in few animals, and only humans are able to grasp with such a level of dexterity. By understanding the workings of the hand, we may gain insights into the general principles used in motor planning that are less apparent when studying simpler systems.

The focus of this thesis is on a behavioral study of grasping. While there have been some insights recently into grasping from neural studies in humans (Buxbaum et al., 2006) and monkeys (Raos et al., 2004, 2006), we are still far from having the ability to deduce the notions of how grasping is performed from such studies. Thus, behavioral research is the primary tool available for inferring the way that the CNS performs grasping.

In this work, the hand is modeled in a similar way to which one might model a robotic system composed of several manipulators acting together. Although the dynamic properties of human muscles cannot be precisely modeled as spring-damper systems, and our joints do not behave exactly as hinge joints do, such modeling allows us to use the tools of robotics in the analysis, and to probe deeper questions. Known biomechanical details are included in the models.

We make the broad assumption that practiced human behavior, such as grasping, is optimal in some sense. This is the underpinning of many models in motor control, although there is significant disagreement on what quantity is being optimized. Although some works have claimed that satisficing¹ is sufficient (Rosenbaum et al., 2001), we nevertheless use the assumption of optimality because it seems likely that in highly skilled tasks such as grasping, the CNS has reached optimal performance.

¹Satisficing, rather than optimizing, is to plan for acceptable performance rather than optimal performance

1.2 Thesis outline

Chapter 2 presents a general overview of previous research on grasping, as well as describing the biomechanical structure of the hand.

Chapter 3 examines the impedance properties of the index finger, which are important for modeling object manipulation by the hand, through geometric modeling of the inertia, and experimental estimation of the stiffness, damping and inertia terms. A technique for interpolating grasp stiffness at novel postures, based on measured grasp stiffnesses, is also presented.

Chapter 4 looks at how the location of the fingers on an object and the hand posture are selected in order to perform different types of object manipulation tasks. The force and velocity capabilities and the stiffnesses of grasps performing different actions on an object are compared, in order to gain insights into what are important in grasp planning. Additionally, the grasps selected are compared to the “optimal” grasps for force or velocity production, or stiffness, in particular directions.

Chapter 5 presents several models for describing the motion of the fingers during grasping. Some of the models are based on independent planning of the path and velocity profiles along the path. The novel models are compared with models presented in previous works. The fit of these models is compared.

Chapter 6 presents two applications of the techniques developed in this work. The first is a telerobotics project, where the goal of a grasp performed by a human operator in a virtual reality environment is transmitted to a robot, which achieves the same goal in a suitable way for its structure and dynamic capabilities. The second application is the determination of the optimal grasps to use for different tasks when the hand has limited movement capabilities, for potential use in rehabilitation.

Appendix A describes the calibration technique used with the CyberGlove.

Appendix B gives a full derivation of the grasp Jacobian, which is used throughout the thesis.

Chapter 2

Background

Grasp selection in humans is largely subconscious. Despite the lack of conscious attention we give to it, grasp selection in the kinematically redundant system of the human hand poses a difficult problem, in that the requirements of a grasp are not clearly specified and it is difficult to define how to generate a grasp in order to best fulfill a given set of attributes. This epitomizes the degrees of freedom problem of Bernstein (1967), due to the larger number of degrees of freedom available in the hand than are necessary for stably grasping an object. In the field of robotics, a large body of literature deals with this question of grasp synthesis (see Shimoga (1996) for a review), which is a testimony to the complexity of the problem.

The study of grasping movements in humans has been mostly addressed from the perspective of reach-to-grasp movements, which have been considered as consisting of two independent components (Jeannerod, 1981) although several experimental studies have shown that external perturbations affect both channels (Haggard, 1994; Soechting & Flanders, 1993). Other studies of grasping movements have mostly focused on grasping kinematics (Mason et al., 2001; Santello et al., 2002; Kamper et al., 2003) or on force distribution among different fingers during object manipulation demonstrating the existence of different force distribution and coordination schemes such as enslaving and force sharing (Zatsiorsky et al., 1998; Danion et al., 2003).

Grasp selection There are many factors that influence us when selecting the grasp to be used for a particular manipulation, and it is unclear which variables should be used to define the goals of a grasp (Smeets & Brenner, 1999). The shape of an object clearly plays a role in determining the grasp, but by itself is insufficient to fully describe the necessary grasp. The mass and coefficient of friction of the object to be grasped will also affect the movement (Pollick et al., 2000), for example, picking up the same bottle when it is empty or full will involve different movement plans. Earlier studies have shown that the kinematic properties of both arm transport and grasp selection are influenced by the object and task properties (Marteniuk et al., 1987; Jakobson & Goodale, 1991). Intrinsic object properties that cause a particular type of interaction, known as affordances (e.g., the size, shape or weight of an object), also affect the type of grasp that is selected. It was found that all the affordances of an object and not only those directly implicated influence grasp selection (Gentilucci, 2002).

Taxonomies To classify the large number of grasps used by humans, grasp taxonomies have been defined. Napier (1993) divided grasps into power grips and precision grips. A power grip involves contact between the object and the surface of the fingers and the palm, and is usually used to constrain the object so that it moves together with the hand. In contrast, a precision grip is performed between the fingertips of the thumb and other fingers. The precision grip can be used for manipulation of an object by the fingers.

Cutkosky (1989) defined a taxonomy of grasps categorized primarily according to their function rather than their shape. The first division was between a power grip and a precision grip. Further divisions in the taxonomy are based on the placement of the fingers (a compact, circular grasp or a long, prismatic grasp), the number of fingers being used and the prehension aperture. This taxonomy is shown in Figure 2.1.

Iberall (1997) divided hand postures during grasping into four categories, grouped by oppositions. The categories were palm opposition (opposition of the palm with some fingers), pad opposition (opposition only of the fingertips), side opposition (opposition of the sides of the fingers) and opposition

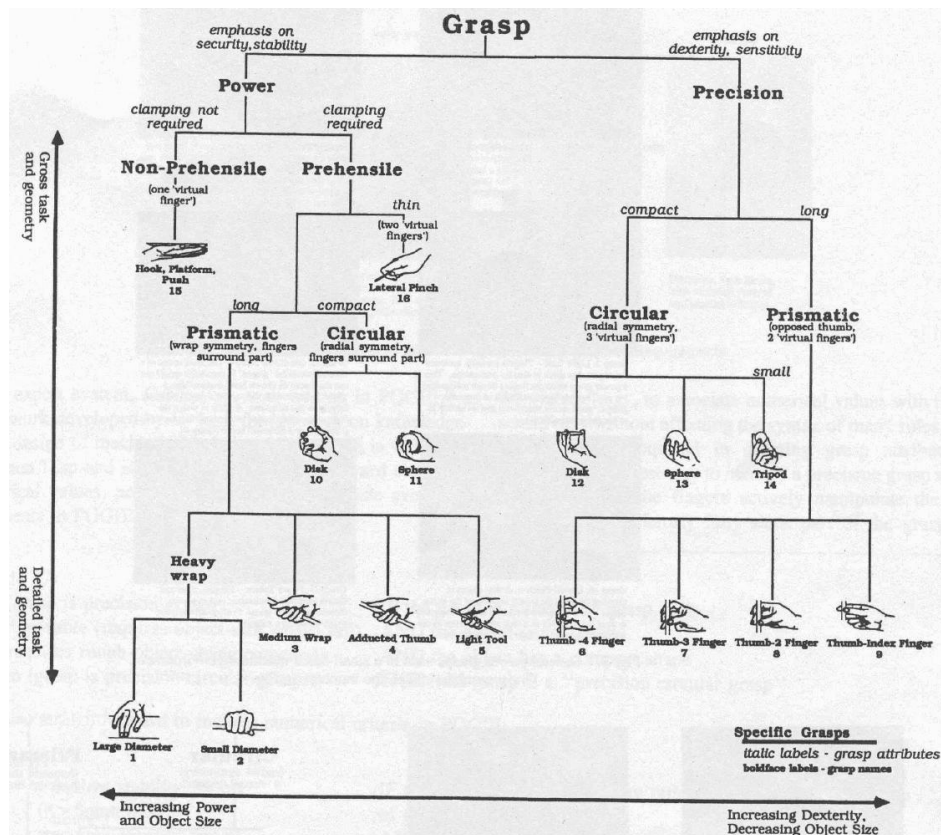


Figure 2.1: Grasp taxonomy defined in Cutkosky (1989).

against gravity. Combinations of these oppositions were also permitted.

Further grasp characterizations include that of Elliott & Connolly (1984), which divided manipulative hand movements into simultaneous and sequential ones. A hierarchy was defined by further decomposition of object manipulation movements, based on which fingers are involved and the similarity of the movements between the fingers.

Motor primitives Grasp formation and manipulation require coordination of many degrees of freedom. Motor primitives, which are a basic set of movements that might subserve as building blocks for more complex movements, may present a simplifying strategy for grasp planning. Computationally, they can be thought of as a set of movements that through combination are sufficient to generate entire movements (Fod et al., 2002). Several dif-

ferent approaches to the use of primitives in grasping have been considered in robotics, where primitives have been proposed that operate in joint space (Speeter, 1991) or in Cartesian task space (Fuentes & Nelson, 1998; Riley & Atkeson, 2002).

Speeter (1991) defined a set of primitives for the Utah/MIT dextrous hand. Each primitive is a coordinated set of joint motions to perform a certain task. New primitives can be defined as a linear combination of primitives, and then motor programs can be defined as a sequence of such commands. Fuentes & Nelson (1998) used a similar technique, but their primitives were learned by minimizing an objective function for a given goal. Their primitives were movements such as moving the fingertips along a certain axis or rotating them. The robotic three-fingered hand, which was modeled as two 3 DOF fingers (using certain redundancies and assumptions), learned these movements using the evolution strategy. These movements could be combined manually to perform tasks using teleoperation, although no method was given for finding the primitives automatically for a general task.

Ilg & Giese (2002) used spatio-temporal morphable models (STMMs) as movement primitives. Prototypical movements were generated from the average of several recorded movements, and the spatial and temporal shifts from a primitive to a given movement are found by minimizing these shifts under certain constraints. These primitives can then be used to generate novel movements, for example, in a different style or with exaggeration.

One other prominent approach in robotics for programming robotic hands to perform compliant tasks has been to specify the task frame in which the manipulation can be defined and the constraints on forces and motions in this frame (Mason, 1981; de Schutter & van Brussel, 1988).

Concerning primitives for human grasping, it has been suggested that they may consist of stored postures (Rosenbaum et al., 1995, 2001; Meulenbroek et al., 2001). A movement between the start and end postures is then computed (Rosenbaum et al., 2001). Smeets & Brenner (1999, 2002) claimed that a much simpler model is sufficient for planning grasping movements. Their model was based on determining the final locations of the fingertips of the thumb and index finger on the object, and then planning the trajectory

that takes the fingertips to those locations. In addition to describing the kinematics of the movement, primitives may also define the applied forces and the dynamic properties of the grasp.

Dimensionality reduction techniques The aforementioned taxonomies suggested for human grasping may enable classification of the movements into different subclasses, although it is unclear whether it is possible to decompose these grasps further into more elementary building blocks. In the past few years, with the development of devices such as the CyberGlove (Immersion), the finer kinematic details of human grasping have been studied. In particular, a number of works have looked at the selection of finger tip locations and joint angles. Principal Component Analysis (PCA) and related techniques for dimensionality reduction have been employed for inferring the underlying joint angle synergies during grasping (Santello et al., 1998; Mason et al., 2001; Santello et al., 2002; Zacksenhouse & Marcovici, 2001). An example of the first two principal components (PCs) for a grasping task is presented in Figure 2.2.

Santello et al. (1998) used PCA to study the posture of the hand. They studied the hand in terms of 15 joint angles. However, they only analyzed the static hand posture at the end of the trial. They found that the first two PCs could account for greater than 80% of the variation, but that higher order PCs are required for more subtle differentiation between the postures.

In a later study, Santello et al. (2002) studied the patterns of covariance between the fingers throughout the movements using PCA. In this case, the PCs were a function of time of all of the joints, not one for each joint (as was the case in Soechting & Flanders (1997), where each joint was considered separately). The first two PCs accounted for more than 70% of the variation. The first PC described where the fingers extended and then reversed to flexion. The second PC only showed significant modulation late in the movement (approximately 70% of the way through the movement) and described all the fingers extending or flexing. Movements of single fingers required further PCs.

A more recent study (Jerde et al., 2003) compared the use of PCA to

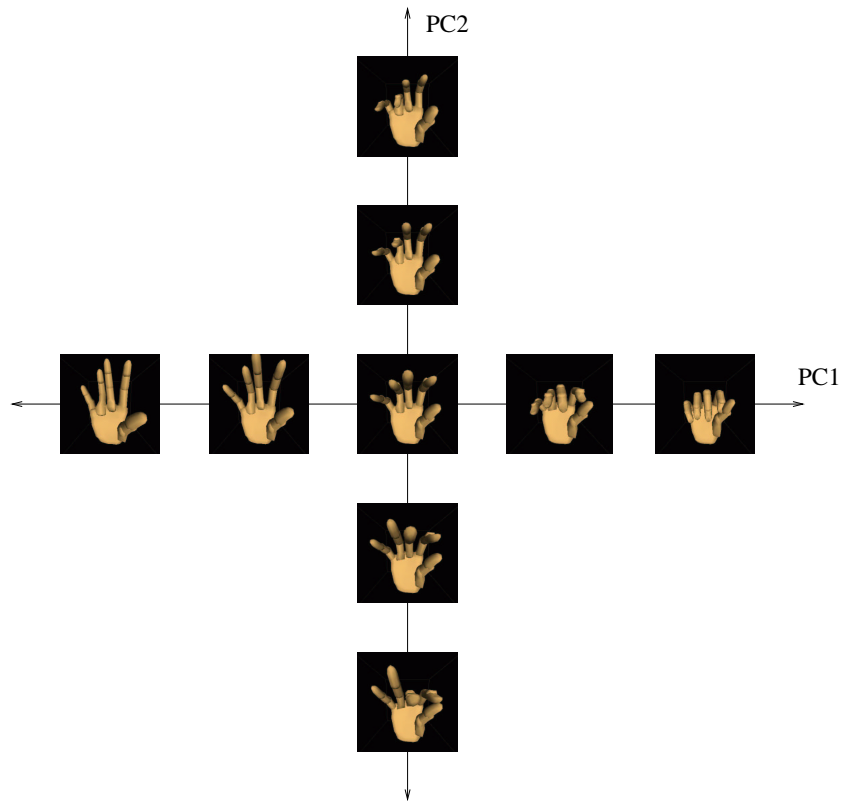


Figure 2.2: The first two principal components (eigenpostures) for grasping tasks. The data were collected with the CyberGlove in a toy experiment, and multiples of the eigenpostures added to the mean posture are rendered.

the selection of a small subset of joint angles. They considered static hand postures used for finger spelling in American Sign Language. Recognition of these postures can be performed with a similar accuracy using an equivalently sized subset of joint angles rather than a vector of weights of the PCs. They suggest that the reduction in degrees of freedom is due to biomechanical and neuromuscular constraints rather than synergetic control.

An alternative to PCA for automatically finding a lower-dimensional expression of hand movements is to use singular value decomposition (Mason et al., 2001). Rather than finding principal components that describe the entire movement, this work found a set of postural synergies, that through combination could describe the posture of the hand. It was found that a small number of “eigenpostures”, consisting of the Cartesian (x, y, z) coordinates

of 21 markers on the hand, could be used to well describe the movement. The first eigenposture explained on average 97.3% of the variation. The time development of the eigenpostures can then be seen through the movements, and were similar between grasps and between subjects. Although the higher eigenpostures represented only a small amount of the variation, they still contributed to the shape of the hand (rather than being noise).

A different approach was taken in Nölker & Ritter (2000), where the grasp was specified by the finger tip positions, and the joint angles were reconstructed using a Parameterized Self-Organizing Map.

Preshape A notion in simplifying grasp planning has been the use of pre-shaping of the hand, that is, moving the hand into a posture with the fingers more open than they need to be to grasp the object, but still close to the desired posture. The preshape selected depends on the object's parameters such as size and shape (Arbib et al., 1985) and the goal of the task (Ansuini et al., 2006). Grasp planning algorithms have been proposed based on pre-shaping (Miller et al., 2003; Wren & Fisher, 1995), where after generating the preshape based on the shape of the object or the task, the fingers then close on the object.

Equilibrium Point Hypothesis The Equilibrium Point Hypothesis (Feldman, 1966) controls movement by appropriately selecting the muscle stiffness and rest length properties. Gu & Ballard (2006) suggested a movement control strategy for grasping by specifying an equilibrium posture of the hand. The equilibrium posture may actually have the fingers inside the object, in which case the actual posture will have the fingers applying forces on the object at the grasp points. By adjusting the stiffness values of the fingers, different forces can be applied. Such models are advantageous in that they can deal better with noise and errors in position, and guarantee object stability.

Robotic Grasp synthesis In the robotics literature, grasp synthesis is usually achieved by optimizing some quality measure (Shimoga, 1996). Many

of these measures are based on the grasp Jacobian, G_h , which defines the relationship between the finger joint velocities, and the velocity of the object being grasped. The grasp Jacobian can be visualized by means of the manipulability ellipsoid (Yoshikawa, 1985), which represents the transmission properties of both velocities and forces between the joints and the object. Object velocity can be optimally produced along the major axis of the velocity transmission ellipsoid, and most accurately controlled along the minor axis. The analogous force transmission ellipsoid can also be derived from the grasp Jacobian. Chiu (1988) defined a measure known as the task compatibility index, which measures the transmission ratio of force or velocity along the direction required by the task. This is calculated as the square of the length of a vector in this direction from the center of the ellipsoid to the surface of the relevant force or velocity transmission ellipsoid. For a given task, Li & Sastry (1988) defined an ideal task ellipsoid whose shape (i.e., the relative lengths of the axes) is determined based on the relative force requirements in the different directions.

Kim et al. (2004) defined a set of performance indices. These measures are normalized by dividing them by the difference between the maximum and minimum possible values and thus they are also non-dimensional. Different weights can be given to the different indices depending on the task.

Impedance Grasping involves more than the placement of the fingers on the object. Due to the redundancy of the hand, the same grasp points on an object can in general be realized in many ways, thus influencing the stability and manipulability of the grasp. Both the stability and the manipulability of a grasp are affected by the grasp impedance. Impedance describes the relationship between externally applied forces and motion. It consists of a static component, the stiffness, which relates forces to displacements, and dynamic components, the damping and inertia, which relate forces to velocity and acceleration, respectively. The passive and active impedances of the human hand help to deal with changes in grasping conditions (Kao et al., 1997). Control of the dynamic behavior during manipulation requires control of the impedance of the hand (Hogan, 1985a).

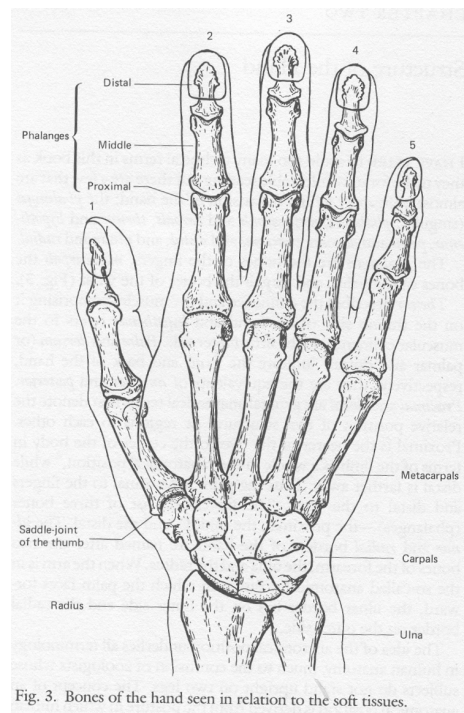


Figure 2.3: The bones in the hand. Figure reproduced from Napier (1993).

Forces In addition to the selection of grasp points, hand posture and stiffness, the distribution of forces applied by the fingers is controlled during grasping. Several phenomena, including enslaving and force sharing, have been observed (Zatsiorsky et al., 1998; Danion et al., 2003). Danion et al. (2003) modeled these phenomena with the mode hypothesis, where a mode is defined as the forces produced by all the fingers resulting from voluntary force production in a single finger. Multiple finger force production can then be modeled by the superposition of modes, with a weight factor dependent on the number of fingers used.

2.1 Structure of the hand

The bones of the hand are shown in Figure 2.3. The bones of the fingers are known as the phalanges, the bones of the palm are known as the metacarpals, and the carpals are the bones of the wrist. The joints between the phalanges

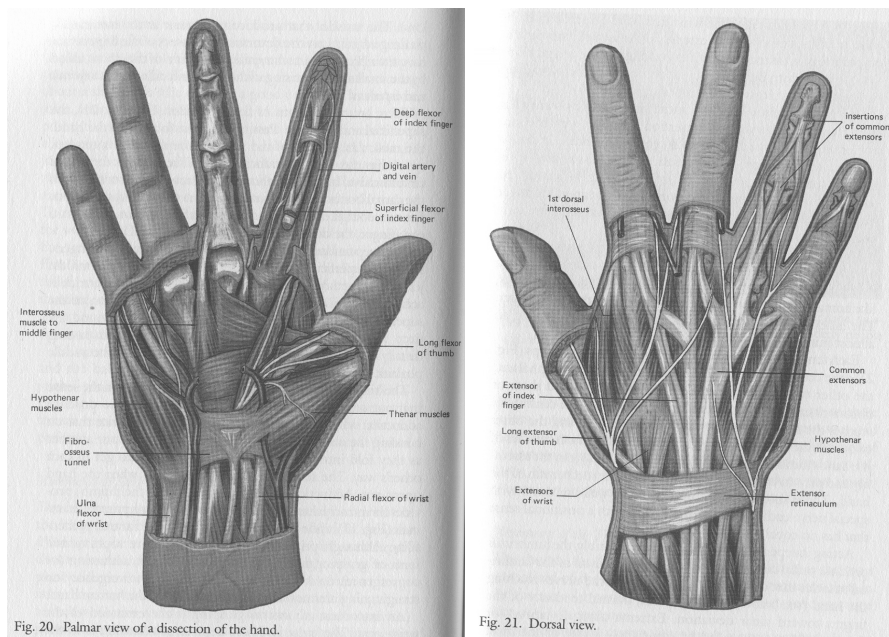


Figure 2.4: The palmar (left) and dorsal (right) view of the muscles in the hand. Figure reproduced from Napier (1993).

are known as the distal and proximal interphalangeal joints, and the fingers can be bent (flexed) or straightened (extended) at these joints. At the joint between the phalanges and the metacarpals, known as the metacarpophalangeal joint, in addition to extension and flexion, side-to-side movements can be performed. Movements away from a line going through the middle finger are known as abduction, those towards it are known as adduction.

The muscles of the hand are shown in Figure 2.4. Most of the muscles in the hand are attached near the elbow, and pass from the forearm to the hand by tendons. These are known as the extrinsic muscles, and are divided into deep tendons, which act mostly on the distal interphalangeal joint, and superficial tendons, which act on the middle joints. Smaller intrinsic muscles, originating in the hand, also play a role. Further details can be found in Napier (1993). The thumb metacarpal joint, unlike the other fingers, is a saddle joint, and can move in three directions (adduction-abduction, flexion-extension, and medial-lateral rotation).

Figure 2.5 shows the tendons of the index finger. Each joint of the finger

has several tendons attached to it. Table 2.1 summarizes these connections.

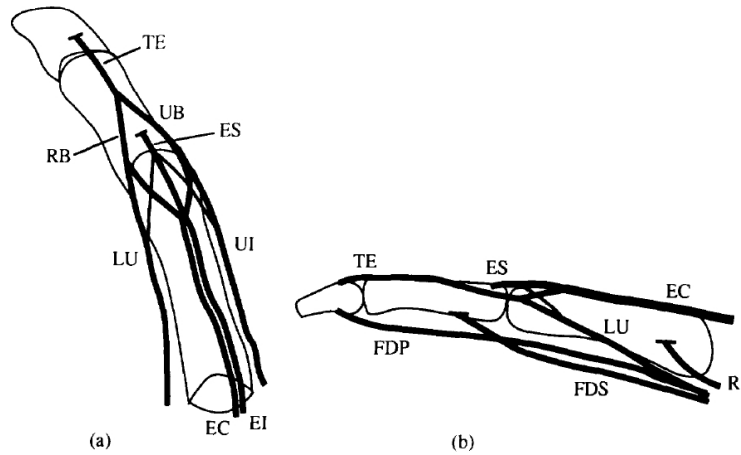


Figure 2.5: Tendons and intrinsic muscles of the index finger. Figure reproduced from Brook et al. (1995).

Joint	Tendon and intrinsic muscles
DIJ	Terminal extensor (TE) Flexor digitorum profundus (FDP)
PIJ	Extensor slip (ES) Radial band (RB) Ulnar band (UB) Flexor digitorum superficialis (FDS) Flexor digitorum profundus (FDP)
MPJ	Extensor digitorum Communis (EC) Extensor indicis (EI) Radial interosseous (RI) Ulnar interosseous (UI) Lumbrical (LU) Flexor digitorum superficialis (FDS) Flexor digitorum profundus (FDP)

Table 2.1: Tendons and intrinsic muscles of the index finger connected to the distal interphalangeal joint (DIJ), proximal interphalangeal joint (PIJ) and the metacarpophalangeal joint (MPJ). Table reproduced from Brook et al. (1995).

Chapter 3

Hand impedance

3.1 Experimental estimation of fingertip impedance

Nomenclature

θ	Joint angles.	c_i	$\cos \theta_i$.
$\dot{\theta}$	Joint velocities.	s_i	$\sin \theta_i$.
$\ddot{\theta}$	Joint accelerations.	M_i	i th link inertia matrix.
τ	Joint torques.	l_i	Length of the i th segment.
\hat{M}	Manipulator inertia matrix.	l_{ci}	Length to segment center of mass.
\hat{B}	Joint damping matrix.	ξ_i	Twist of the i joint.
\hat{K}	Joint stiffness matrix.	J^b	Body Jacobian.
\hat{C}	Joint Coriolis and centrifugal.	m_i	Mass of the i th segment.
\hat{G}	Joint gravity effect.	I_{xi}	Segment moment of inertia about x axis.
M	Endpoint inertia.	Γ_{ijk}	Christoffel symbol.
B	Endpoint Damping.	F_{af}	Force applied to artificial finger.
K	Endpoint Stiffness.	F_{af}	Torque of artificial finger.
C	Endpoint Coriolis and centrifugal.	σ	Fitting error.
G	Endpoint gravity effect.	e_x	Force prediction error in x direction.
J	Joint angles to endpoint Jacobian.	N	Number of samples.

3.1.1 Introduction

A good estimate of the impedance properties of the fingers is essential for modelling the human hand during grasping and manipulation, in particular, for predicting how the hand will interact with an object being grasped (Kowadlo et al., 2005). Impedance, which describes the relationship between externally applied forces and motion, consists of a static component, the stiffness, which relates forces to displacements, and dynamic components, the damping and inertia, which relate forces to velocity and acceleration respectively. While estimation of stiffness and damping values requires either experimental testing or an accurate muscle model, inertia can be calculated using geometric modelling, as several studies have demonstrated for the human finger (Kamper et al., 2002; Grinyagin et al., 2005; Kowadlo et al., 2005). However, there has been no experimental validation of the predicted finger inertia values.

Earlier studies of upper limb impedance have focused mainly on measurements and characterization of the arm stiffness field while maintaining different arm postures in the horizontal plane (Mussa-Ivaldi et al., 1985; Flash & Mussa-Ivaldi, 1990; Tsuji et al., 1995). While maintaining posture, a manipulandum was used to introduce small displacements of the subject's hand in different directions. The resultant measured restoring forces and end-point displacements were used to calculate the hand stiffness matrix and ellipse (Mussa-Ivaldi et al., 1985) which is characterized by three parameters - its size, shape and orientation. Dolan et al. (1993) and Tsuji et al. (1995) extended this technique to estimate damping and inertia. Mussa-Ivaldi et al. (1985) calculated the terms of the stiffness matrix using linear least squares regression. In Tsuji et al. (1995), they estimated the stiffness, damping and inertia terms by integrating twice the equations of motion (to avoid having to take derivatives), then used linear least squares regression. Techniques have also been developed for measuring stiffness during both loaded and unloaded movements (Gomi & Kawato, 1996, 1997; Burdet et al., 2000).

Tee et al. (2004) presented a model of two dimensional arm dynamics, including stiffness, damping and inertia terms. The stiffness was calculated

by assuming that the joint stiffness is a linear function of joint torque. The damping was assumed to be a non-linear function of the stiffness, and the inertia was calculated based on the geometry of the limbs. The predictions of the model agreed well with published findings from other papers. Burdet et al. (2006) used a similar arm model to examine the stability of the arm, which is important when interacting with certain tools or objects.

Human arm stiffness can be controlled depending on the task. Tsuji et al. (2004) showed with a virtual tennis system that participants altered their stiffness depending on the phase of the movement and the mass of the ball. Darainy et al. (2004) demonstrated that subjects learned to alter their arm stiffness in a task requiring posture maintenance during force application.

When considering grasping in three dimensions, a stiffness ellipsoid, rather than an ellipse, is appropriate. Lin et al. (2000) defined a frame-invariant stiffness quality measure which quantifies the grasp stability. However, this measure can not take into account task specific stiffness requirements.

Compared to studies of the whole arm stiffness, relatively few studies have focused on finger and hand stiffness. Hajian & Howe (1997) measured the impedance properties (i.e., stiffness, viscosity and inertia) of the outstretched index finger's metacarpophalangeal (MPJ) joint. Milner & Franklin (1998) studied the effects of finger posture and the direction of the voluntary forces on the resultant finger stiffness ellipses. Unlike for the stiffness of a single joint, where a monotonic relationship was found between joint stiffness and joint torque (Hajian & Howe, 1997), no systematic relationship was found for the whole finger. These authors concluded that finger stiffness can most easily and robustly be controlled by altering the finger posture. Kao et al. (1997) measured the stiffness of the thumb and index finger in a plane. The two-dimensional stiffness of a grasp composed of these two fingers was calculated, and measures from the robotics literature were used to predict the properties of the grasp under external loads. Jindrich et al. (2004) estimated the joint stiffness and damping of the finger during typing, by measuring the joint angles of the finger with miniature goniometers, and the force applied at the endpoint by the finger. They found that the stiffness and damping differed between the loading and unloading stages of the movement.

The stiffness of an external object being grasped was measured by Buttolo (1996) and Van Doren (1998). These calculations were used to compare the stiffness properties of different finger placements (Buttolo, 1996) and the effect of finger span and grasp force (Van Doren, 1998).

A dynamic model of the index finger was constructed in Brook et al. (1995), where they took into account all the muscles acting on the joints of the finger. By calculating the force generated on the joints by the muscles, together with some additional constraints, the model can predict the forces that should be applied by each muscle given the joint driving movements. Sancho-Bru et al. (2001) also presented a model for predicting the muscle forces when given the posture of the finger during the movement.

In this work, we experimentally identify the endpoint inertia, damping and stiffness of the index finger. The experimentally estimated inertia is compared to the predictions of a geometric model. The experimental measurements of impedance are calculated using a novel technique by applying known force perturbations to the index finger with the CyberGrasp (Immersion) and measuring the resultant acceleration, velocity and displacement of the fingertip.

3.1.2 2D Dynamic equations of the index finger

The index finger can be modeled as an open-chain manipulator, as shown in Figure 3.1, where it is assumed that the combined effect of the muscles acting on each joint can be modeled in a similar way to a spring-damper system (Hogan, 1985b; Dolan et al., 1993). The model used here is two dimensional - the abduction / adduction of the metacarpophalangeal joint is not considered. In addition to the spring and damper terms, the inertia, Coriolis and centrifugal effects and gravity are included, giving the model

$$\hat{M}(\theta_0)\ddot{\theta} + \hat{C}(\theta_0, \dot{\theta})\dot{\theta} + \hat{B}(\theta_0)\dot{\theta} + \hat{K}(\theta_0)(\theta - \theta_0) + \hat{G}(\theta_0) = \tau \quad (3.1)$$

where \hat{M} is the inertia matrix, \hat{C} the Coriolis and centrifugal effects, \hat{B} the damping matrix, \hat{K} the stiffness matrix and \hat{G} the gravity term, in joint coordinates. θ is the vector of joint angles and τ the vector of joint torques.

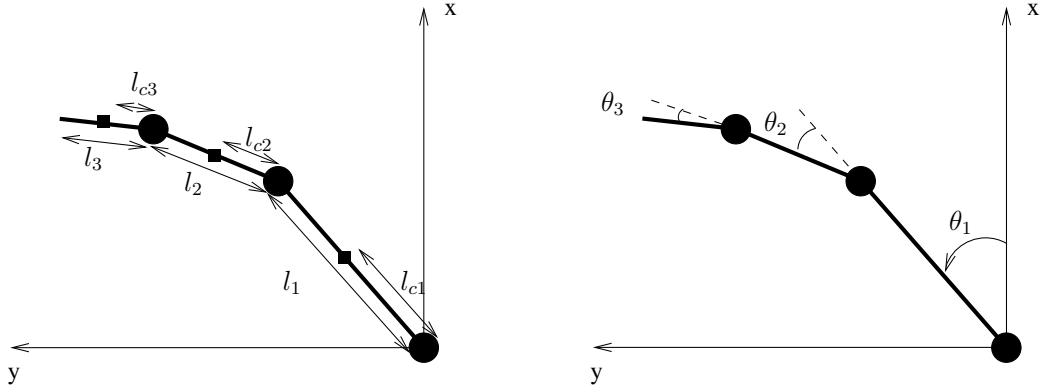


Figure 3.1: The 2D model of the fingers used in this chapter.

The twists ξ representing the three joints of the finger can be written as

$$\xi_1 = \begin{bmatrix} 0 \\ 0 \\ 0 \\ 0 \\ 0 \\ 1 \end{bmatrix}, \quad \xi_2 = \begin{bmatrix} 0 \\ -l_1 \\ 0 \\ 0 \\ 0 \\ 1 \end{bmatrix}, \quad \xi_3 = \begin{bmatrix} 0 \\ -l_1 - l_2 \\ 0 \\ 0 \\ 0 \\ 1 \end{bmatrix}.$$

The body Jacobians for each of the links will then be

$$J_{sl_1(0)}^b = \begin{bmatrix} 0 & 0 & 0 \\ l_{c1} & 0 & 0 \\ 0 & 0 & 0 \\ 0 & 0 & 0 \\ 0 & 0 & 0 \\ 1 & 0 & 0 \end{bmatrix}, \quad J_{sl_2(0)}^b = \begin{bmatrix} s_2 l_1 & 0 & 0 \\ c_2 l_1 + l_{c2} & l_{c2} & 0 \\ 0 & 0 & 0 \\ 0 & 0 & 0 \\ 0 & 0 & 0 \\ 1 & 1 & 0 \end{bmatrix}$$

$$J_{sl_3(0)}^b = \begin{bmatrix} s_3 l_2 + l_1 s_2 \mathfrak{B} & s_3 l_2 & 0 \\ l_{c3} + c_3 l_2 + l_1 c_2 \mathfrak{B} & c_3 l_2 + l_{c3} & l_{c3} \\ 0 & 0 & 0 \\ 0 & 0 & 0 \\ 0 & 0 & 0 \\ 1 & 1 & 1 \end{bmatrix}$$

The link inertia matrix M_i of link i is given by (Murray et al., 1994)

$$M_i = \begin{bmatrix} m_i & & & & & \\ & m_i & & & & \\ & & m_i & & & \\ & & & I_{xi} & & \\ & & & & I_{yi} & \\ & 0 & & & & I_{zi} \end{bmatrix} \quad (3.2)$$

where m_i is the mass of the i th segment of the finger, and I_{xi} , I_{yi} and I_{zi} are the moments of inertia about the x , y and z axes of this segment. In order to find the inertia matrix of the chain, the link inertia matrices need to be transformed into the appropriate coordinate system using the body Jacobians for each link:

$$\hat{M} = \sum_i (J_{sl_i(0)}^b)^T M_i J_{sl_i(0)}^b \quad (3.3)$$

3.1. EXPERIMENTAL ESTIMATION OF FINGERTIP IMPEDANCE 23

The inertia matrix can then be determined by evaluating Equation (3.3):

$$\begin{aligned}
\hat{M}_{1,1} &= (2l_{c3}c_3l_2 + l_2^2 + l_1^2 + 2l_{c3}l_1c_{23} + l_{c3}^2 + 2l_2l_1c_2)m_3 \\
&\quad + m_1l_{c1}^2 + I_{z1} + I_{z2} + I_{z3} + 2m_2c_2l_1l_{c2} + m_2l_{c2}^2 + l_1^2m_2 \\
\hat{M}_{1,2} &= (l_2^2 + l_{c3}^2 + 2l_{c3}c_3l_2 + l_{c3}l_1c_{23} + l_2l_1c_2)m_3 \\
&\quad + m_2c_2l_1l_{c2} + m_2l_{c2}^2 + I_{z2} + I_{z3} \\
\hat{M}_{1,3} &= (l_{c3} + c_3l_2 + l_1c_{23})m_3l_{c3} + I_{z3} \\
\hat{M}_{2,2} &= (l_2^2 + l_{c3}^2 + 2l_{c3}c_3l_2)m_3 + m_2l_{c2}^2 + I_{z2} + I_{z3} \\
\hat{M}_{2,3} &= (l_{c3} + c_3l_2)m_3l_{c3} + I_{z3} \\
\hat{M}_{3,3} &= m_3l_{c3}^2 + I_{z3}
\end{aligned} \tag{3.4}$$

The other three terms of the inertia matrix can be found by the symmetry property of the inertia matrix.

The Coriolis and centrifugal forces can be computed from the partial derivatives of the inertia matrix (Murray et al., 1994):

$$\hat{C}_{ij}(\theta, \dot{\theta}) = \sum_{k=1}^3 \Gamma_{ijk} \dot{\theta}_k = \frac{1}{2} \sum_{k=1}^3 \left(\frac{\partial M_{ij}}{\partial \theta_k} + \frac{\partial M_{ik}}{\partial \theta_j} - \frac{\partial M_{kj}}{\partial \theta_i} \right) \dot{\theta}_k$$

The terms of \hat{C} were calculated to be

$$\begin{aligned}
\hat{C}_{1,1} &= -\dot{\theta}_3 l_1 (m_2 s_2 l_{c2} + m_3 l_2 s_2 + m_3 s_{23} l_{c3}) \dot{\theta}_2 - \dot{\theta}_3^2 m_3 (l_{c3} s_3 l_2 + l_1 s_{23} l_{c3}) \\
\hat{C}_{1,2} &= -\dot{\theta}_3 l_1 (s_2 m_2 l_{c2} + m_3 l_2 s_2 + s_{23} m_3 l_{c3}) \dot{\theta}_1 \\
&\quad - \dot{\theta}_3 (l_1 \dot{\theta}_2 m_3 l_2 s_2 + \dot{\theta}_2 m_3 l_1 s_{23} l_{c3} + \dot{\theta}_3 m_3 l_{c3} s_3 l_2 + \dot{\theta}_2 m_2 s_2 l_1 l_{c2} + \dot{\theta}_3 m_3 l_1 s_{23} l_{c3}) \\
\hat{C}_{1,3} &= \dot{\theta}_3 (-m_3 l_{c3} (s_3 l_2 + l_1 s_{23})) \dot{\theta}_1 + \dot{\theta}_3 (-m_3 l_{c3} (\dot{\theta}_2 + \dot{\theta}_3) (s_3 l_2 + l_1 s_{23})) \\
\hat{C}_{2,1} &= \dot{\theta}_3 (m_2 s_2 l_1 l_{c2} + m_3 l_1 l_2 s_2 + l_1 s_{23} m_3 l_{c3}) \dot{\theta}_1 + \dot{\theta}_3 (-\dot{\theta}_3 m_3 s_3 l_2 l_{c3}) \\
\hat{C}_{2,2} &= -\dot{\theta}_3^2 m_3 s_3 l_2 l_{c3} \\
\hat{C}_{2,3} &= -\dot{\theta}_3 (m_3 s_3 l_2 l_{c3}) \dot{\theta}_1 - \dot{\theta}_3 (m_3 s_3 l_2 l_{c3} (\dot{\theta}_2 + \dot{\theta}_3)) \\
\hat{C}_{3,1} &= \dot{\theta}_3 (m_3 l_{c3} (s_3 l_2 + l_1 s_{23})) \dot{\theta}_1 + \dot{\theta}_3 (\dot{\theta}_2 m_3 s_3 l_2 l_{c3}) \\
\hat{C}_{3,2} &= \dot{\theta}_3 (m_3 s_3 l_2 l_{c3}) \dot{\theta}_1 + \dot{\theta}_3 (\dot{\theta}_2 m_3 s_3 l_2 l_{c3}) \\
\hat{C}_{3,3} &= 0
\end{aligned}$$

The effect of gravity on the joints can be considered by taking the partial derivative of the potential energy with respect to the joint angles. The potential energy is dependent on the height, given by the $-y$ value:

$$\begin{aligned} V &= m_1gh_1(\theta) + m_2gh_2(\theta) + m_3gh_3(\theta) \\ &= -m_1gs_1l_{c1} - m_2g(s_{12}l_{c2} + s_1l_1) - m_3g(s_{123}l_{c3} + s_{12}l_2 + s_1l_1) \end{aligned}$$

The partial derivate $\hat{G} = \frac{\partial V}{\partial \theta}$ was computed to be

$$\begin{aligned} \hat{G}_1 &= -g(m_1c_1l_{c1} + m_2(c_{12}l_{c2} + c_1l_1) + m_3(c_{123}l_{c3} + c_{12}l_2 + c_1l_1)) \\ \hat{G}_2 &= -g(m_2c_{12}l_{c2} + m_3(c_{123}l_{c3} + c_{12}l_2)) \\ \hat{G}_3 &= -gm_3c_{123}l_{c3} \end{aligned}$$

These terms now need to be converted into Cartesian endpoint coordinates, using the Jacobian J , which is the mapping from joint angles to endpoint (this is not equivalent to the body Jacobians). The inertia M , Coriolis and centrifugal effects C , effect of gravity G and force F , all as viewed in endpoint coordinates, are given by (Dolan et al., 1993; Murray et al., 1994)

$$\begin{aligned} M &= J^{-T} \hat{M} J^T \\ C &= J^{-T} \left(\hat{C} J^{-1} + \hat{M} \frac{d}{dt} (J^{-1}) \right) \\ G &= J^{-T} \hat{G} \\ F &= J^{-T} \tau \end{aligned} \tag{3.5}$$

The motion of the endpoint can then be modeled as

$$M(\theta_0)\ddot{x}(t) + C(\theta_0, \dot{\theta}(t))\dot{x}(t) + B(\theta_0)\dot{x}(t) + K(\theta_0)(x(t) - x_0) + G(\theta_0) - F(t) = 0 \tag{3.6}$$

The terms for endpoint damping B and stiffness K will only be estimated based on the experimental endpoint data, and not from the respective joint damping and joint stiffness, as we have not implemented a model for predicting these values.

3.1.3 Methods

Experimental setup

Movements of the index finger were recorded simultaneously by a CyberGlove (Immersion) and an Optotrak (Northern Digital). The subjects wore a CyberGrasp (Immersion) exoskeleton over the CyberGlove. The CyberGlove, which was calibrated as described in Appendix A, measured three joint angles of the index finger (metacarpophalangeal, proximal interphalangeal and distal interphalangeal joints) at 90Hz. Since this sampling rate is too low to accurately model the fingertip acceleration, which is required in the inertia calculations, the Optotrak was also used. Five infrared markers were placed on the exoskeleton and on the index finger, as shown in Figure 3.2, and were sampled at 300Hz.

The base of the CyberGrasp was attached with straps to the back of the hand, with finger loops placed on the medial phalanges and force applicator rings placed over the fingertips. String “tendons” extend from the force applicator rings to the actuator enclosure located in a box on the table, which in turn is connected to a controlling computer. Through application of tensions in the tendons, force (updated at 1000Hz) is applied to the fingertips. The CyberGrasp was calibrated for each subject before use, in order to create a mapping between the joint angles of the hand and the extension of the “tendons”. The tendons are maintained taut when no forces are applied, so as to reduce delay between force application and movement.

CyberGrasp force calibration

The forces that the CyberGrasp produce are controlled by sending commands through the network to the CyberGrasp controller. It is important to know the relation between the commands sent, and the actual force produced by the tendons of the CyberGrasp, as this is required in the inertia calculations. In order to determine this force as a function of time, an artificial finger was built and used. This finger inside the CyberGrasp is shown in Figure 3.3.

The artificial finger had a single joint with a spring. The spring constant (0.2618 Nm/rad) was determined by applying known forces to the finger

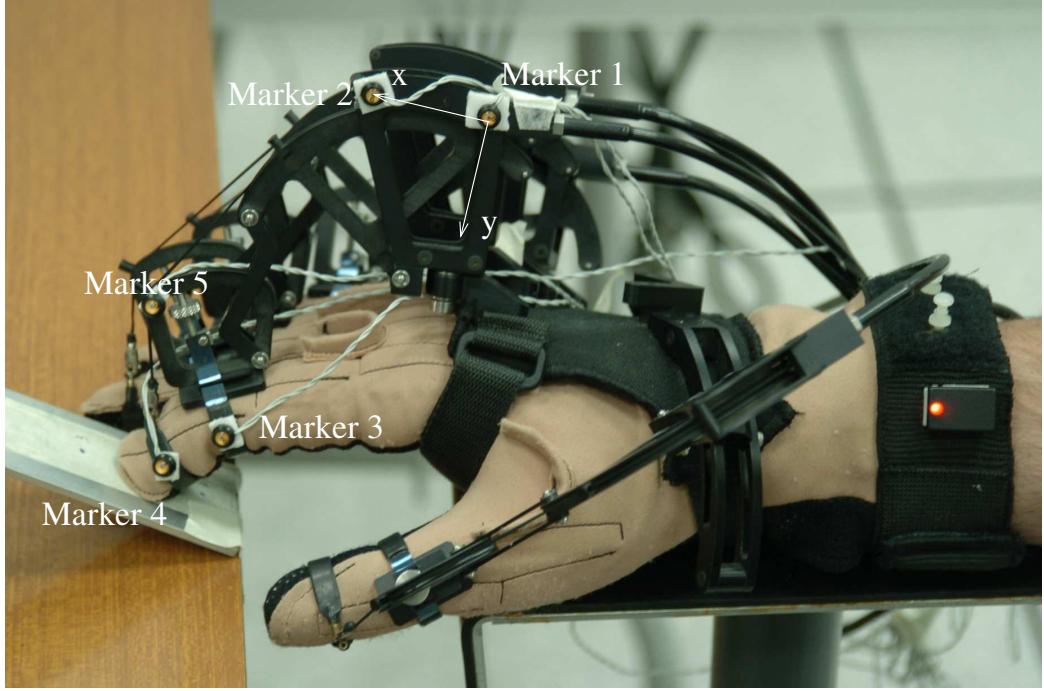


Figure 3.2: Placement of the five Optotrak IRED markers on the exoskeleton and index finger loop. Markers 1 and 2 are fixed relative to the palm and define the x axis, while the y axis is perpendicular to the x and lies in the plane of markers 1,2 and 3. Marker 4 was considered the location of the fingertip, and the force was assumed to be applied along the line from marker 4 to marker 5.

and measuring the angular displacement with the Optotrak. The force-time profile of the artificial finger was then determined by modeling the torque of the joint τ_{af} using the dynamic equations of the finger, assumed to be

$$\tau_{af} = I\ddot{\theta}(t) + K\theta(t) + G(t) \quad (3.7)$$

The force at the point of force application was then calculated from

$$|F_{af}(t)| = \frac{|\tau_{af}|}{|\vec{r}| \sin \theta} \quad (3.8)$$

where r is the vector towards the point of force application, and θ is the angle between \vec{r} and F , which is the equivalent to the angle between the line

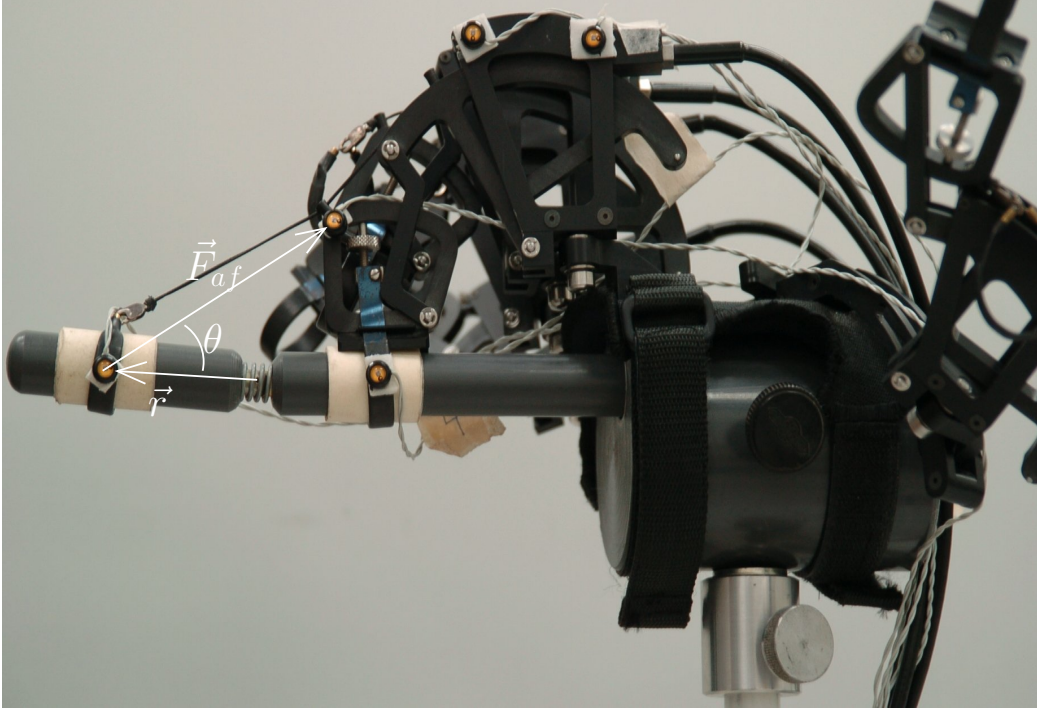


Figure 3.3: The artificial finger used to determine the force profile of the CyberGrasp. F_{af} is the force applied by the CyberGrasp on the artificial finger, and \vec{r} is the position of the point of force application relative to the joint, as specified in Equation (3.8)

joining markers 3 and 4, and the line joining markers 4 and marker 5 (as shown in Figure 3.3).

The “expected” force F_{ex} is the force command given to the CyberGrasp. Then the normalized force profile, defined as $F_{af}(t)/F_{ex}$, was approximated by a 5th order polynomial for the first 0.035s:

$$F(t) = -1.29t^4 + 0.97t^3 + 1.83t^2 - 0.09t - 0.08 \quad (3.9)$$

This polynomial is plotted in Figure 3.4. The force profile does not converge to a constant value during the relatively short duration of force application (although it does eventually), however this does not affect the results, because the time window modeled is the same as the one used in the experiment described below.

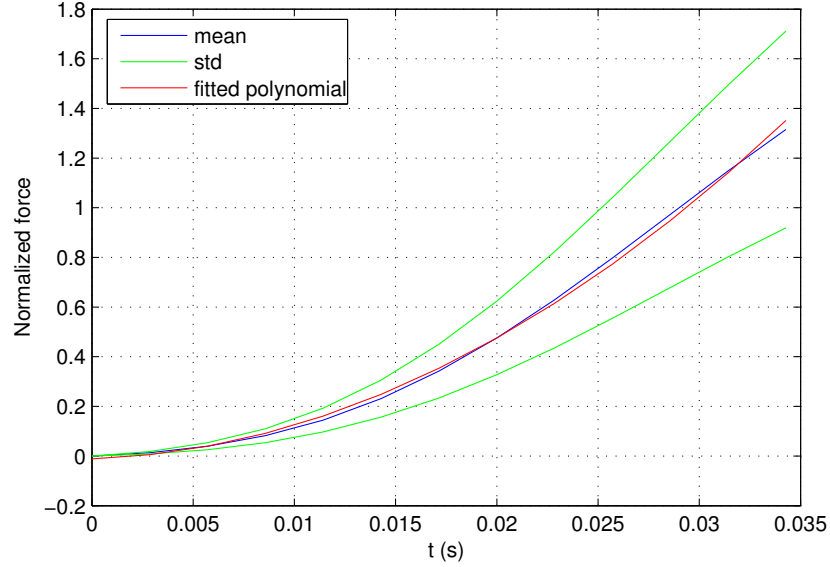


Figure 3.4: The normalized force profile (actual force divided by expected force) of the CyberGrasp acting on an artificial finger, modeled using Equation (3.7). The blue line shows the mean of the normalized force, the green line shows the mean plus or minus one standard deviation, and the red line is the polynomial fit to the data (Equation (3.9)).

Experimental procedure

Three male volunteers participated in the experiment. The subject sat at a table with his right forearm and palm resting on a stand. A triangular wedge, with three points marked on it, was attached to the table under the index finger (see Figure 3.5). During each set of measurements, the subject placed his fingertip on one of the three marked points. The points were selected to span a range of fingertip postures while ensuring that no other part of the finger contacted with the wedge. In each posture, the finger was perturbed by the CyberGrasp fifteen times in the plane containing the major axes of the proximal, medial and distal phalanges, with forces between 1N and 2N for 30ms each. The force was exerted for 30ms to avoid a change in impedance due to activation of the stretch reflex (a response to change in muscle length), the cutaneous slip reflex or voluntary muscle contraction. The perturbations were performed with the fingertip placed, in order, at locations 1, 2, and 3,

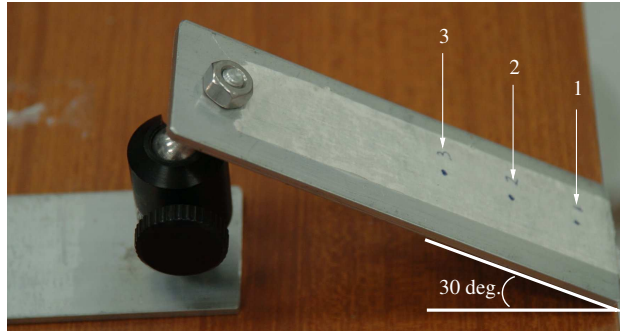


Figure 3.5: The triangular wedge was attached to the table. The points marked indicate the locations where the subjects were required to place their fingertips during the recordings.

and then repeated. Due to the different sizes of the fingers of the subjects, the postures used at the different locations differed between the subjects.

Data Analysis

The Optotrak software was used to obtain the 3D location of each of the markers. The positions of the markers were smoothed using cubic smoothing splines. The position of fingertip (marker 4) was calculated in the exoskeleton frame (x,y) , as shown in Figure 3.2. These axes were selected to be parallel to the axes used in describing the joint locations from the CyberGlove data.

The motion of the fingertip under small perturbations from rest was modeled using Equation (3.6). While the inertia M , damping B and stiffness K are modeled as functions of the posture θ_0 , the Coriolis and centrifugal forces C and the gravity term G are also a function of the joint velocity.

A cubic smoothing spline was fit to $x - x_0$, which allowed the values of $x - x_0$, \dot{x} and \ddot{x} to be calculated at each time step. The values for all the external force levels were combined into one matrix. Perturbations that did not cause the finger to move were not included in the analysis. As the size of the angular perturbations was of a similar magnitude to the resolution of the CyberGlove (≈ 0.5 - 1.0 degrees), a cubic smoothing spline was fitted to the joint angles, to ensure smooth estimations of θ and $\dot{\theta}$. These values were used to calculate C and G .

It was planned to estimate the impedance parameters M, B and K using a linear least squares optimization, by minimizing the square of the left hand side of equation (3.6). However, due to the fact that all the forces applied and the subsequent displacements at each posture were in relatively similar directions, the derivation of M, B and K using this technique was not robust. Hence, additional constraints were applied. From Equation (3.4), it can be observed that $\hat{M}_{3,3}$ (of the joint inertia matrix) is not dependent on the joint angle, and thus should be constant for all the postures. This element of the matrix relates the torque at the third joint (the distal interphalangeal joint) to the angular acceleration at the this joint, and so is independent of the posture. The joint inertia matrix \hat{M} can be calculated from the Cartesian inertia matrix from:

$$\hat{M} = J^T M J \quad (3.10)$$

where J is the Jacobian of the mapping from joint angles to Cartesian endpoint, which will depend on the posture. It can also be observed from Equation (3.4) that $\hat{M}_{1,1} > \hat{M}_{1,2} > \hat{M}_{1,3}$. This constraint was also included in the optimization.

Additionally, as inertia matrices should be positive definite, constraints were added to enforce this, namely that M is symmetric, that the largest element of M is on the diagonal, and that the diagonal elements are positive. Similar constraints were placed on the stiffness matrix K .

The impedance properties M, B and K of all six sets of recordings were derived simultaneously using non-linear optimization where the cost function consisted of both the square sum of the left hand side of (3.6), and terms penalizing the constraints described above with appropriate scale factors. The starting point for the optimization of the inertia was an ellipse with its major axis parallel to the long axis of the distal phalange, while for the stiffness the starting point was the result of the first order stiffness estimation. The use of these additional constraints was successful in producing inertia estimations that were similar to the geometrically predicted values.

The “geometrically predicted” inertia was calculated by converting the manipulator inertia matrix (Equation (3.4)) to the endpoint inertia matrix,

using Equation (3.5):

$$M = J^{-T} \hat{M} J^{-1}$$

where $J^{-T} = (J^{-1})^T$. It should be noted that this equation requires using the pseudo-inverse, because J is not square, and so this may introduce errors. However, it is easier to compare the predictions and experimental results in Cartesian space.

Measurement of fitting error

The average fitting error (between the force predicted using the model, and the measured force) was calculated in a similar way to that used in Dolan et al. (1993):

$$\sigma = \frac{\sqrt{e_x^T e_x}}{N} + \frac{\sqrt{e_y^T e_y}}{N} \quad (3.11)$$

where e_x and e_y are the differences between the geometrically predicted and measured forces in the x and y directions, and N is the number of samples. Five models were considered, with the parameters being estimated shown in bold:

1. The full model (Equation (3.6))

$$\mathbf{M}(\theta_0)\ddot{x}(t) + C(\theta_0, \dot{\theta}(t))\dot{x}(t) + \mathbf{B}(\theta_0)\dot{x}(t) + \mathbf{K}(\theta_0)(x(t) - x_0) + G(\theta_0) - F(t) = 0$$

2. The full model, but without the gravity, Coriolis and centrifugal terms, i.e.

$$\mathbf{M}(\theta_0)\ddot{x}(t) + \mathbf{B}(\theta_0)\dot{x}(t) + \mathbf{K}(\theta_0)(x(t) - x_0) - F(t) = 0 \quad (3.12)$$

3. A second order model, where the geometrically predicted inertia is used, and the stiffness and damping terms estimated from the experimental data:

$$M(\theta_0)\ddot{x}(t) + \mathbf{B}(\theta_0)\dot{x}(t) + \mathbf{K}(\theta_0)(x(t) - x_0) - F(t) = 0 \quad (3.13)$$

4. A first order model, i.e., just stiffness

$$\mathbf{K}(x(t) - x_0) - F(t) = 0 \quad (3.14)$$

5. A first order model where only the total magnitude of force and displacement were used:

$$\mathbf{K}(x_f - x_0) - F = 0 \quad (3.15)$$

where K was fit using the total displacement and force applied for each perturbation (rather than at each sample point, as was performed for the other models).

The differences between the geometrically predicted and experimentally identified inertia ellipses were calculated using the same error measure, where the force required to accelerate the finger due to the inertia was compared between the geometrically predicted and experimentally identified inertia values. In this case, the force vector was that which would be produced by values of \ddot{x} uniformly sampled from a rotating unit input, sampled at 100 points, i.e.

$$F_M = M\ddot{x}, \quad \ddot{x} = \begin{bmatrix} \cos \phi \\ \sin \phi \end{bmatrix}, \phi = [0, \frac{2\pi}{99}, \dots, 2\pi]$$

Reconstruction of trajectories

In order to examine the differences between the geometrically predicted and experimentally estimated inertia matrices, the trajectories of the fingertip were reconstructed using the equation of motion of the finger (Equation (3.6)). The fingertip trajectory was reconstructed using both the experimentally derived and geometrically predicted inertia matrices (in addition to the experimentally determined matrices for the other quantities). It was assumed that the fingertip position could be modeled by a 5th order poly-

mial, with the position, velocity and acceleration initially zero, i.e.,

$$\begin{aligned} x - x_0 &= \begin{bmatrix} a \\ d \end{bmatrix} t^5 + \begin{bmatrix} b \\ e \end{bmatrix} t^4 + \begin{bmatrix} c \\ f \end{bmatrix} t^3 \\ \dot{x} &= \begin{bmatrix} 5a \\ 5d \end{bmatrix} t^4 + \begin{bmatrix} 4b \\ 4e \end{bmatrix} t^3 + \begin{bmatrix} 3c \\ 3f \end{bmatrix} t^2 \\ \ddot{x} &= \begin{bmatrix} 20a \\ 20d \end{bmatrix} t^3 + \begin{bmatrix} 12b \\ 12e \end{bmatrix} t^2 + \begin{bmatrix} 6b \\ 6e \end{bmatrix} t \end{aligned}$$

The stiffness and damping matrices used were those estimated from the experimental data. For the inertia matrix, both the experimentally derived, and geometrically predicted matrices were used. The polynomial parameters $\begin{bmatrix} a & b & c & d & e & f \end{bmatrix}$ were then determined by substituting the inertia parameters, and $(x - x_0)$, \dot{x} and \ddot{x} into equation (3.6), and minimizing the error using a non-linear least squares algorithm (implemented in Matlab). The square of the acceleration was also added to the cost function to ensure reasonable trajectories.

3.1.4 Results

The average fitting errors for the five models are shown in Table 3.1. Generally, the errors for all the models are relatively small when compared to the magnitude of the forces involved (1-2N). The first order model, when only the magnitude of the displacement and the force are considered, performed much worse than the other models. The other four models compared did not differ significantly across all subjects and postures (according to paired t-tests, at the 0.05 significance level). The remainder of the results presented refer to the fit of the full model (Equation (3.6)).

The inertia ellipses calculated from the experimental data, and the inertia ellipses predicted from the geometric model are shown together in Figure 3.6 for the three subjects, at the three different locations (for the second repetition). The ellipses are plotted at the end of the finger. The geometrically predicted and experimentally estimated inertia ellipses are generally of sim-

Subj.	Posture	Model Error ($\times 10^{-2}N$)				
		(3.6)	(3.12)	(3.13)	(3.14)	(3.15)
1	1	1.26	1.27	1.15	1.25	8.49
	2	1.71	1.72	1.64	1.96	12.27
	3	2.34	2.45	1.81	6.58	10.45
2	1	7.93	7.91	7.55	8.09	47.67
	2	3.52	3.51	2.96	2.90	21.71
	3	1.10	1.05	1.26	1.06	7.22
3	1	1.32	1.34	1.26	1.16	7.14
	2	1.36	1.34	1.23	1.28	8.83
	3	1.63	1.45	1.03	0.86	5.39

Table 3.1: Fitting errors for the five models for three subjects. The five models are the full model (Equation (3.6)), the full model without the gravity, Coriolis and centrifugal terms (Equation (3.12)), a second order model using the geometrically predicted inertia (Equation (3.13)), a first order model (Equation (3.14)), and a first order model using total displacement and the applied force (Equation (3.15)). Standard deviations are not shown because these are the errors from a single comparison.

ilar size, shape and orientation although some differences between the two sets are observed. In the third posture (where the finger is most extended), the ellipses are elongated. As the finger becomes more extended, the inertia becomes closer to the inertia that would be observed if the entire finger was one long phalange, in which case, the inertia ellipse would have no width, only a length.

For subject 2, posture 1, the ellipse predicted from the geometric model is quite different to the ellipse from the experimental data. The poor similarity may be due to the relatively small number of usable force / displacement trajectories that were available for the calculation (because the finger did not move during most of the force applications).

The parameters of the ellipses: the angle of the major axis, the shape (ratio of the length of major to minor axis) and the size (the area of the ellipse) are detailed in Table 3.2. There are no errors shown for these values because for each subject at each posture, all the recorded movements are used in generating a single inertia ellipse.

3.1. EXPERIMENTAL ESTIMATION OF FINGERTIP IMPEDANCE 35

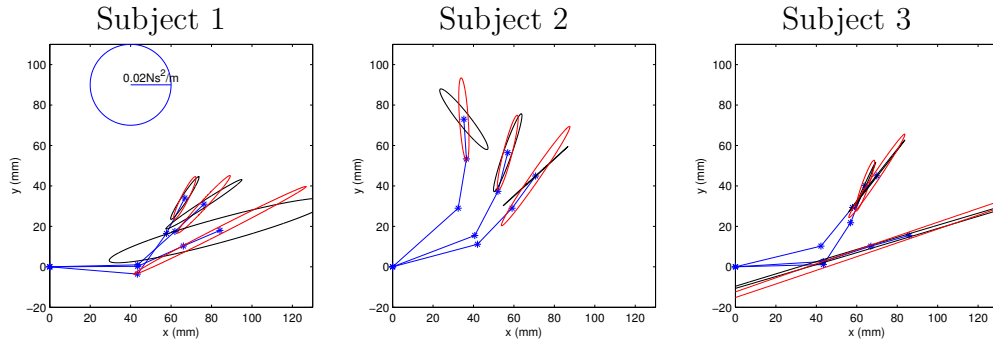


Figure 3.6: Experimentally estimated (black) and geometrically predicted (red) inertia ellipses of the index finger, plotted at the fingertip. The second repetition, at three locations, is shown.

Figure 3.7 and Figure 3.8 show the damping and stiffness ellipses respectively from Equation (3.6), that are calculated from the experimental data.

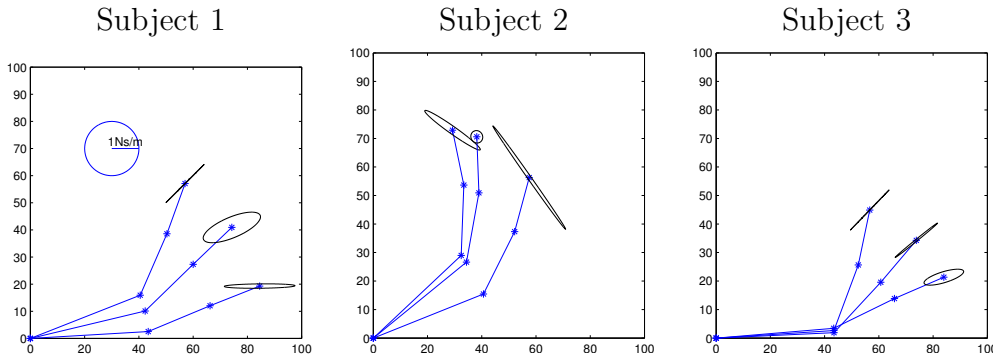


Figure 3.7: Experimentally estimated damping ellipses of the index finger.

Figure 3.9 shows the reconstructions of the position, velocity and acceleration of the endpoint, based on the geometrically predicted and experimentally calculated inertia. The experimentally calculated damping and stiffness were used in both cases. These reconstructions were compared to the actual position, velocity and acceleration. These reconstructions can help to understand the quality of the model. While the reconstructions using the experimental and geometrically predicted inertia matrices predict well the displacement, larger errors are observed in the velocity and acceleration beginning around

Subj.	Posture	Angle (deg.)		Shape		Size ($\times 10^{-4}$)		Error ($\times 10^{-3}N$)
		Pred.	Exp.	Pred.	Exp.	Pred.	Exp.	
1	1	63.32	57.33	6.58	8.21	0.21	0.19	0.25
	2	47.53	33.18	10.90	14.34	0.34	0.35	0.79
	3	26.99	15.48	27.80	9.62	0.82	3.35	1.61
2	1	93.80	-51.99	9.52	6.28	0.44	0.57	1.64
	2	75.76	70.83	8.82	9.79	0.41	0.43	0.29
	3	55.50	42.43	13.91	184.25	0.64	0.03	1.01
3	1	70.43	65.81	8.01	29.67	0.22	0.05	0.23
	2	56.23	51.96	15.28	81.80	0.40	0.06	0.27
	3	18.85	16.64	96.99	148.37	2.51	0.91	3.84

Table 3.2: Parameters of the experimentally estimated and geometrically predicted inertia ellipses of the index finger. The parameters are the angle of the major axis, the shape (ratio of the length of major to minor axis) and the size (the area of the ellipse). The last column shows the error between the forces that would be produced by a rotating unit input for the experimentally estimated and geometrically predicted inertia matrices, calculated with Equation (3.11).

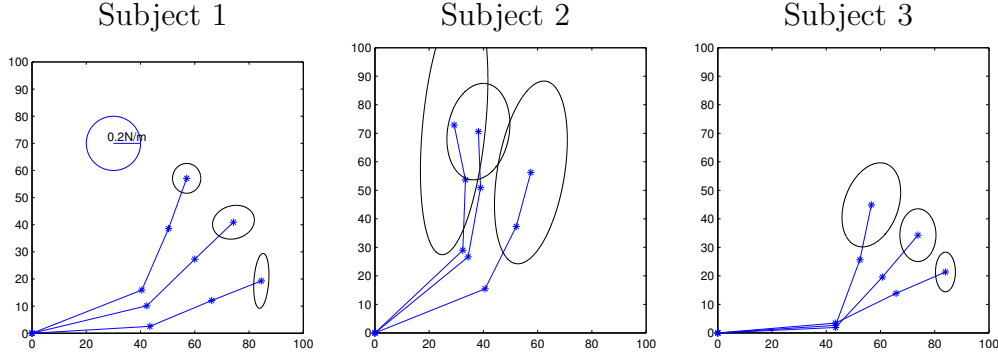


Figure 3.8: Experimentally estimated stiffness ellipses of the index finger.

halfway through the movement. Also, the predictions for the third posture, where the finger is more extended than in the other postures, are worse.

Finally, the 3D inertia ellipsoids for all the fingers are shown, using similar techniques, for a task of lifting a cup, in Figure 3.10. As can be observed, the inertia ellipsoids vary significantly in their size, with the thumb having the largest inertia ellipsoid, and the orientation is a function of the posture of the finger. Thus, the total inertia of the grasp can be controlled by changing

3.1. EXPERIMENTAL ESTIMATION OF FINGERTIP IMPEDANCE 37

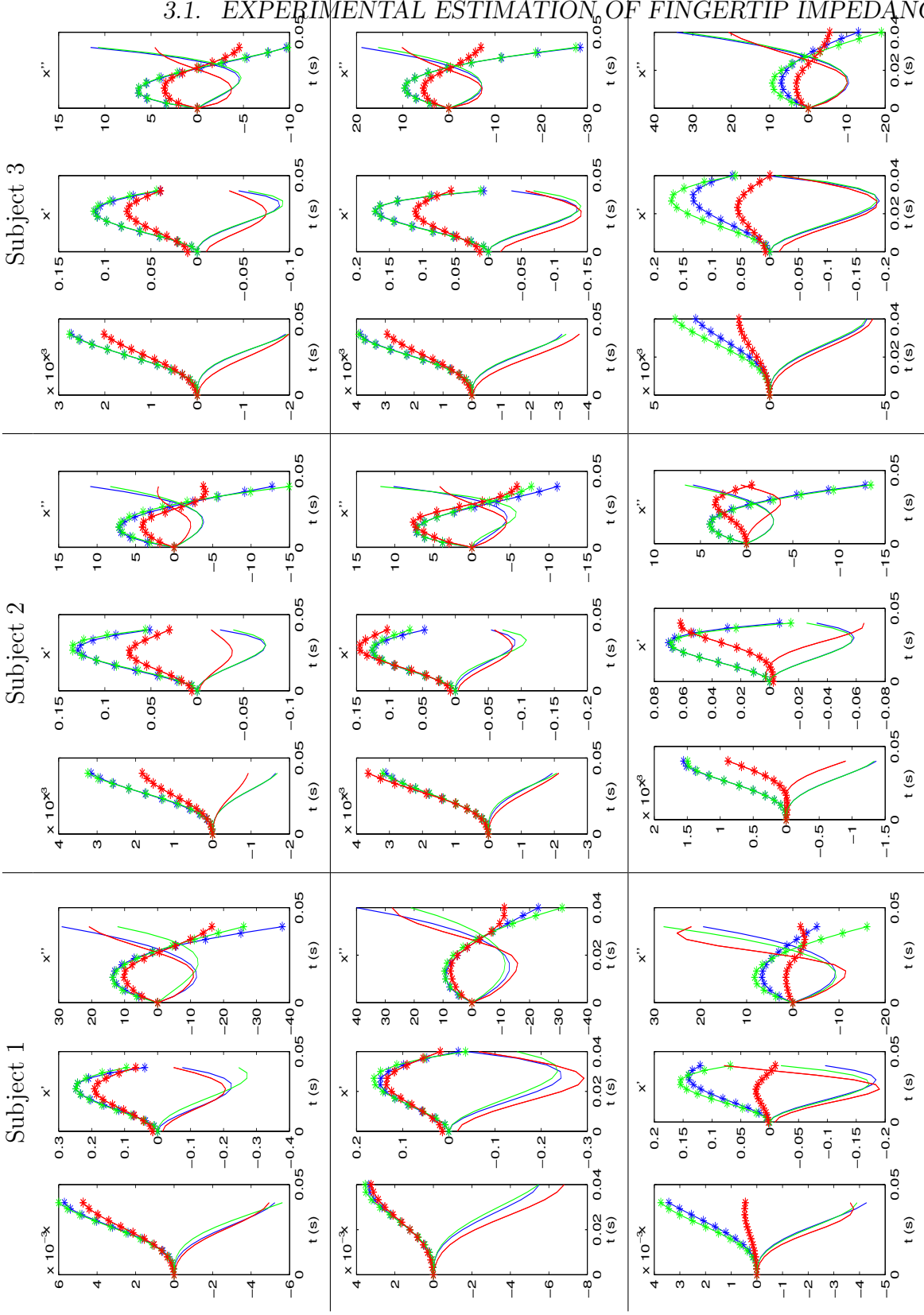


Figure 3.9: Reconstructions of the displacement, velocity and acceleration of the fingertip for the first force perturbation (of many). Each set of three graphs shows the displacement in m (leftmost graph), velocity in m/s (middle graph) and acceleration in m/s^2 (right graph). The red is the experimentally measured trajectory, the blue is the reconstructed trajectory using the experimentally derived inertia, and the green is using the geometrically modeled inertia. The starred trajectories are along the x axis, while those without stars are along the y axis. Each column is a subject, each row a posture.

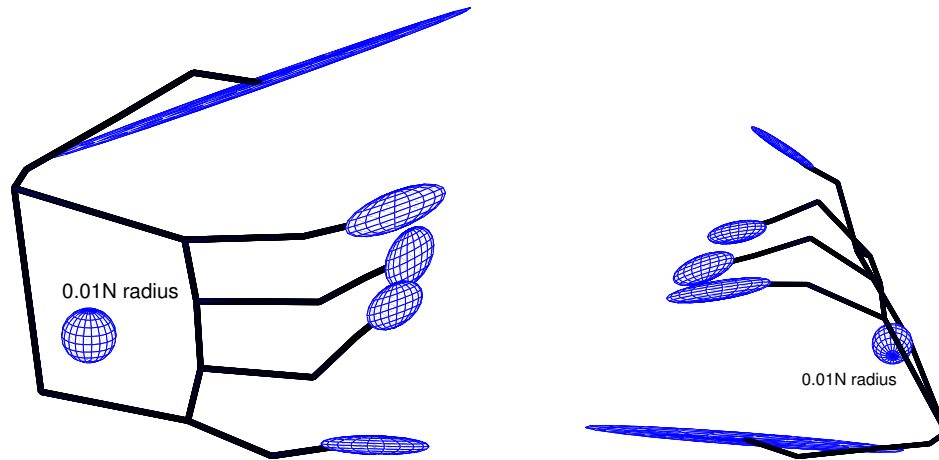


Figure 3.10: Inertia ellipsoids for all the fingers plotted at the fingertips, for the task of lifting a cup, shown from two views. A sphere with radius of $0.01N$ is shown for reference.

the hand posture.

3.1.5 Discussion

In this section, we have experimentally estimated the impedance properties of the human index finger. The calculated inertia values were generally similar to those predicted by a geometric model. The differences between them were quantitatively measured in terms of the average difference in the force to accelerate the fingers for a unit acceleration (over all angles), and were found to be small. It was possible to reconstruct with reasonable accuracy the movements of the fingers when perturbed using the derived parameters. The full impedance model of the finger did not predict the fingertip force significantly better than a first order model, as measured by the fitting error. However, for an accurate model, it was important to model the displacement and force at many time points, rather than only using their total magnitude.

While some success was observed in using this method for estimating the endpoint impedance of the fingertip, it is not an ideal technique, due to the fact that the perturbations on the finger are in a similar direction. This likely led to the failure of a simple least squares technique to estimate the

inertia terms for the finger. This problem is illustrated in Figure 3.11. As the provided data points are all close to one another, and there is some error in their measurement, there are many inertia ellipses that could fit through these points. The additional constraints applied in this paper restricted the allowable ellipses to those that satisfy properties of inertia ellipses (such as being positive definite). Ideally, the perturbations on the finger should be applied very accurately and in all directions.

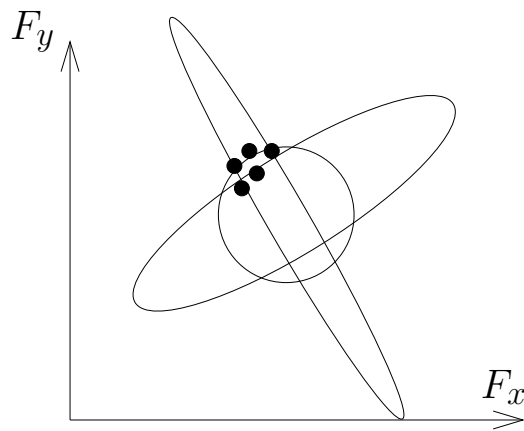


Figure 3.11: The black dots show the forces for a unit displacement. Several possible ellipses that could be fit to these noisy points are shown. To identify the “correct” ellipse, either forces in other directions are necessary, or constraints must be placed on the types of ellipses that are acceptable.

The observed differences in the reconstruction of the trajectories (Figure 3.9) may have been due to the non-symmetry found in some of the inertia matrices. This lack of symmetry may be due to additional terms that should be taken into account when modelling the fingers. The inertia of the glove may have contributed to this error. Also, the greater errors in velocity and acceleration suggest that there may be errors in modelling the velocity-dependent phenomena, although centripetal and centrifugal forces were taken into account. This may also be partly related to wearing the glove during the measurements.

The inertia values found in this study were similar to those presented in Hajian & Howe (1997), although they considered extension of the metacarpophalangeal joint, whereas in this work we considered also extension of the

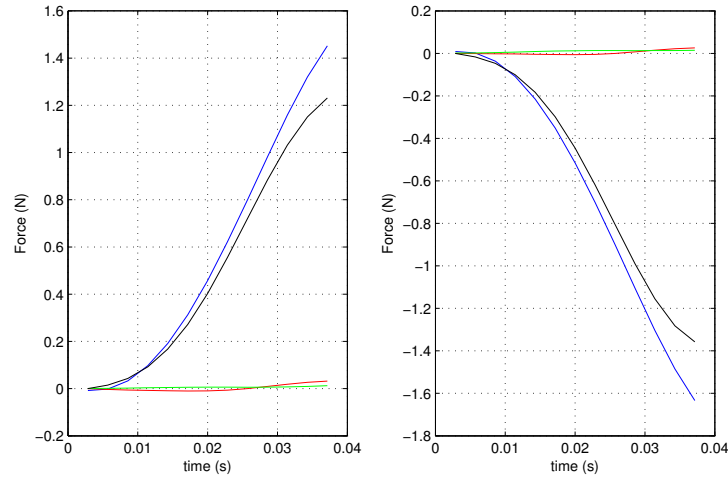


Figure 3.12: Force components in the x direction (left graph) and y direction (right graph), due to inertia (red), damping (green), stiffness (black) and total force (blue) for a typical force perturbation.

interphalangeal joints. This work extends the stiffness measurements of Kao et al. (1997) by including damping and inertia terms, and taking into account dynamic effects.

Figure 3.12 shows the relative magnitude of the contributions of inertia, damping and stiffness to the total force for a typical movement. The deviations between the actual force and the predicted force in the graph are due to the errors in the model, Coriolis and centrifugal effects and gravity effects. The effect of inertia on the total force is much smaller than the effect of stiffness, and it should also be noted that these movements have much higher acceleration than is typical in natural movements. So for many applications, modelling only the stiffness may be sufficient, although for greater accuracy, particularly with fast movements or light objects, the effects of damping and inertia should also be considered.

Based on the findings of this section, it seems reasonable to use such geometric models for estimating the inertia of the fingers, from which the inertia of the hand can be predicted. The technique presented has applications in modeling the interaction of the fingers with different objects (such as when typing or piano playing), in accurately modeling human grasping (such as in Kowadlo et al. (2005)) and for stiffness estimation.

3.2 Grasp stiffness estimation

The stiffness of a grasp is dependent on the muscle activation, as well as the posture of the hand. For the arm, it has been shown that the posture has a strong influence on the endpoint stiffness (Mussa-Ivaldi et al., 1985), and it is expected that a similar statement is true for the fingers. In this section, a technique for interpolating stiffness values for unmeasured finger postures based on stiffness measurements at known postures is presented. This technique is used later in the work to analyze the quality of computer generated grasps.

In this section, for estimating the finger stiffness K_C , a simple first-order impedance model of the fingers was used:

$$F = K_C dX \quad (3.16)$$

While the grasp was held at a particular posture, the fingers were perturbed and the change in position recorded using the CyberGlove. The stiffness was calculated using an optimization procedure to find the symmetric matrix K_C that satisfies Equation (3.16) with the smallest error.

The endpoint stiffness is related to the joint stiffness by (Hogan, 1985b):

$$K_\theta = J^T K_C J \quad (3.17)$$

where J is the Jacobian that converts from joint velocities to fingertip velocities. The Jacobian for the finger, modeled as a three link manipulator, is given by

$$J = \begin{bmatrix} -l_3 s_{123} - l_2 s_{12} - s_1 l_1 & -l_3 s_{123} - l_2 s_{12} & -l_3 s_{123} \\ l_3 c_{123} + l_2 c_{12} + c_1 l_1 & l_3 c_{123} + l_2 c_{12} & l_3 c_{123} \end{bmatrix}$$

From analysis of experimental data, Kamper et al. (2002) found that the relationship between a joint angle and the joint's stiffness can be reasonably modeled by a quadratic equation. Based on this, the relationship between the joint angles and the joint stiffnesses, calculated from Equation (3.17) was

modeled in this way, where the coefficients of the quadratic equation were determined using robust linear regression (implemented using Matlab).

The transformation of the stiffness to the endpoint from joint stiffness requires using the pseudo-inverse because the Jacobian J is not square:

$$K_C = J^{-T} K_\theta J^{-1} \quad (3.18)$$

Using the Moore-Penrose inverse gave poor results, in that the order of magnitude of the endpoint stiffness matrix was several times larger than typical values. Instead, an optimization procedure is used, where the endpoint stiffness of the novel posture was required to be symmetric, and “close” to the endpoint stiffness of the closest recorded posture.

$$\begin{aligned} K_C^* = \min_{K_C} & (J^T K_C J - K_\theta)^2 \\ & + 10^4 ((K_{C_{1,1}} - K_{C_{n_{1,1}}})^2 + (K_{C_{2,2}} - K_{C_{n_{2,2}}})^2 + (K_{C_{1,1}} - K_{C_{n_{1,2}}})^2) \end{aligned} \quad (3.19)$$

The last term in Equation (3.19) prevented unrealistically large values of the stiffness matrix. The minimization was implemented using the optimization toolkit of Matlab.

The technique described above was verified using known endpoint stiffness matrices, and was used in later sections to estimate the stiffnesses of the fingers at novel, unmeasured postures, from which the grasp stiffness could be derived.

Chapter 4

Grasp selection

Nomenclature

G_h	Grasp Jacobian.
\dot{x}_o	Object velocity.
$\dot{\theta}$	Joint velocities (of the fingers).
V_f	Fingertip velocity.
J_f	Finger Jacobian.
F_{ci}	Force on object from contact i .
f_{ci}	Force applied by finger i .
B_{ci}	Soft finger constraint.
μ	Coefficient of friction.
γ	Coefficient of torsional friction.
G	Grasp map.
F_o	Force applied on the object.
τ_o	Torque applied on the object.
K	Stiffness.
K_{ext}	Stiffness of the metacarpophalangeal joint in the extension direction.
K_{abd}	Stiffness of the metacarpophalangeal joint in the abduction direction.
K_C	Stiffness at the contacts.
K_o	Grasp stiffness.
C	Task compatibility index.
u	Direction of desired force or velocity.

4.1 Introduction

During our day-to-day life, we interact with objects in the world using our hands in many different ways but give little thought to how we select where to place our fingers on the object, what posture our hand takes, and the impedance properties that we impart to the grasping hand. This section explores the relationship between the manipulation properties of grasps selected for various tasks, and the requirements of the task.

The way that we grasp an object is influenced by our perception of the physical properties of the object such as size and shape, as well as our intention for the action (see Rosenbaum et al. (2006) for a review). Affordances of the object, a term introduced by Gibson (1979), are intrinsic properties that afford a particular type of manipulation. The affordances of an object affect how the grasp is selected for an object (Gentilucci, 2002).

In robotics, there are three broad approaches to the problem of grasp synthesis - geometric, taxonomy or optimization based (Coelho & Grupen, 1997). The geometric approach plans grasps that satisfy form-closure or force-closure. Form-closure means that the object being grasped is unable to move, whereas force closure is when the contacts are able to apply any wrench to the object, or alternatively, are able to resist any perturbation (Mason, 2001). Form-closure does not imply force-closure or vice versa. A force- or form-closure grasp, if one exists, can be selected from the geometry of the object. However, the use of force-closure may be an overly strict constraint when stable grasps are required (Brook et al., 1998).

Taxonomy based grasp selection is where the grasp to use is selected from a predefined taxonomy, such as the taxonomies proposed by Cutkosky (1989) and Iberall (1997). The selection is made based on the type of grasp desired (for example, power or precision grasp) and the geometry of the object.

An alternative approach is based on optimization. This is where the grasp is selected to be optimal in terms of some measure. Shimoga (1996) presented a comprehensive review of different properties that can be optimized, such as dexterity, stability or dynamic behavior. Hester et al. (1999) used the velocity transmission and force transmission properties (from the joint angles to the

object being grasped) to select the optimal grasps.

The work described in this chapter is based on the optimization approach, but looks at the problem from an inverse perspective. Here, it is assumed that human grasps are optimal in some sense. Based on this assumption, the optimality of the grasps selected for different tasks is examined in terms of measures of force and velocity transmission properties, and stiffness.

The results of the first part of this work are published in Friedman & Flash (2007).

4.2 Methods

Five right handed and two left handed male subjects aged between 25 and 37 (mean 31) gave informed consent to participate in the experiments. Stiffness measurements were not performed for one of the subjects.

The CyberGlove (Immersion) was used to measure 22 joint angles of the hand during the grasping movements. The joint angles were sampled at 90Hz throughout the recordings, and smoothed using cubic splines. The 3D locations of the joints (including the fingertips) were estimated using a model of the hand described in Appendix A. Simultaneously, the position and orientation of the wrist were recorded at 120Hz using the Fastrak (Polhemus), which records the 3D position and orientation by sensing an AC electromagnetic field. The Fastrak data were resampled to 90Hz so that the data coincided with those from the CyberGlove. The Fastrak and CyberGlove data were combined to give the joint locations relative to the laboratory fixed reference frame. The joint locations were then transformed into a reference frame with its center located at the center of mass of the object. During stiffness measurements, the CyberGrasp (Immersion) exoskeleton was placed on the subject's hand over the CyberGlove.

Nine different grasps involving 5 different objects were tested. These grasps consisted of lifting a plastic cup, from the side and from the top, stirring with and lifting a teaspoon, unscrewing and lifting the lid of a narrow jar, unscrewing and lifting the lid of a wide jar and lifting a puzzle piece. The objects and grasps are shown in Table 4.2.













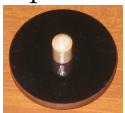

Object	Dimensions	Grasps	
Plastic cup 	4.3cm diameter at base, 8.3cm diameter at top, 10.9cm height	 (1) Lift from side(*)	 (2) Lift from top(*)
Narrow jar 	8cm height of jar, 1.4cm height of lid, 3cm diameter	 Unscrew lid	 Lift lid
Wide jar 	5.6cm height of jar, 1.5cm height of lid, 6cm diameter	 (3) Unscrew lid(*)	 (4) Lift lid(*)
Teaspoon 	13.7cm length	 (5) Lift(*)	 (6) Stir(*)
Puzzle piece 	base is 5.6cm diameter, 0.6cm height, rod is 1.0cm diameter, 1.5cm long	 Pick up	

Table 4.1: The five objects and nine grasps tested in the experiment. Those marked with (*) were subject to detailed analysis.

All the grasps in this study were pad opposition grasps, that is, grasps that contact the object only at the fingertips and not at the palm. The subjects were instructed to use only their fingertips (and not their palms), and adherence to this instruction was visually confirmed.

The experimental setup is shown in Figure 4.1. The subject sat upright next to a table, with his or her arm resting on the table at approximately waist level. Each trial began with the subject's hand at a marked starting position. The objects were manually placed at the marked object position before each manipulation. The objects were attached firmly to the table using strong Velcro during the stiffness measurement, and when the manipulation involved the lid of the object.

The experiment was divided into two parts. The purpose of the first part was to measure the joint angles and wrist location and orientation at the onset of the manipulation task as well as during object manipulation. In the second part, the stiffness of the hand was estimated by asking the subjects to produce finger and hand configurations that matched those used at the onset of the manipulation task, and by applying forces to the fingertips and measuring their displacement.

The first part began with a procedure to calibrate the glove for the subject, as described in Appendix A. Before each movement, the subject rested his or her arm on the table. Each trial, initiated by the experimenter when the subject was ready, began with a beep. The subject then moved his or her hand and held the object, and waited until the second beep (2.5 seconds later). He or she then manipulated the object for 2 seconds as instructed, after which a final beep was heard. At this time, he or she returned the object to the table (if appropriate). For each object, the static forearm, hand and finger configuration before the manipulation began (at the time of the second beep) were measured. The number of fingers used for each grasp was noted by the experimenter. The manipulation with each type of grasp was repeated 3 times, i.e. 27 grasps were performed with the 9 manipulations. The first block of trials took approximately 20 minutes. Sufficient periods of rest were given to the subject between manipulations and at the end of the block.

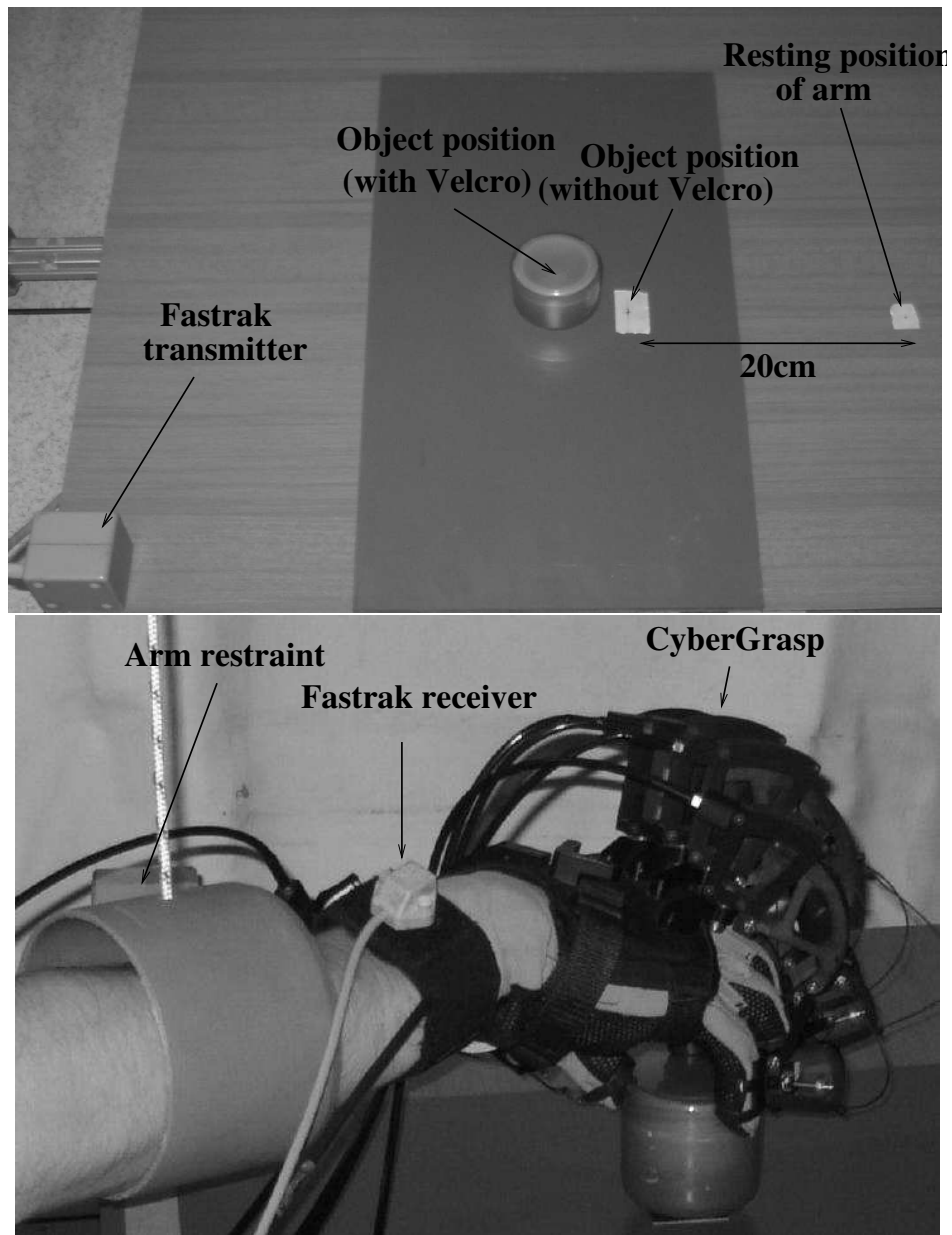


Figure 4.1: Experimental setup. The appropriate object was placed at the marked position before each manipulation. When necessary, the object was attached to the table with strong Velcro (e.g. the base was attached to the table when unscrewing the lid). Joint angles of the hand were recorded by the CyberGlove worn on the hand, and the position and orientation of the wrist were measured with the Fastrak. During measurements of the stiffness, the CyberGrasp was placed over the CyberGlove and the forearm was restrained with a plastic loop.

After a short break, the second part began. The CyberGrasp (Immersion) was placed on the subject's hand over the CyberGlove, and the calibration procedures for the CyberGlove and CyberGrasp were performed. Each trial began with a beep, and in response the subject moved his or her hand in order to grasp the object and was instructed to maintain the initial posture they would use if they were to manipulate the object. Two seconds after the first beep, a second beep was generated. At this time, a force was applied to all fingers participating in the grasp for 300ms, causing the fingers to move. After the 300ms of force application the force was removed and the fingers returned to their initial position. After a random time, between 700ms and 2000ms after the end of the previous force application, another force was applied. A total of 25 forces were applied in each trial. During this entire procedure, the forearm was supported by a plastic loop hanging from a cantilever above. The displacements of the fingertips caused by the applied forces, generally between 5mm and 20mm, were calculated from the joint angles measured with the CyberGlove. The wrist sometimes moved slightly (up to 3mm) as a result of the force application.

Forces of 1.0N, 1.25N, 1.5N, 1.75N, 2.0N were applied. Each force was repeated 10 times with small variations added to the force (-0.05N, -0.025N, +0N, +0.025N, +0.05N), each repeated twice.

Analysis

Grasp Jacobian The analysis was based on the grasp Jacobian at the start of the manipulation. Full details of the derivation can be found in Appendix B. The grasp Jacobian, sometimes known as the grasp matrix (e.g., in Mason & Salisbury (1985)), G_h , is the transformation from finger joint velocities to the velocity of the object.

$$\dot{x}_o = G_h \dot{\theta} \quad (4.1)$$

It takes into account the transformations for each finger from joint velocities to fingertip Cartesian velocity, the contact relationships (i.e., in which directions force can be transmitted from the fingertips to the object), and the

transformations from the fingertip frames of reference to the object frame of reference.

The transformation from the joint velocities $\dot{\theta}$ to the spatial velocity V_f of the finger tip is defined by the finger Jacobian $J_f(\theta)$

$$V_f = J_f(\theta)\dot{\theta} \quad (4.2)$$

which is a function of the posture. At the contact between the finger tip and the object, forces can only be applied in certain directions, due to friction. These constraints are formally stated using a grasp contact model B_{c_i} . Here, the soft-finger model (Mason & Salisbury, 1985) is used as an approximation to the human finger, which assumes that force can be applied in three directions, as well as torques about the surface normal of the fingertip. The force F_{c_i} felt by the object as a result of applied finger forces f_{c_i} is defined by

$$F_{c_i} = B_{c_i}f_{c_i}, \quad \sqrt{f_1^2 + f_2^2} \leq \mu f_3, f_3 \geq 0, |f_4| \leq \gamma$$

$$B_{c_i} = \begin{bmatrix} 1 & 0 & 0 & 0 \\ 0 & 1 & 0 & 0 \\ 0 & 0 & 1 & 0 \\ 0 & 0 & 0 & 0 \\ 0 & 0 & 0 & 0 \\ 0 & 0 & 0 & 1 \end{bmatrix}$$

where μ is the coefficient of friction, and γ is the coefficient of torsional friction.

The individual finger Jacobians are combined, together with the change of reference frame and taking into account the contact relationships, to form the hand Jacobian J_h :

$$J_h(\theta, x_0)\dot{\theta} = \dot{x}_c$$

where \dot{x}_c is the velocity at the contact points. The effect of the contact

forces on the object are determined by the grasp map G

$$F_o = Gf_c$$

where the grasp map takes into account the contact relationships of the fingers, and the change of coordinate system from the contacts to the object. The forces applied by all the fingers are then summed to give the force applied on the object, F_o .

The grasp Jacobian consists of the combination of the hand Jacobian and the grasp map. The hand Jacobian transforms the joint angles (torques) to the contact velocities (forces), while the grasp map transforms the contact velocities (forces) to the object velocities (forces), as applied by the grasp. The definition of the grasp Jacobian is thus

$$G_h = G^{+T} J_h$$

where G^{+T} is the transpose of the generalized inverse of the grasp map.

Ellipsoids The force transmission ellipsoids are a function of the grasp Jacobian, and are defined by

$$F_o^T (G_{h(trans)} G_{h(trans)}^T) F_o \leq 1 \quad (4.3)$$

where F_o are the forces acting on the object. Similarly, the torque transmission ellipsoid is defined by

$$\tau_o^T (G_{h(angular)} G_{h(angular)}^T) \tau_o = 1 \quad (4.4)$$

where τ_o are the torques acting on the object. The direction with maximum velocity transmission ratio will also be the direction with minimum force transmission ratio. This relationship is a result of the conservation of energy - the work performed by the fingers results in the same amount of work performed on the object (excluding friction). These ellipsoids do not describe the actual velocity or force being applied, rather, they represent the velocity

and force production capabilities of the grasp on the object as a function of the hand and finger configuration.

Stiffness A first order model of stiffness was used here (i.e., damping and inertia terms were not considered), as was applied by Kao et al. (1997) and Milner & Franklin (1998) for measuring the finger's stiffness. Initially, the two dimensional stiffness matrix for each fingertip in the plane containing the major axes of the proximal, medial and distal phalanges was derived. The total displacement vector at the end of the 300ms of force application was used. The direction of the applied force was assumed to be perpendicular to the major axis of the distal phalange and in the plane described above. The parameters of the stiffness matrix K were found by minimizing the error in the overdetermined equation

$$F = Kx \quad (4.5)$$

under the condition that K is symmetric and positive definite. This was implemented using the Optimization toolbox of Matlab.

In order to determine the three dimensional stiffness matrix for each finger, the unmeasured abduction stiffness was estimated. It was assumed that there is a linear relationship between applied force and stiffness, as observed in Hajian & Howe (1997). Based on Tables 1 and 2 from the aforementioned paper, the extension and abduction stiffness were estimated to be

$$K_{ext} = a_{ext}F_{ext} + c_{ext}$$

$$K_{abd} = a_{abd}F_{abd} + c_{abd}$$

$$a_{ext} = 40.9m^{-1}$$

$$c_{ext} = 92.5N/m$$

$$a_{abd} = 49.5m^{-1}$$

$$c_{abd} = 126.0N/m$$

where F_{ext} and F_{abd} are the applied extension and abduction forces, and K_{ext} and K_{abd} are the extension and abduction Cartesian stiffness. Two stiffness ellipsoids were generated for each fingertip. The first uses the assumption

that no force was applied in the abduction direction, hence the abduction stiffness is 126.0 N/m . The second assumes that the maximal abduction force is applied. The maximum abduction force that can be applied without slipping can be calculated using the contact relationship, which is dependent on the coefficient of friction. It is assumed here that the coefficient of friction for all objects is $\mu = 0.45$, based on the reported skin - polythene coefficient of friction (from Figure 2a in Comaish & Bottoms (1971)). This value was used as an approximation to the glove-object coefficient of friction, for which no data were available. The maximum abduction force that can be applied is then $F_{abd} = \mu F_{ext}$, under the assumption that the extension force is applied in the normal direction. Hence the maximal abduction stiffness using the above equations is

$$K_{abd} = \mu \frac{a_{abd}}{a_{ext}} (K_{ext} - c_{ext}) + c_{abd} \quad (4.6)$$

The assumption that the extension force is in the direction of the normal force is clearly violated in two cases: for the middle finger while stirring with the spoon, and for the last finger (ring or little finger, depending on the subject) while unscrewing the jar. In these cases, the normal force is in the abduction direction, and so the maximum abduction force will instead be $F_{abd} = \frac{F_{ext}}{\mu}$. Hence in these cases the maximum abduction stiffness was estimated as

$$K_{abd} = \frac{a_{abd}}{\mu a_{ext}} (K_{ext} - c_{ext}) + c_{abd} \quad (4.7)$$

In order to combine the fingertip stiffness matrices to form the grasp stiffness matrix, the contact relationship must be taken into consideration. The stiffness matrices of all the fingers can be combined to give K_c , which is the stiffness at the contacts. This is achieved by a change of coordinate system to the fingertip (the contact), by T_{C_i} :

$$K_c = \begin{bmatrix} T_{C_1}^{-1} K_1 T_{C_1} & & \\ & \ddots & \\ & & T_{C_5}^{-1} K_5 T_{C_5} \end{bmatrix}$$

This relates movements of the contacts to the force at the contacts. The relationship to the force on the object can then be written using the grasp map

$$F_o = GK_c(X - X_0)$$

where X is the location of the contacts. However, what is wanted is the stiffness relationship between the movement and resultant force of the object. This can be achieved by expressing the relationship in terms of the object location:

$$F_o = GK_cG^T(x_o - x_{o0})$$

and hence the grasp stiffness can be written as

$$K_o = GK_cG^T$$

The object grasp stiffness matrix K_o is a 6×6 matrix. The upper left quadrant of this matrix represents the relationship between the translational forces and translational motion. This quadrant has been visualized as the translational stiffness ellipsoid. Similarly, the bottom right quadrant of the grasp stiffness matrix represents the relationship between angular motion and torques. This quadrant has been visualized as the rotational stiffness ellipsoid. The stiffness ellipsoids are visualized from the quadrant of the matrix by multiplying a hypothetical rotating input displacement (Mussa-Ivaldi et al., 1985):

$$K_o \begin{bmatrix} \cos(t_1) \sin(t_2) \\ \sin(t_1) \sin(t_2) \\ \cos(t_2) \end{bmatrix} \quad 0 < t_1 < 2\pi, 0 < t_2 < \pi$$

Task compatibility and mean ellipsoids The task compatibility index defined by Chiu (1988) was computed for generating velocities and torques along the axes of the coordinate system. This is the square of the distance from the center of the ellipsoid to the surface in the desired direction. For

forces / torques, the task compatibility index C is defined by

$$C = \frac{1}{u^T(G_h G_h^T)u} \quad (4.8)$$

and for velocities by

$$C = \frac{1}{u^T(G_h G_h^T)^{-1}u} \quad (4.9)$$

where u is the desired force or velocity direction (in this case, along the coordinate axes).

The “mean” ellipsoids for each quantity and task of each subject were determined by taking the mean of the directions of the major axes, and the mean of the shape parameters. Ellipsoids with major axis directions that were more than two standard deviations away from the mean direction (in spherical coordinates), or shape parameters more than two standard deviations from the mean shape parameters were not used in computation of the mean ellipsoid. The same procedure was used for finding the mean ellipsoids across subjects.

4.3 Results

Six of the grasps where patterns could be clearly observed are described in this section in detail. Results were omitted for the narrow jar and puzzle piece.

The fingertip positions on the objects for these grasps for all subjects are presented in Figure 4.2. The color of the line represents the finger used, and the location of the line on the circle represents the position of the fingertip on the surface of the object (projected onto the horizontal (XZ) plane). As can be observed from this figure, for each type of manipulation, the subjects selected different postures, including when the same object was manipulated as part of different tasks. Differences were observed in the number of fingers used in the grasp (for example, when lifting the lid, the number of fingers used ranged between 3 and 5) and in the placement of the fingers (for example, significant variation was seen in the thumb position). Variation was often

seen in the consecutive repetitions by the same subject, although this usually involved the same rotation of all the fingers relative to the object. The contact between the fingertips and the object was generally on the inner side of the finger, apart for unscrewing the lids and stirring the spoon, where the side of one finger was used.

The calculated fingertip stiffness matrices have diagonal elements ranging from approximately 50 N/m to 1000 N/m (see Equation (4.5)). These values are of a similar range to those observed in Kao et al. (1997) and Milner & Franklin (1998).

Qualitatively, observations on the grasp features were made based on the shape and orientation of the mean ellipsoids, represented by the parameters of the ellipsoids. The mean ellipsoids are presented graphically, in Figures 4.3 and 4.4, and their parameters are presented in Tables 4.2 and 4.3. An approximate wire-frame rendering of the object is superimposed on the graphs of the ellipsoids to aid in the analysis. The orientation of the ellipsoid (defined by the azimuth, elevation and torsion parameters) determines the directions in which object velocity or force can be most efficiently actuated (for velocity and force ellipsoids respectively), or the direction of maximum stiffness (for the stiffness ellipsoid). The shape parameters determine the isotropy of velocity or force production (for the velocity or force ellipsoids), or stiffness. If in some direction, a large velocity can be generated on the object by the grasping fingers (with a unit joint velocity vector magnitude), in this direction the force that can be generated (with a unit joint torque vector magnitude) will be small. This is due to the principle of virtual work.

The log of the values of the compatibility index for all subjects for six grasps are plotted for force and velocity production (Figure 4.5) and for stiffness (Figure 4.6), along the x (left-right), y (vertical) and z (front-back) axes. The compatibility measures were calculated only along these axes because of their connection to axes of movement and force production involved in the manipulation tasks. Significant differences in the compatibility measure at the $p < 0.1$ and $p < 0.05$ levels between different tasks being performed on the same object are marked in the figures by (*) and (**) respectively. The comparison was performed using the Wilcoxon signed rank test (Gib-

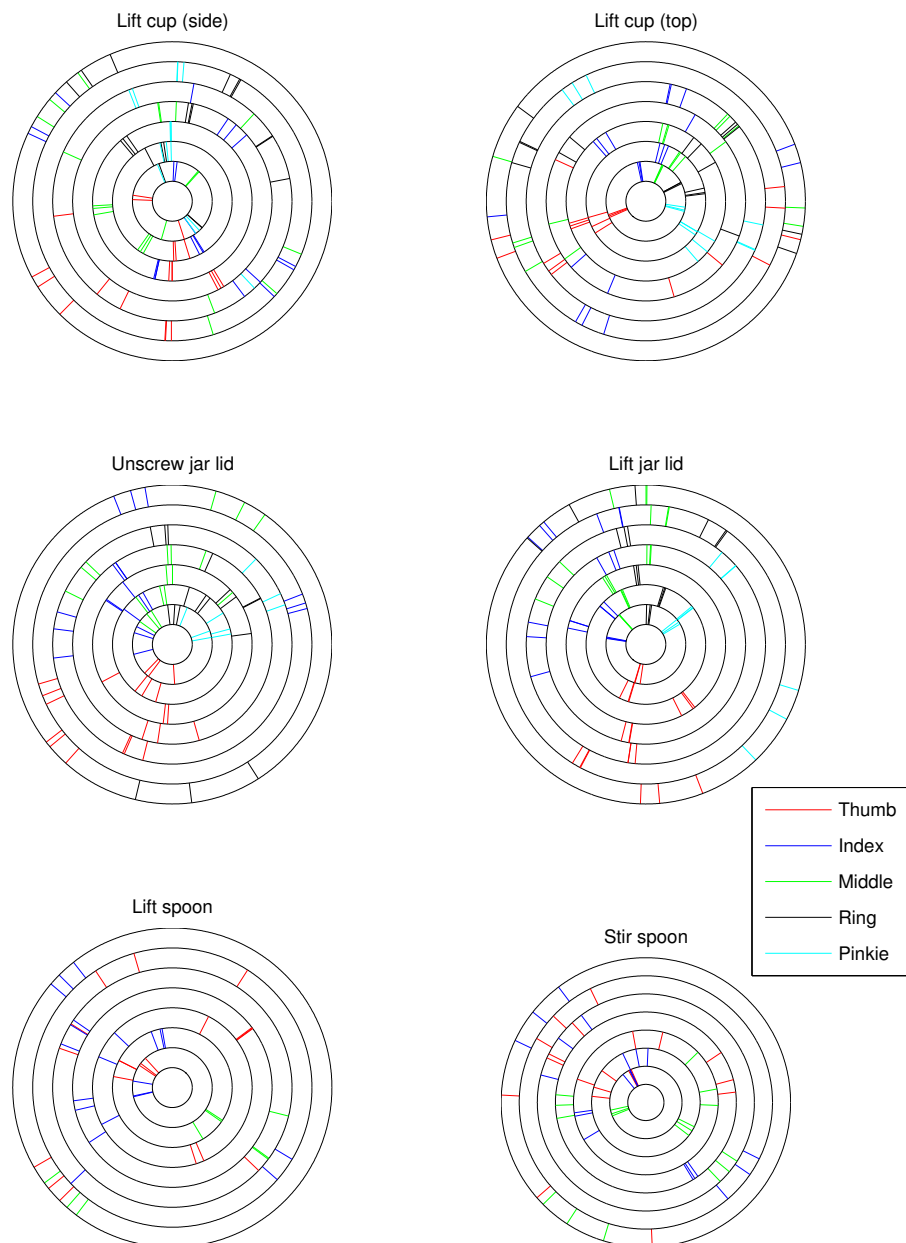


Figure 4.2: Locations of the fingertips on the object for six tasks in the horizontal (XZ) plane. Each concentric circle represents a single subject. The position of a line represents the placement of the appropriate fingertip on the circumference of the object. Only fingers that participated in the grasp are plotted.

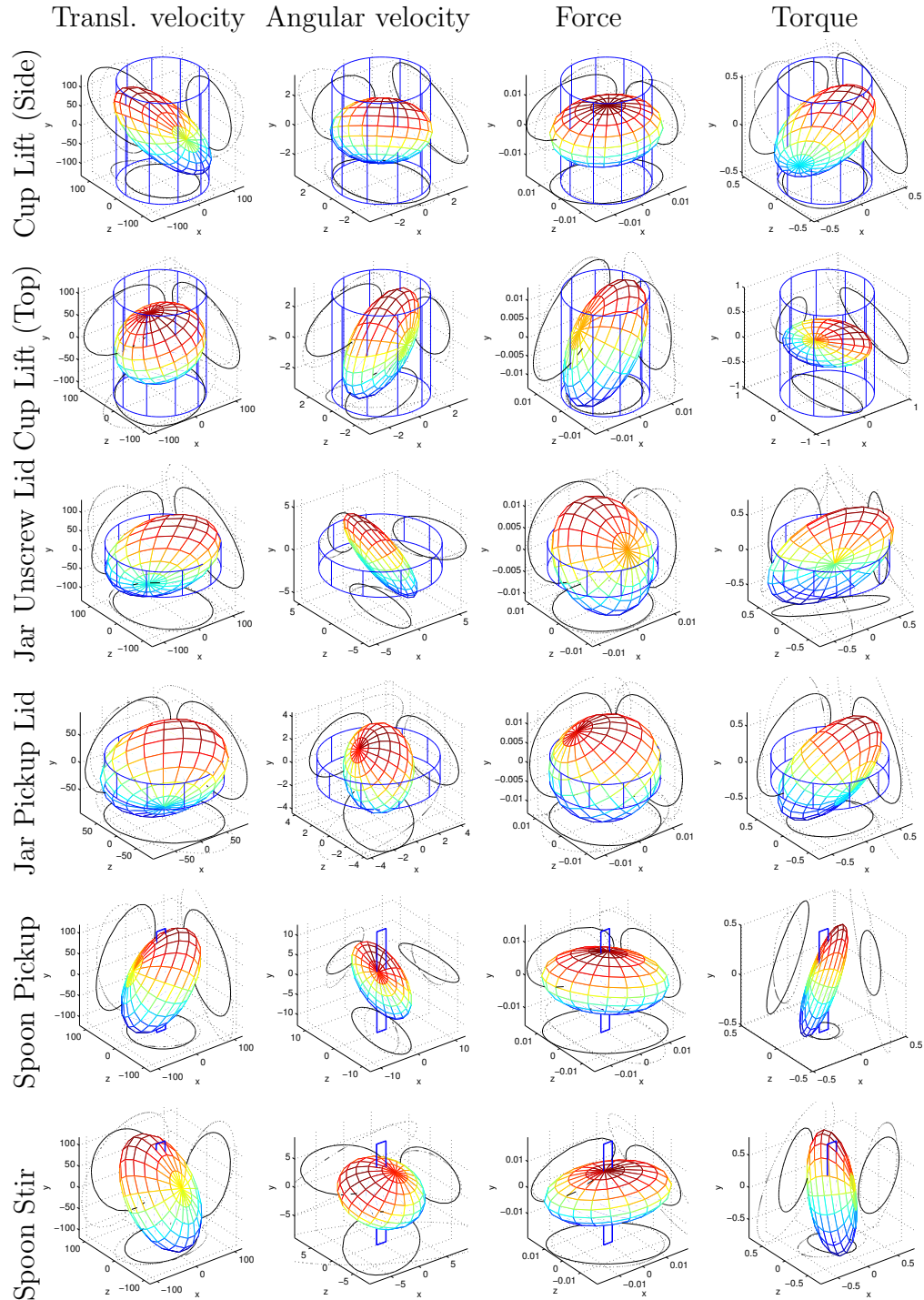


Figure 4.3: Mean translational velocity, angular velocity, translational force and torque ellipsoids for lifting the cup from the side (1st row) and from the top (2nd row), unscrewing (3rd row) and lifting (4th row) the lid of a jar, and lifting (5th row) and stirring with (6th row) a spoon over the seven subjects. The solid and dashed black lines are the projections of the mean and the mean plus one standard deviation respectively onto the XY, YZ and XZ planes. A wire-frame not-to-scale rendering of the object is superimposed on the graphs. The distance from the center of the ellipsoid to the surface in a certain direction is the amount of velocity (force) that can be produced as a result of a joint velocity (torque) vector with unit magnitude.

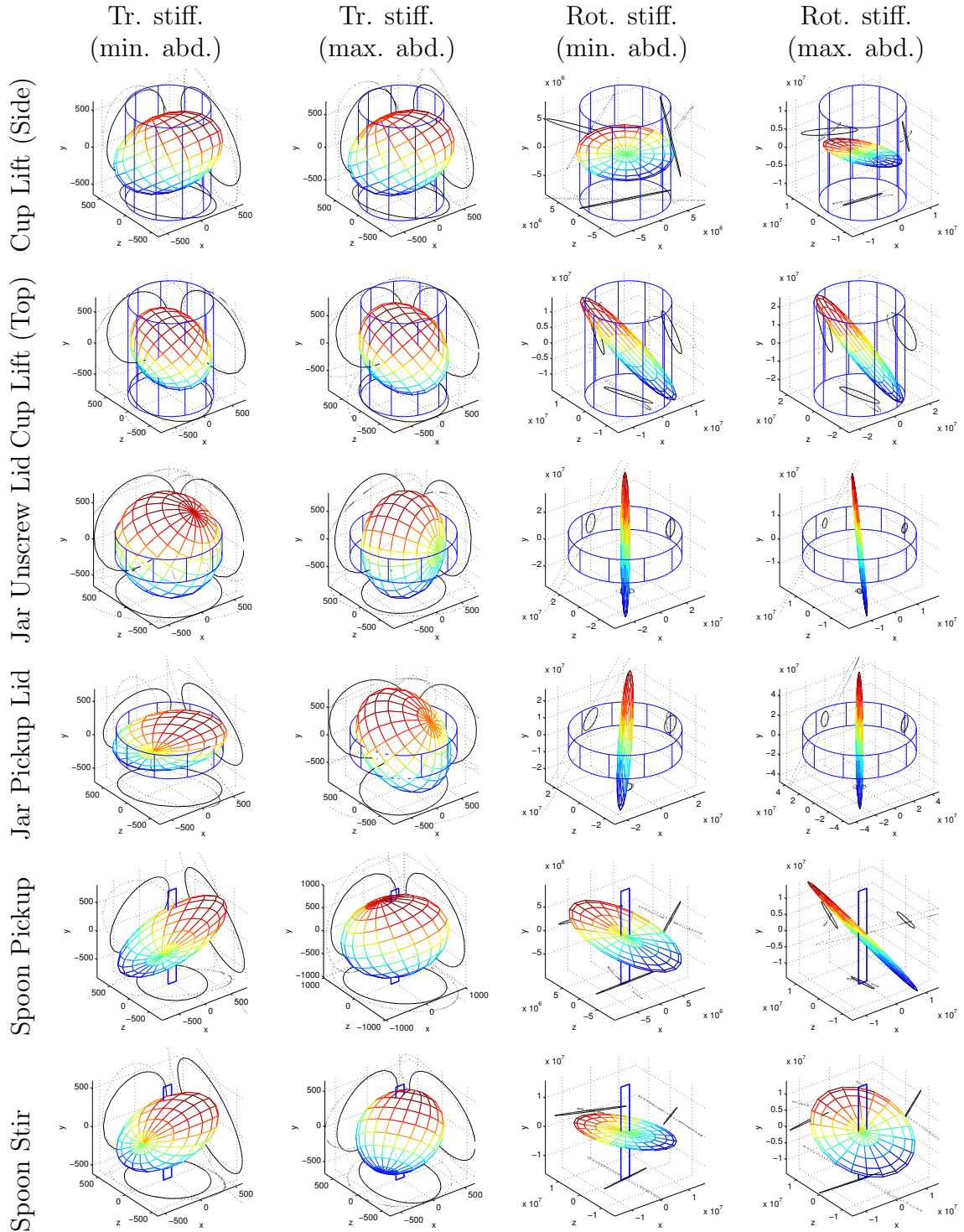


Figure 4.4: Mean translational stiffness under the assumption of minimum (first column) and maximum (second column) abduction stiffness, and mean rotational stiffness for minimum (third column) and maximum (fourth column) abduction stiffness. The rows represent the same objects as in Figure 4.3. The stiffness ellipsoids represent the relative stiffness of the grasp in different directions.

	Azimuth (rad)	Elevation (rad)	Torsion (rad)	Volume	Shape 1	Shape 2
<i>Cup lift (side)</i>						
Transl. Vel.	0.15(±0.91)	0.88(±0.15)	-2.88(±0.94)	$3.60(\pm 3.52) \times 10^6$	2.68(±1.21)	1.95(±0.72)
Ang. Vel.	0.16(±1.12)	0.41(±0.30)	-1.08(±0.34)	68.60(±47.88)	0.61(±0.28)	1.17(±1.01)
Transl. Force	-1.30(±0.19)	-0.13(±0.51)	1.56(±0.16)	$8.54(\pm 2.07) \times 10^{-6}$	0.72(±0.72)	1.35(±0.70)
Torque	1.45(±0.39)	-0.71(±0.17)	-0.39(±0.95)	0.39(±0.20)	2.06(±1.56)	1.32(±1.31)
<i>Cup lift (top)</i>						
Transl. Vel.	-0.92(±0.73)	0.15(±0.39)	1.88(±0.15)	$3.37(\pm 0.75) \times 10^6$	1.43(±0.53)	1.94(±0.89)
Ang. Vel.	-0.51(±1.02)	-0.38(±0.19)	0.22(±1.34)	43.89(±22.02)	2.28(±1.53)	2.53(±0.76)
Transl. Force	-0.14(±0.97)	-0.90(±0.14)	1.90(±0.15)	$5.03(\pm 1.99) \times 10^{-6}$	1.83(±0.46)	1.91(±0.90)
Torque	1.43(±0.33)	-0.31(±0.11)	-2.63(±1.55)	0.56(±0.41)	2.56(±1.15)	3.59(±2.52)
<i>Jar Unscrew Lid</i>						
Transl. Vel.	1.12(±0.82)	-0.51(±0.27)	-0.26(±0.81)	$5.36(\pm 4.30) \times 10^6$	1.88(±0.54)	1.53(±0.19)
Ang. Vel.	-1.49(±0.29)	-0.28(±0.19)	-2.77(±1.51)	104.59(±134.49)	2.59(±1.23)	3.66(±1.56)
Transl. Force	1.10(±0.76)	1.00(±0.18)	1.21(±0.47)	$5.22(\pm 2.05) \times 10^{-6}$	1.17(±0.44)	1.34(±0.91)
Torque	0.44(±1.03)	-0.56(±0.10)	3.07(±0.87)	0.39(±0.29)	1.49(±0.33)	4.69(±4.01)
<i>Jar Lift Lid</i>						
Transl. Vel.	-2.28(±0.62)	0.44(±0.19)	0.43(±1.12)	$2.36(\pm 1.00) \times 10^6$	1.56(±0.44)	1.35(±0.57)
Ang. Vel.	-0.99(±0.64)	-0.06(±0.17)	-0.88(±0.55)	124.69(±131.51)	1.90(±0.91)	2.23(±1.10)
Transl. Force	-0.70(±0.86)	-0.24(±0.38)	-1.01(±0.33)	$8.56(\pm 5.92) \times 10^{-6}$	0.87(±0.41)	1.00(±0.63)
Torque	0.67(±0.74)	-0.90(±0.22)	2.29(±0.58)	0.65(±0.91)	1.76(±0.79)	2.03(±1.21)
<i>Spoon Pickup</i>						
Transl. Vel.	0.75(±0.91)	-1.11(±0.08)	-1.82(±0.73)	$2.77(\pm 0.89) \times 10^6$	1.74(±0.38)	1.98(±0.73)
Ang. Vel.	-1.26(±0.40)	-0.16(±0.31)	-1.24(±0.61)	758.19(±778.05)	2.73(±1.60)	5.04(±3.39)
Transl. Force	0.61(±1.01)	0.10(±0.29)	-1.42(±0.38)	$7.33(\pm 1.94) \times 10^{-6}$	1.42(±0.40)	2.05(±0.93)
Torque	0.10(±1.20)	-1.21(±0.05)	-1.26(±0.64)	0.04(±0.05)	3.72(±1.95)	4.22(±2.09)
<i>Spoon Stir</i>						
Transl. Vel.	1.11(±1.19)	1.08(±0.09)	1.43(±0.73)	$2.84(\pm 2.43) \times 10^6$	1.52(±0.39)	2.21(±0.87)
Ang. Vel.	-0.65(±1.05)	0.23(±0.38)	1.08(±0.17)	$1.15(\pm 0.94) \times 10^3$	1.64(±1.14)	2.67(±2.77)
Transl. Force	0.59(±0.60)	-0.12(±0.29)	-1.65(±0.21)	$1.11(\pm 0.75) \times 10^{-5}$	1.57(±0.30)	2.44(±1.09)
Torque	1.93(±0.70)	1.14(±0.04)	-0.73(±1.54)	0.28(±0.64)	3.71(±1.56)	2.56(±0.86)

Table 4.2: Ellipsoid parameters for the mean (across subjects) velocity and force ellipsoids. The orientations azimuth, elevation and torsion (in radians) define the direction in which force or velocity can be most efficiently effected, and the shape parameters (volume, shape1 and shape2) define the magnitude and degree of isotropy of velocity or force production. Units of volume for translational velocity, angular velocity, translational stiffness and angular stiffness are m^3s^{-3} , rad^3s^{-3} , N^3 and N^3m^3 respectively.

bons, 1971) on the values of the compatibility index. When a compatibility measure is consistently higher for one task compared to a second task being performed on the same object, this invariance may represent a task-related property of the grasp (for example, torque production about the vertical axis) that the CNS is trying to optimize.

4.3.1 Cup

A plastic cup, shaped like a truncated elliptical cone, was picked up with two different grasps, from the side (task 1) and from the top (task 2). In

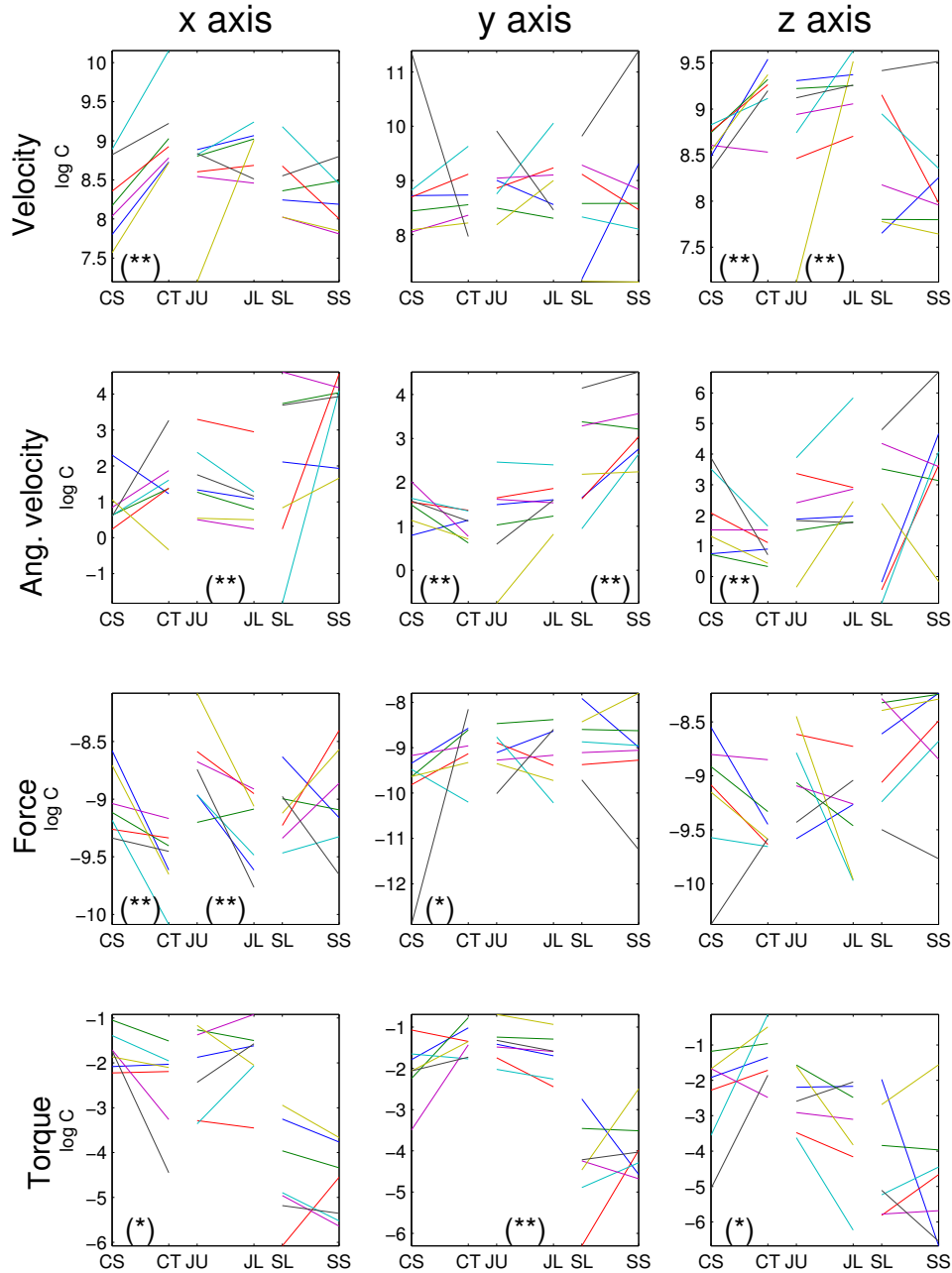


Figure 4.5: Kinematic task compatibility indices. The task compatibility indices for translational velocity (first row), angular velocity (second row), translational force (third row) and torque (fourth row) along the x (first column), y (second column) and z (third column) directions, for lifting the cup from the side (CS) and top (CT), unscrewing (JU) and lifting (JL) the lid of the jar, and lifting (SL) and stirring (SS) with the spoon. Log scales are used on the graphs. Lines join different actions on the same object. (*) and (**) represent significantly different values at $p < 0.1$ and $p < 0.05$ levels on the Wilcoxon signed rank test between the two actions performed on the object.

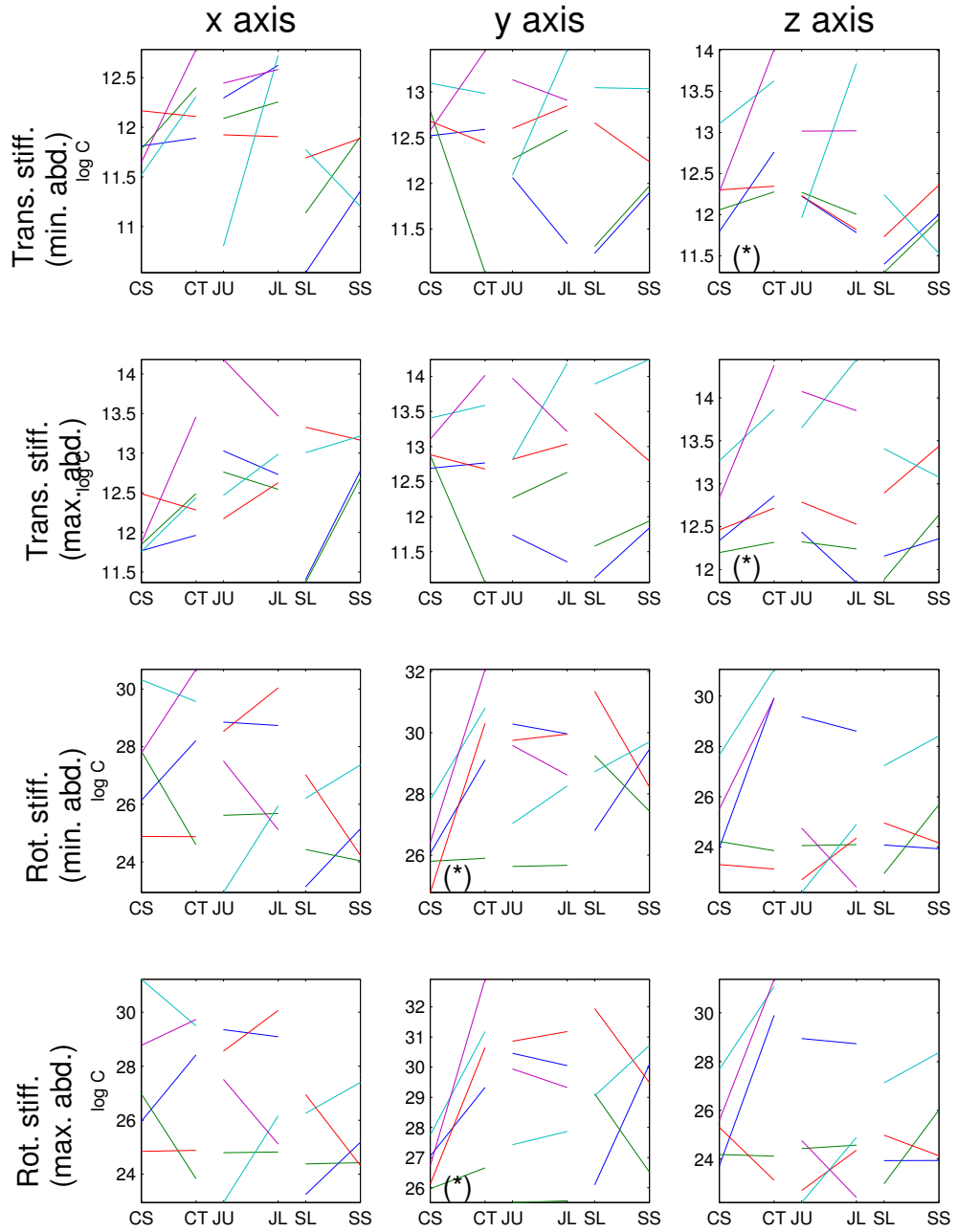


Figure 4.6: Stiffness task compatibility indices. The format of the graphs are the same as in Figure 4.5.

	Azimuth (rad)	Elevation (rad)	Torsion (rad)	Volume	Shape 1	Shape 2
<i>Cup lift (side)</i>						
Tr. stiff. (*)	1.08(±1.08)	-0.60(±0.35)	1.78(±0.55)	$5.65(\pm 1.60) \times 10^8$	1.97(±0.83)	1.70(±0.46)
Tr. stiff. (+)	1.13(±1.15)	-0.63(±0.35)	1.62(±0.47)	$8.50(\pm 3.17) \times 10^8$	1.97(±0.82)	1.59(±0.67)
Rot. stiff. (*)	-0.06(±0.99)	0.65(±0.23)	-0.49(±1.03)	$4.39(\pm 4.35) \times 10^{19}$	1.68(±0.95)	49.93(±50.20)
Rot. stiff. (+)	-0.14(±0.74)	0.57(±0.28)	2.72(±1.16)	$6.52(\pm 6.77) \times 10^{19}$	4.69(±7.08)	49.53(±45.39)
<i>Cup lift (top)</i>						
Tr. stiff. (*)	-1.26(±0.57)	0.17(±0.41)	0.61(±1.24)	$9.73(\pm 9.40) \times 10^8$	1.30(±0.62)	1.52(±0.42)
Tr. stiff. (+)	-1.26(±0.52)	0.11(±0.31)	0.61(±1.17)	$1.82(\pm 2.01) \times 10^9$	1.14(±0.49)	1.35(±0.72)
Rot. stiff. (*)	0.92(±0.83)	0.83(±0.21)	1.15(±0.72)	$4.69(\pm 6.10) \times 10^{20}$	22.03(±27.75)	3.05(±4.14)
Rot. stiff. (+)	1.05(±0.80)	0.88(±0.28)	1.17(±0.69)	$2.93(\pm 5.54) \times 10^{21}$	14.53(±29.18)	3.39(±4.74)
<i>Jar Unscrew Lid</i>						
Tr. stiff. (*)	-0.25(±0.91)	0.18(±0.35)	1.03(±0.37)	$1.09(\pm 1.05) \times 10^9$	0.96(±0.56)	1.03(±0.86)
Tr. stiff. (+)	-0.30(±1.09)	0.34(±0.32)	0.11(±0.88)	$1.63(\pm 1.10) \times 10^9$	0.83(±0.29)	1.12(±0.91)
Rot. stiff. (*)	-0.92(±0.98)	-0.80(±0.14)	-1.49(±0.69)	$2.55(\pm 5.56) \times 10^{21}$	17.88(±28.12)	10.28(±18.08)
Rot. stiff. (+)	-1.05(±1.07)	-0.82(±0.17)	-1.53(±0.64)	$1.26(\pm 1.09) \times 10^{20}$	32.93(±52.68)	19.85(±23.08)
<i>Jar Lift Lid</i>						
Tr. stiff. (*)	1.01(±0.51)	-0.33(±0.38)	-2.94(±0.95)	$6.43(\pm 3.97) \times 10^8$	2.14(±1.49)	1.56(±0.55)
Tr. stiff. (+)	-0.37(±1.15)	0.33(±0.28)	0.78(±0.79)	$1.97(\pm 2.35) \times 10^9$	1.02(±0.16)	1.54(±0.77)
Rot. stiff. (*)	-0.82(±0.86)	-0.85(±0.11)	-1.11(±0.72)	$1.58(\pm 3.35) \times 10^{21}$	11.47(±14.80)	11.24(±20.56)
Rot. stiff. (+)	-0.92(±0.82)	-0.88(±0.11)	-1.36(±0.66)	$3.59(\pm 7.71) \times 10^{21}$	21.99(±29.30)	12.20(±22.02)
<i>Spoon Pickup</i>						
Tr. stiff. (*)	1.06(±0.10)	-0.72(±0.08)	3.00(±0.85)	$1.02(\pm 1.16) \times 10^9$	2.83(±2.23)	2.13(±0.12)
Tr. stiff. (+)	1.00(±0.24)	-0.41(±0.21)	-1.56(±0.09)	$2.88(\pm 4.70) \times 10^9$	1.54(±0.68)	1.50(±0.52)
Rot. stiff. (*)	0.38(±0.78)	0.63(±0.26)	-2.50(±1.41)	$3.98(\pm 5.43) \times 10^{19}$	2.59(±4.06)	78.93(±70.94)
Rot. stiff. (+)	0.95(±0.61)	0.76(±0.20)	2.44(±1.40)	$1.13(\pm 1.93) \times 10^{20}$	5.93(±10.63)	56.40(±42.25)
<i>Spoon Stir</i>						
Tr. stiff. (*)	1.26(±0.07)	-0.71(±0.05)	-3.01(±0.85)	$5.33(\pm 4.99) \times 10^8$	2.04(±0.87)	1.75(±0.35)
Tr. stiff. (+)	1.47(±0.02)	-0.38(±0.11)	-0.79(±0.70)	$6.27(\pm 4.65) \times 10^8$	1.75(±0.58)	1.26(±0.19)
Rot. stiff. (*)	0.18(±1.11)	0.43(±0.31)	0.69(±1.34)	$5.38(\pm 6.07) \times 10^{19}$	3.64(±2.99)	122.79(±85.09)
Rot. stiff. (+)	0.44(±0.69)	0.55(±0.34)	-2.49(±1.42)	$1.30(\pm 1.96) \times 10^{20}$	1.41(±0.98)	94.85(±65.35)

Table 4.3: Ellipsoid parameters for the stiffness ellipsoids. Interpretation of the parameters is the same as Table 4.2. (*) indicates the minimum abduction stiffness assumption was used, (+) indicates that the maximum abduction stiffness assumption was used.

both cases, only the fingertips contacted the object, and not the palm. The movements involved lifting the cup vertically (along the positive y direction), generally with negligible rotation.

Lifting a cup primarily requires movement of the arm rather than the fingers. Hence, the role of the grasp is to stabilize the object and prevent undesirable movement. Lifting from the side generally involved placing the thumb on one side, and the other fingers close together (see Figure 4.2, top left). When lifting from the top, the subjects spread their fingers around the rim of the cup, although not uniformly. The values of the task compatibility indices in Figure 4.5 indicate that the two postures have different interaction capabilities with the object.

Lifting from the side has translational velocity compatibility indices in the

x (left-right) and z (front-back) directions significantly smaller than those for lifting from the top (Figure 4.5, top row). A significantly larger compatibility index is also observed in the x direction for the force variable for lifting from the side rather than from the top (Figure 4.5, third row). These results mean that when lifting from the side, larger forces can be produced in this direction.

Seemingly contradictory results are observed when considering the stiffness, where lifting from the top has a significantly higher translational stiffness compatibility index than lifting from the side in the z direction and generally higher translational stiffness although not statistically significant in the x direction. The explanation for this can be found in the fact that the grasp stiffness measures the response of the grasp to applied forces as a result of the elastic properties of the muscles, tendons and joints, rather than the ability of the grasp to actively generate forces.

In terms of angular velocities, lifting from the top has a significantly smaller task compatibility index for angular velocity in the y and z directions than for lifting from the side, meaning that the velocity can be better controlled in these directions. Additionally, the rotational stiffness compatibility index in the y direction for both types of estimation of the abduction stiffness are considerably higher for lifting from the top. Thus, lifting from the top is able to better actively control angular velocities about the y axis and additionally passively respond to external disturbances about this axis. It appears that the choice of grasping from the side or top should depend on whether translational or rotational disturbances are more likely.

The rotational stiffness ellipsoids were highly anisotropic, long and thin, with low stiffness in the z direction for lifting from the side and in the x direction for lifting from the top (see Figure 4.4, first two rows, third and fourth columns). The direction of the major axis was roughly perpendicular to the direction of the *opposition axis*, defined here as the line connecting the thumb and the average of the other fingers positions. The rotational stiffness ellipsoids were similar for both cases of abduction stiffness.

4.3.2 Wide jar

Two grasps were performed on the wide jar - unscrewing the lid (task number 3), and lifting the lid after it was already unscrewed (task number 4). It was observed that unscrewing the lid involves primarily an anti-clockwise rotation about the y axis. Lifting the lid, in contrast, involves a translation in the positive y direction, with negligible rotation.

For lifting the lid, the subjects generally placed their thumbs on the side of the object closest to their chest and the other fingers on the other side of the object, relatively close to each other with even spacing between the fingers. When unscrewing the same lid, the thumb was rotated clockwise, and the last finger used in the grasp was placed such that the contact with the object was with the side of the finger.

In order to unscrew the lid, it is necessary to apply a torque about the y axis. Although the difference in the orientation of the torque ellipsoids for unscrewing and lifting the lids is small, the task compatibility index for applying a torque in the y axis is significantly larger for the unscrewing task than for the lifting task ($p < 0.05$).

The difference in torque production capabilities of the two grasps is due to the different finger placement. The placement of the last finger used in the grasp such that it contacts the object with the side of the finger allows rotation of the object by this finger by the extension of three joints (metacarpophalangeal, proximal and distal interphalangeal) rather than only by the abduction of the metacarpophalangeal joint. In addition, the rotation of the thumb clockwise on the object moves it closer to its limit such that it can rotate the lid over a larger angle.

The clear difference in task compatibility observed for torque production in the y direction is not observed for translational velocity or force production in this direction. Varied results were observed regarding the grasp for which the velocity in the vertical (y) direction can be most efficiently produced.

The translational stiffness ellipsoids observed differ between the two tasks. When unscrewing the lid (task number 3) the stiffness ellipsoids are fairly isotropic, while the stiffness ellipsoids are “flatter” for lifting the lid, with

greater stiffness in the horizontal (x and z) directions. These stiffness values are large in a direction perpendicular to the velocity involved in lifting, which is along the vertical (y) direction.

The mean rotational stiffness ellipsoid has greater stiffness in the vertical (y) direction for both types of grasp, which would appear to be counterproductive for torque production about this axis. However, large amounts of variation were observed in the rotational stiffness for this task.

4.3.3 Spoon

Two different types of manipulation were performed with the spoon - lifting the spoon (task number 5), and stirring with the spoon (task number 6). Whereas the task of lifting the spoon vertically (in the y direction) is primarily performed by the arm, stirring the spoon (generally about the vertical (y) axis) was performed by movements of the fingers.

For lifting the spoon, subjects used two or three fingers. Large amounts of variation were observed in the placement of the fingers on the spoon. All subjects apart from one (who used two fingers) used three fingers for stirring with the spoon. Generally, the spoon was grasped with the side of the middle finger. Stirring with the spoon was significantly better for applying an angular velocity, about the vertical (y) axis than for lifting the spoon. It should be noted that this is different from the unscrewing of the lid where a preference was observed for applying torque about the y axis. In contrast, the best grip for applying an angular velocity along the x and z axes varied greatly between subjects.

Stiffness ellipsoids were not constructed for one subject due to insufficient movement of the fingers resulting from the force application. The translational stiffness ellipsoids for stirring and lifting the spoon were fairly isotropic, although the volume of the translational stiffness ellipsoid for lifting the spoon was much larger than that for stirring with the spoon although two fingers were generally used for picking up the spoon as opposed to three for stirring with it. This finding reflects the different task requirements of the grasps, because for lifting the spoon the grasp is required only to hold

securely the object while lifting is performed by the arm.

4.3.4 General discussion

A large amount of variance was observed in the postures selected across subjects for the same type of manipulation. Nevertheless, similarities have been observed when comparing the force or velocity production capabilities, and stiffness properties, between different types of manipulations on the same object.

Throughout this section, the grasps have been analyzed in the frame of reference of the object. Various works in robotics (for example, Mason (1981) and de Schutter & van Brussel (1988)) have proposed planning control of a robotic manipulator by specifying the task constraints in terms of the task frame. However, it is difficult to know what constraints need to be specified for a given task. For example, it is not intuitively clear whether it is more desirable to be able to generate a high angular velocity or torque in order to unscrew a lid. In this work, the goal is the inverse of that in robotics studies - to determine which characteristics humans give to grasps in order to perform different tasks.

The use of the velocity and force ellipsoids to measure task compatibility for generating optimum grasps for robotic manipulators was proposed by Chiu (1988). Buttolo (1996) compared the stiffness of different pen grasps by comparing the stiffness ellipsoids of the grasp. He found that different three fingered grasps gave similar stiffness ellipsoids, which were more suitable for fine control than using a single finger because of larger stiffness values.

For all of the tasks, a large amount of variation in finger placement on the objects was observed. The velocity and force transmission ellipsoids are a function of the hand posture, and so the variation in finger placement caused significant variations in the resulting velocity and force transmission ellipsoids. The grasp stiffness, as visualized by the stiffness ellipsoids is also dependent on the hand posture (as well as the finger stiffnesses). Thus, some of the variation in the stiffness ellipsoids was probably due to variations in the posture. However, despite these significant variations, patterns were observed

in the compatibility of the grasps for controlling or effecting force and velocity in salient task directions. For example, a larger torque can be produced about the vertical (y) axis for unscrewing the lid of the jar rather than for lifting the lid. Based on this and similar findings, it appears that for the same object, different preferred directions of velocity and force production were selected depending on the task being performed. This is important to note, because it implies that grasp planning cannot be performed based purely on the geometry of the object but rather must take into account the desired manipulation.

Greater variance was observed in the task compatibility measures between subjects for some of the parameters where there was no obvious connection between the parameter and the task. This suggests that control or actuation of force or velocity in these directions is less important for a successful completion of the task.

For the rotational stiffness, the major axis of the stiffness ellipsoid was often perpendicular to the opposition axis (the line connecting the thumb and the average of the other finger positions). This may be a result of forces being applied parallel to this axis to hold the object stably.

The translational stiffness ellipsoids under the assumption of maximum abduction stiffness have a larger volume than the stiffness ellipsoids under the assumption of minimum abduction stiffness for the same task. This is because the finger stiffness ellipsoids under the assumption of maximum abduction will have a larger volume, and the grasp stiffness ellipsoids are the result of the summation of the finger stiffness ellipsoids (after rotation into the appropriate frame of reference).

It appears that the stiffness may be selected by making the grasp compliant (i.e., low stiffness) in the directions in which forces or movement are to be applied, and stiff in the directions in which movement is not desired (Cutkosky, 1985). Using more fingers in a grasp will generally increase the stiffness. Although the net force on the object will be zero when the object is not moving (so that the object is in equilibrium), in spite of the “canceling out” of the applied forces, the stiffness of the fingers sum.

Throughout the measurements performed in this section, the subjects

wore the CyberGlove. While the inner surface of the glove, where the hand is in contact with the object is relatively thin, it is expected that wearing the glove will change in a small way the grasping behavior observed. The glove also restricts slightly the range of movement of the fingers. Despite these differences, the subjects easily performed successfully the tasks, and thus we expect that the differences in grasping when wearing the glove compared to grasping without the glove will be small, and will not affect adversely the overall patterns of behavior.

In the construction of the grasp stiffness ellipsoid, it was assumed that the fingers are not coupled. However, some of the muscles serve all fingers (Li et al., 2002; Leijnse, 1997). Hence, it is expected that there will be some coupling between the fingers. The magnitude of the coupling should be determined through further experiments.

4.4 Optimal grasp selection

In the previous section, the grasps that were selected for different tasks on the same object were compared. Different values for the task compatibility index were observed between the tasks for force or torque generation in directions related to the task. For example, when unscrewing a lid, a larger torque could be applied about the y axis than when lifting the lid. These differences in capabilities are due to the different postures of the hand. This naturally raises the question of which posture should be selected to be able to produce the *largest* torque, and whether the grasps we select are optimal in this sense. This section examines the broader question of what, if anything, is being optimized when we perform grasping. The candidates for quantities that are being optimized that are considered here are the force and velocity transmission capabilities, and stiffness, as described in the previous section.

4.4.1 Methods

In order to determine the optimality of the grasps subjects selected during the experiment, these grasps were compared to a large number of computer generated grasps. The comparison was in terms of the velocity and force compatibility measures, and their stiffness.

For each object that was used in the experiment, grasps were generated with the same number of grasping fingers as the subject used in the experiment (from two to five fingers). Ten joint angles uniformly dividing the joint ranges the subjects used across all movements were selected for each joint. It should be noted that the joint ranges varied between fingers, and did not in general agree with standard tables of joint ranges (such as those found in Norkin & White (1985)).

It was assumed that the ratio between the proximal interphalangeal joint (PIJ) and the distal interphalangeal joint (DIJ) is constant, based on findings that there is a linear linkage between these joints (Hahn et al., 1995). The ratio used was the average of the ratio between these joints observed in the data, which was generally close to the value published in the aforementioned work (0.76). All possible combinations of the joint angles spanning the range

were then considered for the entire finger (i.e., for the thumb 10^4 postures were considered, for the other fingers 10^3 postures). For grasps involving more than 3 fingers, the palm arch (see Figure A.1) was also allowed to vary (over 5 different values). A sample of the postures for the index finger is shown in Figure 4.7. Thus the number of possible grasps for 2, 3, 4 and 5 fingered grasps is 10^7 , 10^{10} , 5×10^{13} and 5×10^{16} respectively.

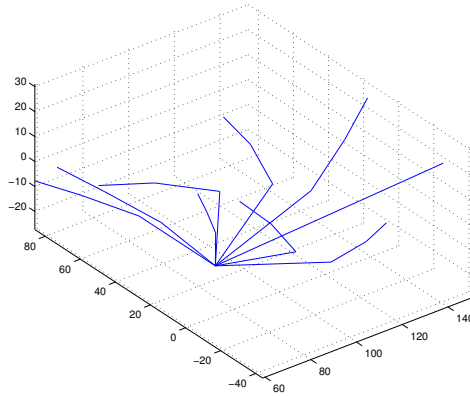


Figure 4.7: A sample of the postures considered for the index finger in the optimization. In total, 1000 postures were generated for the index finger.

Generating such a large number of grasps would take a long time, so a Monte Carlo method was used instead. A grasp was constructed by first randomly selecting a thumb and index posture. At this point, several tests for the feasibility of the grasp were performed. The relevant tests were performed as soon as possible, so that infeasible grasps could be quickly discarded. The tests performed at this point checked that the fingers did not cross over, and that the distance between the thumb and index fingers was not so large that grasping the object would be impossible. If the grasp passed these tests, additional fingers were added, with the posture of the next finger selected randomly, until the number of fingers equaled the number used in the experiment. For all of the grasps except for lifting the cup from the side, the fingertips of the subjects were all approximately in the horizontal plane. Based on this, only postures where the fingertips were in a plane were considered. Lifting the cup from the side was not included in this analysis. After the addition of each finger, similar feasibility tests were applied.



Figure 4.8: Two rendered views of a feasible grasp, showing a wire-frame hand grasping a cylindrical shaped object. A large number of such feasible grasps were generated.

After all the fingers were added, the best fit of the fingertips to the circumference of a disc (or the edges of a rectangle), whose dimensions were the same as the objects used in the experiment (from Table 4.2) was calculated. The grasp was considered feasible only if the distance of all fingers to the surface of the disc / rectangle was less than 1cm. Additionally, it was required that the fingers contact the object with the fingertips (and not the back of the finger), and that all the fingers not be on one side of the object. This last requirement is necessary so that a stable, force closure grasp will be possible. An example of a feasible grasp is shown in Figure 4.8.

For the feasible grasps, the wrist orientation was selected such that the disc (or rectangular prism) was parallel to the horizontal plane, as was the case in the experiment. This was repeated until either 100,000 candidate grasps were constructed, or a total of 1000 feasible grasps were generated. This number of grasps was considered enough to sample sufficiently the space of possible grasps on the object.

For each generated grasp, the grasp Jacobian was calculated and from this, the task compatibility measures were calculated for force, torque, velocity and angular velocity generation along the x , y and z axes. The grasp stiffness was modeled using the technique described in Section 3.2. The magnitudes of translational and rotational stiffnesses along the Cartesian axes were calculated. In order to compare between the different measures, which have

different units, the *normalized compatibility measure* was defined, calculated as the fraction of computer generated grasps that have smaller compatibility measures than the experimental compatibility measure, on the same object, with the same hand geometry and number of fingers. Thus, all normalized compatibility measures lie between 0 and 1. If a normalized compatibility measure is close to 1, this means that the experimentally selected grasp was close to optimal for this particular measure.

4.4.2 Results and Discussion

The task compatibility scores of the computer generated grasps are compared to the results from the experiments for Subject 3 in Figures 4.9 and 4.10. These graphs show the values of relevant compatibility measures, selected based on the conclusions in the previous section. The sorted compatibility measures for the computer generated grasps are shown as the continuous blue lines. The compatibility measures for the experimentally recorded grasps are shown as the stars, and they have been plotted at the same horizontal location as the computer generated grasp with the closest compatibility score. Hence if a star appears at a high value, this means that this grasp is close to optimal in terms of this particular quantity. Figure 4.9 shows these results for the force/velocity compatibility, while Figure 4.10 shows the results for the stiffness measures.

As can be observed in these figures, a large range of compatibility measures can be obtained by selecting different grasps on the same object. Most of the graphs have a similar shape - roughly linear for most of the range, with sharp increases at low and high values.

For example, for lifting the lid of the jar, and lifting the lid of the narrow bottle, the grasps selected by the subject were close to optimal for applying velocity in the direction of the task (vertical y), as seen in the second and third graphs in the right column in Figure 4.9. In contrast, for unscrewing the lid of the jar (second graph on the left column), the unscrewing action, although able to produce more torque than for the lifting grasp, is suboptimal. However for this same task, the stiffness in the x direction (second

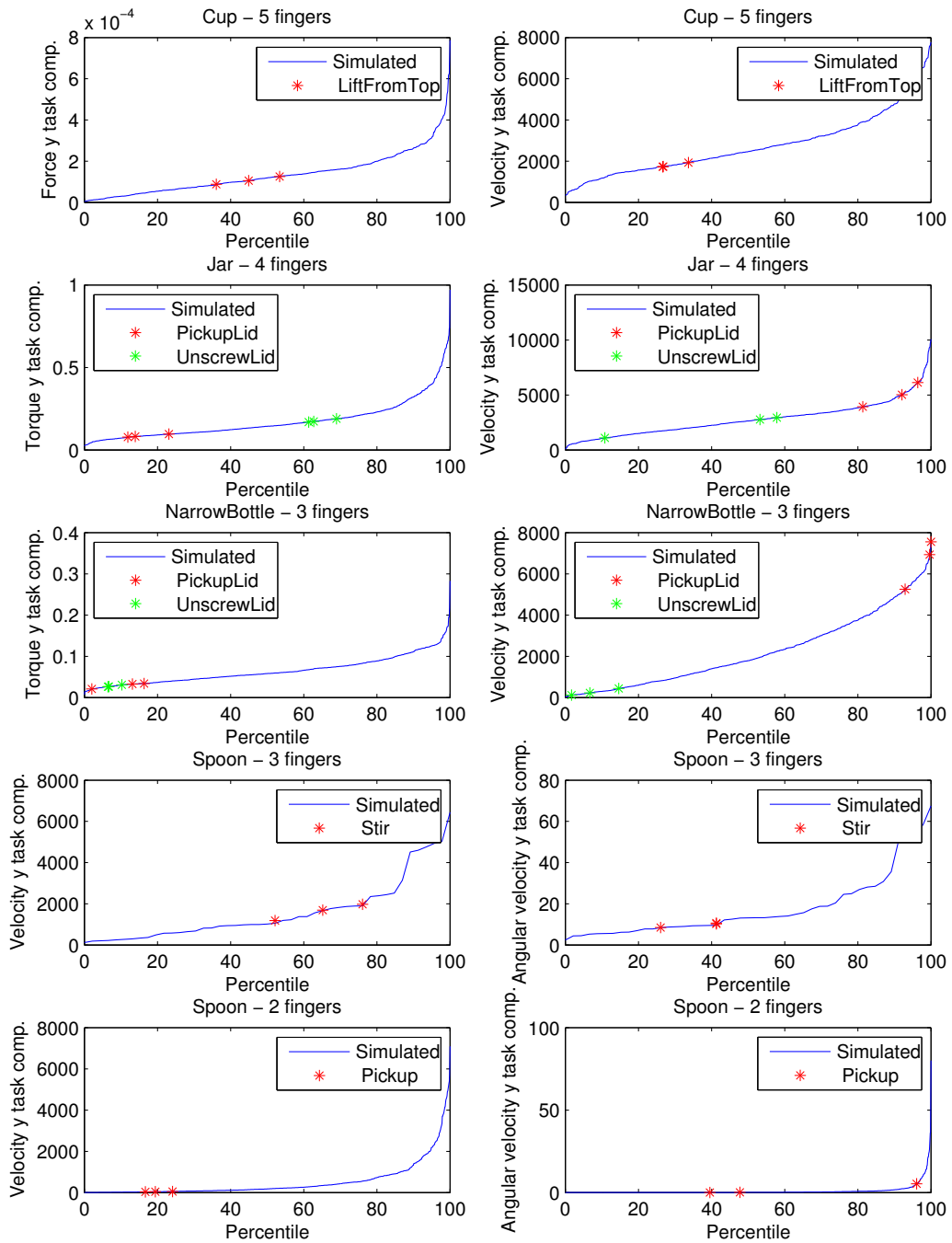


Figure 4.9: Task compatibility measures for Subject 3, for relevant compatibility measures. The continuous blue line is the sorted task compatibility measures of the computer generated grasps. The stars represent the grasps selected by the subjects.

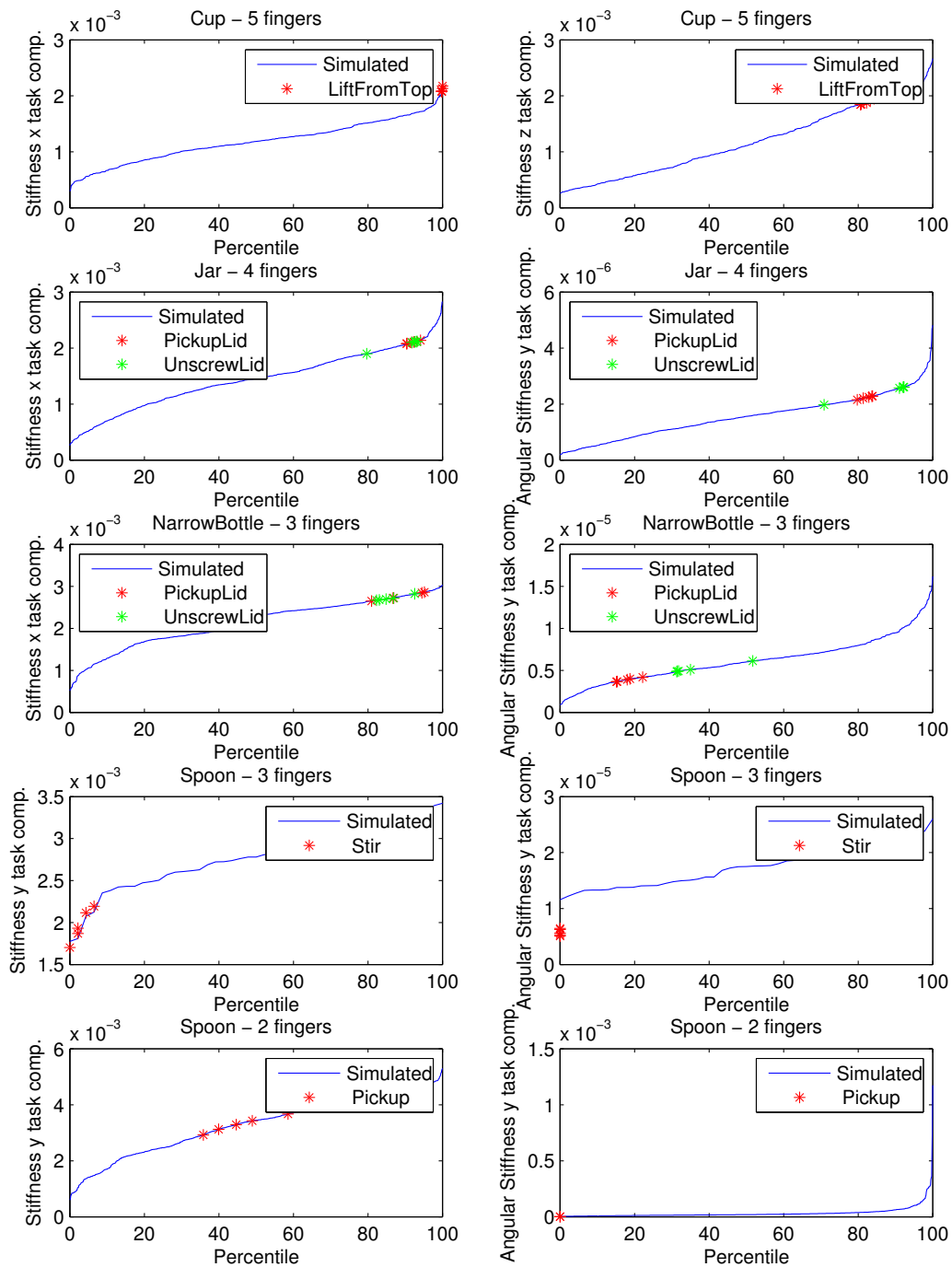


Figure 4.10: Task compatibility measures for Subject 3, for relevant stiffness compatibility measures. The continuous blue line is the sorted task compatibility measures of the computer generated grasps. The stars represent the grasps selected by the subjects.

graph on the left column in Figure 4.10) is close to optimal. The compatibility measures of these two quantities for the computer generated graphs, and the experimentally selected grasps, are shown in Figure 4.11.

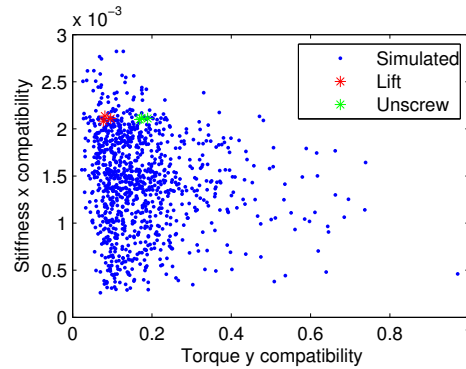


Figure 4.11: The trade-off between stiffness in the x direction, and torque production about the y axis. Each blue point represents one sample from the simulation. The points with high torque production ability have low stiffness. The stiffness / torque production ability selected by the subject had high stiffness.

In this figure, it can be seen that there are relatively few postures that have high torque production ability, and those that do, also have lower stiffness in the horizontal (x) direction. The grasps with the highest stiffness in the x direction have the lowest values for torque production. Thus, a trade-off must be made between the two. In this case, it appears that the subjects chose to optimize stiffness in the x direction (which was observed in Figure 4.10 to be close to optimal), rather than torque production ability about the y axis. It is possible that a task which requires a larger amount of torque would have caused the subjects to sacrifice stiffness in the x direction in order to have the ability to produce a larger torque in the required direction.

Mason (1981); de Schutter & van Brussel (1988) specified the task constraints for performing various compliant tasks in terms of forces and velocities, and proposed controllers for implementing these constraints with a robot. The stiffness was selected while constructing the controller, rather than as a specific task requirement. For example, in the task described above,

it may have been that the requirement was that there be zero force in the horizontal direction (so as not to interfere with the task), and this constraint can be realized by requiring high stiffness in the x direction.

Based on one subject, it is difficult to determine what is actually being optimized, because although a particular measure may be optimal, it may be that the CNS is actually trying to optimize some other measure and the optimality observed is simply a consequence of this. One way to partially overcome this problem is to study many objects, and many subjects. If the same patterns are observed across subjects and objects, this strengthens the claim that such measures are being optimized and reduces the probability that the findings are a consequence of optimization of some other quantity. While we only have data from a relatively small number of objects, the pooled data from six subjects can give a better basis for analysis.

This analysis is performed by looking at the normalized compatibility measures. If the pooled (for all subjects and repetitions) normalized compatibility measures for a given task on an object show a mean value significantly different from 0.5, this suggests that this quantity may be optimized (maximized if the value is greater than 0.5, or minimized if the value is less than 0.5). This analysis was performed on all the compatibility measures along the 3 coordinate axes. Tables 4.4 and 4.5 show the mean and standard deviation of the normalized compatibility measures for the eight tasks for the kinematic and stiffness measures respectively.

The values are colored in red if the mean of the normalized compatibility measure is significantly greater than 0.5, and colored in blue if the normalized compatibility measure is less than 0.5. This test is performed using a Student's t -test, with significance at the 0.05 level.

It is immediately apparent from Table 4.5 that the rotational stiffness is low (mean of less than 0.5) for nearly all the tasks. In order to have high rotational stiffness, the fingers need to be spread out around the circumference of the object, something which was not generally done. Rather, the fingers used were generally placed opposite the thumb. This finding suggests that, at least for the tasks selected, having high rotational stiffness is not required, or on the contrary, the grasps may have been selected to be highly

Grasp	τ_x	τ_y	τ_z	f_x	f_y	f_z
Cup Lift From Top	0.59 ± 0.31	0.38 ± 0.32	0.97 ± 0.08	0.11 ± 0.11	0.66 ± 0.27	0.33 ± 0.28
Jar Pickup Lid	0.77 ± 0.37	0.43 ± 0.18	0.53 ± 0.40	0.24 ± 0.25	0.48 ± 0.32	0.25 ± 0.29
Jar Unscrew Lid	0.60 ± 0.25	0.75 ± 0.19	0.75 ± 0.22	0.67 ± 0.29	0.55 ± 0.24	0.46 ± 0.31
Bottle Pickup Lid	0.58 ± 0.35	0.65 ± 0.36	0.37 ± 0.21	0.75 ± 0.28	0.24 ± 0.22	0.36 ± 0.22
Bottle Unscrew Lid	0.44 ± 0.24	0.50 ± 0.42	0.58 ± 0.19	0.80 ± 0.34	0.44 ± 0.32	0.36 ± 0.23
Puzzle Piece Pickup	0.60 ± 0.26	0.70 ± 0.23	0.51 ± 0.31	0.31 ± 0.41	0.33 ± 0.28	0.19 ± 0.21
Spoon Pickup	0.33 ± 0.38	0.23 ± 0.23	0.29 ± 0.30	0.25 ± 0.14	0.34 ± 0.27	0.38 ± 0.25
Spoon Stir	0.70 ± 0.19	0.36 ± 0.23	0.44 ± 0.35	0.40 ± 0.35	0.34 ± 0.29	0.40 ± 0.28
Grasp	v_x	v_y	v_z	ω_x	ω_y	ω_z
Cup Lift From Top	0.55 ± 0.35	0.13 ± 0.16	0.73 ± 0.26	0.35 ± 0.31	0.57 ± 0.25	0.03 ± 0.08
Jar Pickup Lid	0.22 ± 0.25	0.48 ± 0.23	0.73 ± 0.31	0.13 ± 0.14	0.56 ± 0.35	0.31 ± 0.26
Jar Unscrew Lid	0.10 ± 0.15	0.50 ± 0.18	0.57 ± 0.26	0.39 ± 0.27	0.50 ± 0.35	0.25 ± 0.24
Bottle Pickup Lid	0.02 ± 0.06	0.69 ± 0.14	0.55 ± 0.09	0.25 ± 0.40	0.22 ± 0.40	0.49 ± 0.28
Bottle Unscrew Lid	0.01 ± 0.04	0.45 ± 0.24	0.39 ± 0.24	0.34 ± 0.27	0.38 ± 0.41	0.28 ± 0.19
Puzzle Piece Pickup	0.02 ± 0.04	0.67 ± 0.30	0.46 ± 0.17	0.28 ± 0.30	0.22 ± 0.23	0.38 ± 0.34
Spoon Pickup	0.42 ± 0.10	0.49 ± 0.19	0.61 ± 0.32	0.45 ± 0.28	0.38 ± 0.34	0.20 ± 0.17
Spoon Stir	0.44 ± 0.32	0.63 ± 0.10	0.35 ± 0.22	0.40 ± 0.32	0.29 ± 0.29	0.53 ± 0.34

Table 4.4: The mean and standard deviation of the normalized compatibility measures (torque τ , force f , velocity v and angular velocity ω about the x , y and z axes), pooled across the six subjects for the eight tasks. Those shown in red have a mean which is significantly greater than 0.5, those in blue have a mean significantly less than 0.5, according to a t-test.

Grasp	<i>Minimum abduction stiffness assumption:</i>					
	k_x	k_y	k_z	kr_x	kr_y	kr_z
Cup Lift From Top	0.67 ± 0.38	0.49 ± 0.28	0.45 ± 0.25	0.29 ± 0.30	0.17 ± 0.28	0.20 ± 0.26
Jar Pickup Lid	0.45 ± 0.32	0.77 ± 0.17	0.56 ± 0.24	0.48 ± 0.23	0.29 ± 0.29	0.28 ± 0.26
Jar Unscrew Lid	0.45 ± 0.29	0.56 ± 0.29	0.43 ± 0.28	0.33 ± 0.28	0.21 ± 0.31	0.18 ± 0.26
Bottle Pickup Lid	0.24 ± 0.33	0.55 ± 0.12	0.34 ± 0.24	0.38 ± 0.27	0.32 ± 0.29	0.27 ± 0.15
Bottle Unscrew Lid	0.34 ± 0.34	0.60 ± 0.27	0.44 ± 0.24	0.21 ± 0.18	0.21 ± 0.21	0.15 ± 0.14
Puzzle Piece Pickup	0.45 ± 0.30	0.38 ± 0.35	0.26 ± 0.22	0.03 ± 0.06	0.00 ± 0.00	0.00 ± 0.00
Spoon Pickup	0.25 ± 0.26	0.20 ± 0.27	0.44 ± 0.40	0.00 ± 0.00	0.00 ± 0.00	0.00 ± 0.00
Spoon Stir	0.37 ± 0.45	0.26 ± 0.39	0.25 ± 0.27	0.01 ± 0.02	0.03 ± 0.10	0.16 ± 0.37

Grasp	<i>Maximum abduction stiffness assumption:</i>					
	k_x	k_y	k_z	kr_x	kr_y	kr_z
Cup Lift From Top	0.56 ± 0.40	0.42 ± 0.28	0.28 ± 0.26	0.28 ± 0.29	0.12 ± 0.26	0.17 ± 0.25
Jar Pickup Lid	0.32 ± 0.30	0.64 ± 0.20	0.40 ± 0.32	0.34 ± 0.14	0.17 ± 0.29	0.22 ± 0.24
Jar Unscrew Lid	0.21 ± 0.23	0.44 ± 0.33	0.27 ± 0.27	0.23 ± 0.25	0.13 ± 0.29	0.16 ± 0.26
Bottle Pickup Lid	0.13 ± 0.26	0.41 ± 0.15	0.22 ± 0.24	0.25 ± 0.21	0.18 ± 0.17	0.23 ± 0.13
Bottle Unscrew Lid	0.17 ± 0.23	0.45 ± 0.18	0.29 ± 0.22	0.14 ± 0.17	0.12 ± 0.18	0.13 ± 0.13
Puzzle Piece Pickup	0.09 ± 0.16	0.32 ± 0.33	0.15 ± 0.14	0.02 ± 0.03	0.00 ± 0.00	0.00 ± 0.00
Spoon Pickup	0.19 ± 0.24	0.15 ± 0.21	0.30 ± 0.31	0.00 ± 0.00	0.00 ± 0.00	0.00 ± 0.00
Spoon Stir	0.00 ± 0.01	0.20 ± 0.28	0.13 ± 0.18	0.00 ± 0.00	0.01 ± 0.05	0.15 ± 0.34

Table 4.5: The mean and standard deviation of the normalized stiffness compatibility measures (translational stiffness k and rotational stiffness kr about the x , y and z axes), calculated across the six subjects for the eight tasks. The top table is with the minimum abduction stiffness assumption, the lower table with the maximum abduction stiffness assumption (see page 52). Those shown in red have a mean which is significantly greater than 0.5, those in blue have a mean significantly less than 0.5, according to a t-test.

rotationally compliant (the opposite of stiffness).

For some of the tasks, the compatibility measures being optimized are similar to the findings described in the previous section, and can be related to salient task-related properties. However, it should be noted that this is a different type of analysis. Whereas in the previous section, two different grasps on the same object were compared, here each grasp individually is compared with an approximation to the space of all possible grasps on the object.

For example, for unscrewing the jar, the ability to produce torque about the y axis has a mean value significantly greater than 0.5, which suggests that the grasps are chosen to be able to produce torque in this direction to succeed in the unscrewing task.

For lifting the lid of the bottle, and lifting the puzzle piece, the mean velocity in the vertical y direction is significantly greater than 0.5. This may be related to the requirements of the task, that is, to lift the object vertically.

In terms of the stiffness, for the spoon the mean of the normalized stiffness values in the y direction is significantly lower than 0.5.

For many of the other values which are significantly different from 0.5, there is not a clear connection between the value and the task being performed. For other tasks, there is a large amount of variance between subjects which resulted in no measures being different from 0.5. It is also possible, due to the symmetry of the objects, that the different strategies used by different subjects caused the large amount of variation observed.

In conclusion, this technique shows promise for determining the potential quantities being optimized during grasp selection. In order to make more decisive statements about what is being optimized during grasping, it would be necessary to study a larger range of objects with similar task requirements, and to then observe the common patterns in terms of the compatibility scores across the same tasks on different objects.

Chapter 5

Trajectories of the fingers

Nomenclature

θ	Joint angles of the finger.	t_f	Time at conclusion of movement.
$\dot{\theta}$	Joint velocities of the finger.	$\phi_k^{(m)}$	Basis functions.
τ	Joint torques of the finger.	λ	Arbitrary parameter.
r	Fingertip radius from knuckle.	s	Arc length along the fingertip path.
θ_r	Fingertip angles from knuckle.	$M(\theta)$	Manipulator inertia matrix.
C_E	Kinetic energy-like cost.	$C_{k,m}$	Normalization factor for Jacobi polynomial.
C_T	Minimum torque-change cost.	$P_k^{(2m,2m)}$	Jacobi polynomial.
t	Time.	$RMSE$	Root mean square error.
t_0	Time at start of movement.		

t_n	Normalized time (normalized by the duration of the movement).
k	Ratio of widths of successive whorls in a logarithmic spiral.
z	Complex number representation of the fingertip location.
l_i	Length of the i th link of the finger.
θ_{MPJ}	Extension / flexion of the metacarpophalangeal joint.
θ_{PIJ}	Extension / flexion of the proximal interphalangeal joint.
θ_{DIJ}	Extension / flexion of the distal interphalangeal joint.
a	Logarithmic spiral parameter that determines its size.
b	Logarithmic spiral parameter that determines its growth rate.
E_{xy}	RMSE of the fingertip position with respect to the arc length.
E_{vel}	RMSE of the fingertip velocity with respect to time.
$E_{posture}$	RMSE of the joint angles with respect to time.

5.1 Introduction

This section examines the trajectory of the index finger during grasping movements, in particular, which endpoint paths and joint angle trajectories are used during these movements. Different models from the literature, in addition to some novel models, are compared for their ability to describe the observed experimental data.

The study of grasping movements in humans has been mostly addressed from the perspective of reach-to-grasp movements, which have been considered as consisting of two independent components (Jeannerod, 1981), one for bringing the hand to the location of the object, and the other for shaping the hand for the grasp. The focus of this section is on the component responsible for shaping the fingers during the grasp.

There have been relatively few studies looking at the trajectories of the fingertips during grasping. In the model of Rosenbaum et al. (2001), where the final grasping posture is selected based on stored postures, the velocity profiles of all the joints are set to have bell shaped velocity profiles from their current value, through a via point, to the predetermined goal values. In contrast, the model of Smeets & Brenner (1999) suggested that it is the grasping fingers that move to the object in extrinsic space, and in their model,

the movement of the fingertips were modeled by minimum jerk trajectories in Cartesian space (rather than joint space).

An alternate approach to studying the trajectories of finger movements during grasping has been to use dimensionality reduction techniques. These techniques use a number of repetitions of different tasks to specify prototypical trajectories of the fingers during such tasks, which can be linearly combined in various combinations. Mason et al. (2001) used singular value decomposition (SVD) to approximate the 3D position of 21 markers on the hand at 180 time samples while grasping a variety of objects. They showed that the trajectory can be reconstructed well using a small number of eigenpostures (97.3% of the variance described for the first set of eigenpostures, and 1.9% for the second set). Similarly, Santello et al. (2002) demonstrated that using principal component analysis on 15 joint angles at 120 time samples, the first two principal components can describe 75% of the variance of the movement. The first principal component consisted of the fingers simultaneously extending together to a maximum opening, then flexing together to close in on the object. However, the eigenpostures generated by these techniques are dependent on the types of tasks used to generate them, and so may not be generalizable, and they do not offer an explanation for the underlying principle that produced these particular trajectories.

5.1.1 Logarithmic spirals for describing finger motion

Littler (1973) noted from observation that the paths taken by the fingertips approximately follow a logarithmic (sometimes called equiangular) spiral, although he did not provide experimental proof of this. Gupta et al. (1998) performed measurements of the paths taken by the fingers using a motion capture system and confirmed this finding, although they did not test any alternative parameterizations of the path. Recently, the index finger was measured during grasping, and a logarithmic spiral was found to be a good fit to the fingertip paths (Kamper et al., 2003), and better than the fit of a parabola.



Figure 5.1: An example of a shell, a chambered Nautilus, whose shape corresponds to a logarithmic spiral. Reproduced from Thompson (1992).

The logarithmic spiral was first described by Descartes in 1638 (Thompson, 1992). Jacob Bernoulli also studied the logarithmic spiral in 1691-93, and described several of its properties (Archibald, 1918). It has the feature that the rate of change of the radius of the spiral is proportional to the angular rotation θ_r . As a result of this, the total shape of the spiral remains constant, despite its growth. This implies that the radius r on a given whorl¹ is a constant multiple k of the radius on the previous whorl, i.e.

$$r(\theta_r + 2\pi) = kr(\theta_r), \quad \forall \theta_r \quad (5.1)$$

The equation for a logarithmic spiral can be written in polar coordinates by

$$r = ae^{b\theta_r} \quad (5.2)$$

where the parameters a and b describe the spiral. By substituting Equation (5.2) into Equation (5.1), we get the value k in terms of b

$$k = e^{2\pi b} \quad (5.3)$$

¹A whorl is a single, complete 360° turn in the growth of a spiral (Thompson, 1992).

Thompson (1992) presents many examples of where logarithmic spirals can be observed in nature, such as sea shells (see Figure 5.1), with differing values of k . The ratio will affect how tight the curve is. One particular value of k of interest is that of $\phi = \frac{\sqrt{5}+1}{2} \approx 1.618$, the golden ratio. It has been suggested that the ratios of the segment lengths in the finger follow this ratio (Littler, 1973). Park et al. (2003) attempted to prove this by taking X-rays of 100 hands and measuring the bone lengths. Although their findings did not support this assumption, they suggest that the ratio may hold if instead the length is calculated between the centers of rotation (although this has not been tested). Based on this assumption, Markley (2003) predicted that the logarithmic spiral produced by the motion path of the fingers should have a $k = \phi$, although this has not been experimentally confirmed.

Mathematical representation of the fingertip location The equation of the fingertip can be written using complex numbers, where

$$z = x + iy$$

The location of the fingertip is given by

$$\begin{aligned} x &= l_1 \cos(\theta_{\text{MPJ}}) + l_2 \cos(\theta_{\text{MPJ}} + \theta_{\text{PIJ}}) + l_3 \cos(\theta_{\text{MPJ}} + \theta_{\text{PIJ}} + \theta_{\text{DIJ}}) \\ y &= l_1 \sin(\theta_{\text{MPJ}}) + l_2 \sin(\theta_{\text{MPJ}} + \theta_{\text{PIJ}}) + l_3 \sin(\theta_{\text{MPJ}} + \theta_{\text{PIJ}} + \theta_{\text{DIJ}}) \end{aligned} \quad (5.4)$$

where θ_{MPJ} , θ_{PIJ} and θ_{DIJ} are the metacarpophalangeal joint, proximal interphalangeal joint and distal interphalangeal joint angles of the finger respectively. This can be written compactly as z_{ft}

$$z_{ft} = e^{i\theta_{\text{MPJ}}} [l_1 + e^{i\theta_{\text{PIJ}}} (l_2 + e^{i\theta_{\text{DIJ}}} l_3)] \quad (5.5)$$

The fingertip location corresponding to a logarithmic spiral, z_{ls} is

$$z_{ls} = ae^{(i+b)\theta_r} \quad (5.6)$$

where θ_r is the angle of the fingertip in polar coordinates. If the trajectory

of the fingertip is indeed a logarithmic spiral, then Equations (5.5) and (5.6) should be equivalent, although it is not clear how this can be achieved.

When the long axes of the phalanges of the finger are parallel to the palm, the finger lies along the y axis. In the posture where $\theta_r = \theta_{MPJ} = \theta_{PIJ} = \theta_{DIJ} = 0$, the a value can be determined:

$$a = l_1 + l_2 + l_3 \quad (5.7)$$

The value of θ_r can be calculated as it is the argument of the complex number z_{ft} , which can be determined by $\tan^{-1}\left(\frac{y_{ft}}{x_{ft}}\right)$:

$$\begin{aligned} \theta_r &= \tan^{-1}\left(\frac{y_{ft}}{x_{ft}}\right) \\ &= \tan^{-1}\left(\frac{l_1 \sin(\theta_{MPJ}) + l_2 \sin(\theta_{MPJ} + \theta_{PIJ}) + l_3 \sin(\theta_{MPJ} + \theta_{PIJ} + \theta_{DIJ})}{l_1 \cos(\theta_{MPJ}) + l_2 \cos(\theta_{MPJ} + \theta_{PIJ}) + l_3 \cos(\theta_{MPJ} + \theta_{PIJ} + \theta_{DIJ})}\right) \end{aligned}$$

A first order approximation that will be reasonably close over the range of movement is given by

$$\theta_r \approx \theta_{MPJ} + \frac{l_2 + l_3}{l_1 + l_2 + l_3} \theta_{PIJ} + \frac{l_3}{l_1 + l_2 + l_3} \theta_{DIJ}$$

The distance to the fingertip can be calculated from $r = \sqrt{x_{ft}^2 + y_{ft}^2}$

$$r = \sqrt{l_1^2 + l_2^2 + l_3^2 + 2l_2l_3 \cos(\theta_{DIJ}) + 2l_1l_2 \cos(\theta_{PIJ}) + 2l_1l_3 \cos(\theta_{DIJ} + \theta_{PIJ})}$$

A first order approximation to $b\theta_r$ was then calculated after rearranging Equation (5.2):

$$\begin{aligned} b\theta_r &= \log \frac{r}{a} \\ &\approx -\frac{l_1l_3\theta_{PIJ}\theta_{DIJ}}{(l_1 + l_2 + l_3)^2} \end{aligned}$$

Then b is given by

$$\begin{aligned} b &\approx -\frac{l_1 l_3 \theta_{PIJ} \theta_{DIJ}}{(l_1 + l_2 + l_3)^2} \frac{l_1 + l_2 + l_3}{(l_1 + l_2 + l_3) \theta_{MPJ} + (l_2 + l_3) \theta_{PIJ} + l_3 \theta_{DIJ}} \\ &= -\frac{l_1 l_3 \theta_{PIJ} \theta_{DIJ}}{(l_1 + l_2 + l_3) \theta_{MPJ} + (l_2 + l_3) \theta_{PIJ} + l_3 \theta_{DIJ}} \end{aligned}$$

This allows the relationship between two of the joint angles to be computed if the third (and b is known)

$$\begin{aligned} \theta_{DIJ} &= -\frac{bl_1 \theta_{MPJ} + (l_2 + l_3)(\theta_{MPJ} + \theta_{PIJ})}{l_3(b + l_1 \theta_{PIJ})} \\ \theta_{PIJ} &= -\frac{b(l_3 \theta_{DIJ} + (l_1 + l_2 + l_3) \theta_{MPJ})}{b(l_2 + l_3) + l_1 l_3 \theta_{DIJ}} \\ \theta_{MPJ} &= \frac{bl_3 \theta_{DIJ} + b(l_2 + l_3) \theta_{PIJ} + l_1 l_3 \theta_{DIJ} \theta_{PIJ}}{b(l_1 + l_2 + l_3)} \end{aligned}$$

If, as is often assumed, θ_{DIJ} is linearly related to θ_{PIJ} (Hahn et al., 1995), then (where $\theta_{DIJ} = m\theta_{PIJ}$)

$$\theta_{MPJ} = \frac{b(l_2 + l_3 + l_3 m) \theta_{PIJ} + l_1 l_3 m \theta_{PIJ}^2}{b(l_1 + l_2 + l_3)} \quad (5.8)$$

So if θ_{DIJ} and θ_{PIJ} are linearly related, then θ_{MPJ} and θ_{PIJ} can not be linearly related, if the fingertip follows a logarithmic spiral. Thus it is not theoretically possible for the joint angles to be linearly related (as is the case in the minimum angular jerk model) and for the endpoint path to be a logarithmic spiral.

5.1.2 Prediction of path from minimization of kinetic energy-like function

While the logarithmic spiral trajectory of the fingertip may have some attractive geometric properties, alternative models were considered based on energetic considerations. This was partly motivated by the recent work of Biess et al. (2006a), which models the path of the arm by minimizing a cost function related to the kinetic energy of the movement. Here, a similar procedure

is followed for the finger, and similarly, the path is predicted independently of the velocity profile.

The kinetic energy E_k of a multiple link open-chain manipulator like the finger can be written in terms of the manipulator inertia matrix (Murray et al., 1994):

$$E_k(\theta, \dot{\theta}) = \frac{1}{2} \dot{\theta}^T M(\theta) \dot{\theta}$$

where the 3x3 matrix M is known as the manipulator inertia matrix. The derivation of M for this model of the finger can be found in Equation (3.4). The cost function used here is similar to this, but the parameter is an arbitrary one (λ), rather than time. Thus it is not equivalent to kinetic energy. The definition is given by

$$C_E = \frac{1}{2} \int \dot{\theta}(\lambda)^T M(\theta(\lambda)) \dot{\theta}(\lambda) d\lambda \quad (5.9)$$

5.1.3 Time course of the movements

In Kamper et al. (2003), it was claimed that the path of the fingertip does not follow a minimum jerk solution (Flash & Hogan, 1985), where the integral of the squared sum of the jerk in Cartesian coordinates is minimized. According to the original minimum jerk formulation, this would require the path to be a straight line, which it clearly is not. In the work of Kamper et al. (2003), it was shown that even if the endpoint constraint that the acceleration is zero at the start and end of the movement is removed, the trajectory is still does not minimize the jerk cost.

However, an alternative approach is to consider minimizing jerk on the Euclidean arc length (Biess et al., 2006a), i.e., that the squared arc length jerk cost

$$C = \int_{t=0}^{t_f} \ddot{s}(t)^2 dt \quad (5.10)$$

is minimized. The arc length is the length along the curve, and can be calculated by

$$s = \int \sqrt{x'(\lambda)^2 + y'(\lambda)^2} d\lambda \quad (5.11)$$

5.2 Methods

The experimental data used here was taken from four of the subjects of the grasping experiments described in Chapter 4. During a typical grasping movement, the fingers first open, before closing in on the object (Jeannerod, 1981). The part of the movement that is examined here is from the time of maximum aperture of the fingers to when the fingers grasp the object. The segmentation was performed by selecting the last continuous region before the grasp where all the relevant joint velocities are positive. The movement was considered to have been finished when the mean square velocities of the joints in the finger were below a threshold of $0.10 \text{ rad}^2\text{s}^{-2}$. Only grasping movements which started from rest (at the moment of maximum aperture) were considered.

The lengths and radii of the fingers were measured using calipers. The mass was estimated by assuming that the phalanges are cylinders, with a density of 1200 kg m^{-3} (Dempster, 1955). These data were used in calculating the inertia matrices for the fingers.

If the finger trajectories selected are indeed a result of energetic considerations, then changes in these trajectories should be observed if the inertia of the finger is changed. In order to test this, the experiments were repeated for the four subjects examined with the addition of a weight of 20g to the medial phalange of the index finger. This weight was in the form of a lead spiral, worn symmetrically around the phalange such that the inertia of the phalange would increase in a uniform way in all directions. This weight was much larger than the typical mass of this phalange (around 3g). The lead spiral was sufficiently small that it could be worn inside the CyberGlove and did not adversely affect the movements.

Logarithmic spiral parameters The best fit logarithmic spirals were fit to each movement, which required finding the a and b parameters in Equation 5.2. These values were compared to the values expected from Equation 5.7, and the suggestion in the literature that $k \approx 1.618$.

Time course In order to test how close the arc length trajectories of the movements are to the minimum arc length jerk trajectories, the parameters of a fifth order polynomial were fit to the arc length

$$s(t_n) = s(1) (a_1 t_n^5 + a_2 t_n^4 + a_3 t_n^3), \quad s(0) = 0, \quad t_n = \frac{t - t_0}{t_f - t_0}. \quad (5.12)$$

An ideal minimum jerk trajectory, with initial and final velocity and acceleration of zero will have the parameters (Flash & Hogan, 1985)

$$\begin{aligned} a_1 &= 6 \\ a_2 &= -15 \\ a_3 &= 10 \end{aligned}$$

For comparison, the fit to $\theta_{MPJ}(t)$, $\theta_{PIJ}(t)$ and $\theta_{DIJ}(t)$ are also shown. This is equivalent to selecting a minimum angular jerk trajectory, and is similar to the technique used in Rosenbaum et al. (2001), where they generated movements with bell-shaped angular velocity profiles. In general, the jerk can not be minimized simultaneously for the arc length and the joint angles, due to the non-linear relationship between them.

Models Four different models were compared for predicting the trajectories of the index finger.

For the first two models, the time course was set such that the squared jerk of the Euclidean arc length along the path (Equation (5.10)) was minimized. The optimal arc length jerk trajectory can be written as

$$s(t_n) = s(1)(6t_n^5 - 15t_n^4 + 10t_n^3), s(0) = 0, t_n = \frac{t - t_0}{t_f - t_0}. \quad (5.13)$$

The arc length at each sample point during the modeled movement was calculated using Equation (5.11), and the movement was then resampled so that the arc length jerk would be minimized. The paths of the two models were calculated by

- i. The path was selected to minimize the integral of the weighted squared

joint derivatives along the path (Equation (5.9)).

- ii. The path was selected to be the best fit logarithmic spiral (Equation (5.6)).

For model (i), the joint angles of the metacarpophalangeal (θ_{MPJ}) and proximal interphalangeal (θ_{PIJ}) joints were modeled using Jacobi polynomials (Wada et al., 2001; Biess et al., 2006b). Full details of the technique used can be found in Biess et al. (2006b). Each joint was modeled as a function of a parameter λ (which is a parameter that increases monotonically along the path, but generally is not linearly related to either the arc length or time) by

$$\theta(\lambda) = \theta_0 + (\theta_f - \theta_0)\lambda + \sum_{k=0}^N c_{ik} \phi_k^{(1)}(\lambda), \quad 0 \leq \lambda \leq 1 \quad (5.14)$$

The first two terms here, which describe a straight line from the initial to final joint angle, ensure that the boundary conditions are met. The basis functions are described in terms of Jacobi polynomials. Each basis function satisfies homogeneous boundary conditions. The basis functions, are defined by (Wada et al., 2001; Biess et al., 2006b)

$$\phi_k^{(m)}(\lambda) = C_{k,m} 2^{2m} \lambda^m (1 - \lambda)^m P_k^{(2m, 2m)}(2\lambda - 1) \quad (5.15)$$

where m is the order of the highest derivative in the cost functional, $C_{k,m}$ is a normalization factor, the term $\lambda^m(1 - \lambda)^m$ ensures that the basis function vanishes at the boundary points, and $P_k^{(2m, 2m)}$ is the Jacobi polynomial, defined by

$$P_n^{(\alpha, \beta)}(x) = \frac{1}{2^n} \sum_{k=0}^n \binom{n + \alpha}{k} \binom{n + \beta}{n - k} (x - 1)^{n-k} (x + 1)^k$$

Jacobi polynomials are used because they define a set of orthogonal functions on $[0, 1]$, while satisfying the correct boundary conditions. This means that by using a sufficiently large number of polynomials, any (smooth) trajectory of θ can be captured (in the least squared sense). In practice, the

first three polynomials were used (because the coefficients became very small after this). The value of the cost function was evaluated at 1000 steps of λ .

For model (ii), the best fit logarithmic spiral

$$r = ae^{b\theta}$$

was fit to the trajectory in fingertip space, in a least squares sense. The joint angles that produce this endpoint were uniquely determined, because of the assumption made about the relationship between the proximal and distal interphalangeal joints, and were found by modeling each joint angle as a 5th order polynomial and then selecting the parameters such that the forward kinematics are best satisfied.

The third model used was:

- iii. The minimum torque-change model (Uno et al., 1989), which was used to predict the path and the time course.

For this model, Jacobi polynomials were also used:

$$\theta(t_n) = \theta_0 + (\theta_f - \theta_0) (6t_n^5 - 15t_n^4 + 10t_n^3) + \sum_{k=0}^N c_{ik} \phi_k^{(3)}(t_n), \quad 0 \leq t_n \leq 1 \quad (5.16)$$

In this case, the first two terms describe a polynomial that satisfies the boundary conditions of the minimum torque-change model, namely, that the velocities and accelerations at the start and end are zero, as described in Nakano et al. (1999). For this model, the joint angles are modeled as a function of normalized time $t_n = \frac{t}{t_f}$, because the path and velocity profiles cannot be derived independently as with the previous models. In this case, the Jacobi polynomials are constructed with a basis where $m = 3$, corresponding to an expansion scheme of order $m = 3$.

The cost function used for the minimum torque-change model was

$$C_\tau = \frac{1}{2} \int \left(\frac{d\tau(\theta)}{dt} \right)^T \left(\frac{d\tau(\theta)}{dt} \right) dt \quad (5.17)$$

The torque is calculated using the first two terms (inertia and Coriolis) in

Equation (3.1). The effects of gravity are neglected.

The fourth model was

- iv. The minimum angular jerk model (Okadome & Honda, 1999; Hermens & Gielen, 2004) was used to predict the path and the time course. That is, each joint will have a trajectory determined by Equation (5.13), except the parameter will be the joint angle, rather than the arc length. This implies that there is a linear relationship between the metacarpophalangeal joint and the proximal interphalangeal joint.

This model does not require the use of optimization to determine its trajectory.

For all the models, the distal interphalangeal joint (θ_{DIJ}) was assumed to be determined by the proximal interphalangeal joint, based on the findings of previous papers (Hahn et al., 1995). For each movement, the relationship between θ_{PIJ} and θ_{DIJ} was modeled by a 3rd order polynomial:

$$\theta_{DIJ} = p_1\theta_{PIJ}^3 + p_2\theta_{PIJ}^2 + p_3\theta_{PIJ} + p_4$$

This was used, rather than a linear relationship as was suggested in Hahn et al. (1995), because at the extremes of the joint range, the linear relationship does not hold.

The minimization of the cost functions was performed in Matlab, using the non-linear optimization function in the Optimization toolkit. The torque for all the movements was estimated using the first two terms (inertia and Coriolis) in Equation (3.1). The effects of gravity are not included.

Quality of fit The quality of the predictions was compared by calculating the root mean square error (RMSE) between the predictions and the experimental data for Cartesian (xy) endpoint data E_{xy} with respect to the normalized arc length σ , and for the Cartesian endpoint velocities E_{vel} and

the joint angles $E_{posture}$ with respect to normalized time:

$$\begin{aligned}
 E_{xy} &= \sqrt{\frac{1}{N} \sum_{i=1}^N (x_e(\sigma_i) - x_p(\sigma_i))^2 + (y_e(\sigma_i) - y_p(\sigma_i))^2} \\
 E_{vel} &= \sqrt{\frac{1}{N} \sum_{i=1}^N (\dot{x}_e(t_i) - \dot{x}_p(t_i))^2 + (\dot{y}_e(t_i) - \dot{y}_p(t_i))^2} \\
 E_{\theta} &= \sqrt{\frac{1}{N} \sum_{i=1}^N (\theta_e(t_i) - \theta_p(t_i))^2} \\
 E_{posture} &= E_{\theta_{MPJ}} + E_{\theta_{PIJ}} + E_{\theta_{DIJ}}
 \end{aligned} \tag{5.18}$$

The subscript p denotes the prediction of the model, and e the experimentally recorded data. The error in terms of the posture (joint angles) was calculated by summing the errors over the angles.

The first error measure considers differences only in the endpoint paths, whereas the second measure also considers the velocity profiles. The third error measure captures the differences in the joint angle trajectories with respect to time.

The errors of the different models in terms of the RMSE for the path, Cartesian endpoint velocity, and joint angle data were compared using multiple t-tests, with the Bonferroni correction applied to prevent spurious results due to the multiple comparisons. All results stated as being significant are at the 0.05 confidence level, after the Bonferroni correction.

5.3 Results

Logarithmic spiral parameters The logarithmic spiral parameters a and b were fit for each movement, and are plotted for each subject in Figures 5.2 and 5.3.

The a parameter varies very little, although it was not found to be equal to the length of the outstretched finger, as was suggested in Equation 5.7. The b parameter shows considerable variation, and was not found to equal the value

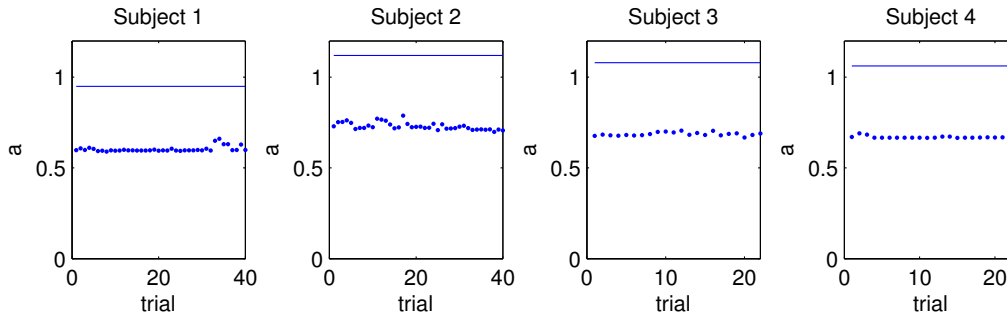


Figure 5.2: The logarithmic spiral a value from Equation (5.2), plotted for the four subjects compared to the trial number. The solid line is the value of the length of the outstretched finger $l = l_1 + l_2 + l_3$ (Equation 5.7), which varies between subjects.

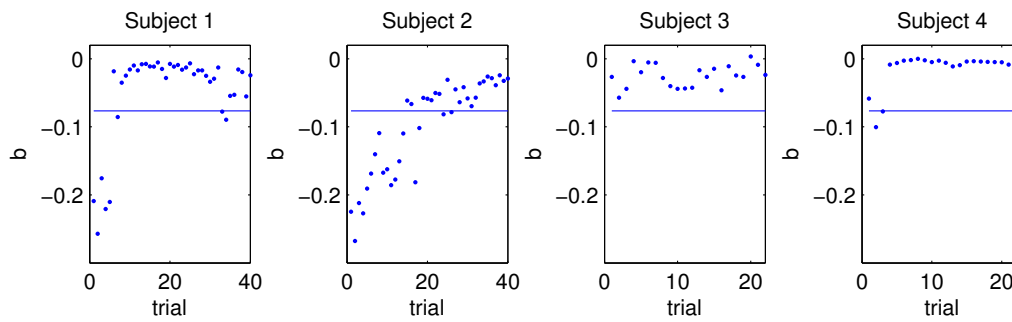


Figure 5.3: The logarithmic spiral b value from Equation (5.2), plotted for the four subject compared to the trial number. The solid line is the value of b that would be expected if $k = \phi \approx 1.618$, i.e., $r(\theta + 2\pi) = 1.618r(\theta)$.

expected if the ratio between radii on successive whorls was $k = \phi \approx 1.618$. Rather, for many of the movements, the b value was close to zero. A b value of zero (equivalent to a k value of 1) means that the logarithmic spiral becomes a circle.

5.3.1 Minimum jerk fit

The fit of the parameters of 5th order polynomials to the arc length $s(t)$ and the three joint angles $\theta_{MPJ}(t)$, $\theta_{PIJ}(t)$ and $\theta_{DIJ}(t)$ for the four fingers, across the four subjects, are shown in Tables 5.1 and 5.2. To demonstrate this visually, the arc length is plotted against time for the index finger and compared to a minimum arc length jerk trajectory in Figure 5.4.

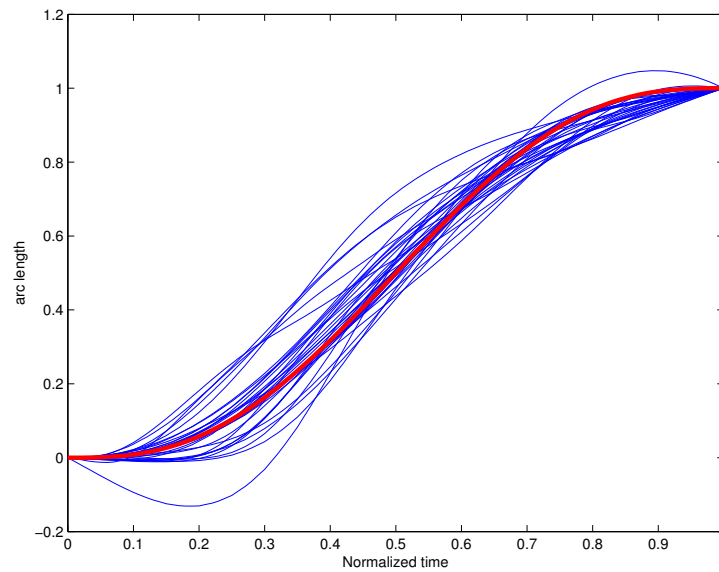


Figure 5.4: Normalized arc length plotted against normalized time for Subject 1, index finger for the grasping movements (in blue), compared to an ideal minimum arc length jerk cost trajectory (in red).

For many of the subjects and fingers, the arc length trajectory is reasonably close to a minimum jerk one. As can be observed in Figure 5.4, although there is some variation, the arc length trajectories all have a similar shape to the minimum jerk trajectory.

	Subject 1			Subject 2		
	a_1 (6)	a_2 (-15)	a_3 (10)	a_1 (6)	a_2 (-15)	a_3 (10)
<i>Finger 1</i>						
θ_{MPJ}	7.99 ± 4.45	-18.34 ± 7.73	11.36 ± 3.36	13.37 ± 2.51	-27.46 ± 4.68	15.15 ± 2.22
θ_{PIJ}	2.16 ± 5.32	-8.07 ± 9.90	6.88 ± 4.65	3.43 ± 8.12	-10.79 ± 14.22	8.32 ± 6.20
θ_{DIJ}	-2.63 ± 3.08	2.11 ± 5.68	1.49 ± 2.91	4.46 ± 5.21	-11.34 ± 9.50	7.89 ± 4.43
s	7.10 ± 3.39	-16.73 ± 5.71	10.64 ± 2.36	9.43 ± 2.31	-20.70 ± 3.77	12.29 ± 1.51
<i>Finger 2</i>						
θ_{MPJ}	11.16 ± 6.58	-23.77 ± 11.65	13.64 ± 5.12	5.54 ± 5.65	-13.60 ± 9.67	9.06 ± 4.11
θ_{PIJ}	2.27 ± 4.08	-9.08 ± 7.30	7.75 ± 3.38	13.60 ± 7.50	-28.49 ± 13.10	15.94 ± 5.68
θ_{DIJ}	-7.41 ± 5.58	10.81 ± 8.90	-2.47 ± 3.62	13.27 ± 5.81	-27.62 ± 10.09	15.41 ± 4.36
s	8.13 ± 4.47	-18.52 ± 7.66	11.40 ± 3.24	7.73 ± 2.54	-17.73 ± 4.15	11.01 ± 1.65
<i>Finger 3</i>						
θ_{MPJ}	5.74 ± 6.50	-14.33 ± 11.21	9.58 ± 4.81	6.33 ± 5.13	-15.27 ± 9.01	9.94 ± 3.97
θ_{PIJ}	7.73 ± 5.62	-19.75 ± 10.17	12.98 ± 5.08	9.64 ± 4.04	-21.39 ± 7.63	12.77 ± 3.62
θ_{DIJ}	-16.76 ± 17.36	25.95 ± 31.13	-8.37 ± 13.91	7.64 ± 3.52	-17.53 ± 6.33	10.90 ± 2.89
s	4.72 ± 2.38	-12.96 ± 3.78	9.22 ± 1.44	7.00 ± 2.74	-16.54 ± 4.49	10.55 ± 1.79
<i>Finger 4</i>						
θ_{MPJ}	9.90 ± 10.02	-21.50 ± 17.48	12.63 ± 7.55	9.17 ± 4.67	-20.07 ± 8.01	11.93 ± 3.42
θ_{PIJ}	13.78 ± 6.80	-28.83 ± 11.80	16.10 ± 5.10	12.62 ± 8.42	-26.42 ± 14.71	14.86 ± 6.41
θ_{DIJ}	-2.70 ± 14.07	1.48 ± 26.07	2.17 ± 12.66	-0.68 ± 9.36	-2.12 ± 16.62	3.76 ± 7.39
s	12.42 ± 9.61	-26.15 ± 16.56	14.77 ± 7.05	9.49 ± 2.81	-20.78 ± 4.75	12.32 ± 1.99

Table 5.1: Fit of a fifth order polynomial (Equation (5.12)) to $\theta_{MPJ}(t), \theta_{PIJ}(t), \theta_{DIJ}(t)$ and the arc length s for Subjects 1 and 2. The ideal parameters are shown at the top of columns in brackets. Finger 1 is the index finger, 2 the middle finger, 3 the ring finger and 4 the pinkie finger. The numbers shown are the mean ± standard deviation across all the closing finger movements as part of a grasping movement. The numbers shown in black are significantly different from the expected minimum jerk value, according to a t-test at 0.05 significance level. The numbers shown in red are not significantly different from the expected value.

	Subject 3			Subject 4		
	a_1 (6)	a_2 (-15)	a_3 (10)	a_1 (6)	a_2 (-15)	a_3 (10)
<i>Finger 1</i>						
θ_{MPJ}	14.03 ± 4.74	-29.24 ± 8.33	16.26 ± 3.65	3.35 ± 2.83	-10.50 ± 5.15	8.13 ± 2.35
θ_{PIJ}	-3.25 ± 11.60	1.22 ± 20.54	2.93 ± 9.06	4.93 ± 5.77	-12.53 ± 11.18	8.59 ± 5.52
θ_{DIJ}	-3.97 ± 7.57	4.64 ± 12.87	0.29 ± 5.67	-20.15 ± 42.53	29.12 ± 69.33	-8.21 ± 27.44
s	11.15 ± 4.84	-24.15 ± 8.47	14.02 ± 3.67	3.77 ± 3.36	-11.24 ± 5.80	8.44 ± 2.48
<i>Finger 2</i>						
θ_{MPJ}	8.68 ± 8.65	-19.55 ± 15.06	11.88 ± 6.50	3.58 ± 3.68	-11.44 ± 6.67	8.82 ± 3.05
θ_{PIJ}	-0.35 ± 6.62	-3.45 ± 12.11	4.75 ± 5.58	1.78 ± 5.57	-6.80 ± 10.05	6.01 ± 4.54
θ_{DIJ}	0.23 ± 6.12	-4.47 ± 10.80	5.19 ± 4.78	7.24 ± 36.73	-14.86 ± 65.58	8.67 ± 29.29
s	6.69 ± 2.90	-16.10 ± 4.83	10.41 ± 1.97	2.59 ± 2.23	-9.25 ± 3.88	7.62 ± 1.68
<i>Finger 3</i>						
θ_{MPJ}	7.29 ± 7.77	-16.46 ± 13.08	10.20 ± 5.49	2.38 ± 4.70	-9.29 ± 7.58	7.86 ± 2.98
θ_{PIJ}	3.77 ± 4.70	-12.29 ± 8.21	9.45 ± 3.89	1.81 ± 5.22	-7.57 ± 9.36	6.72 ± 4.22
θ_{DIJ}	5.08 ± 8.41	-14.77 ± 17.07	10.63 ± 8.74	11.43 ± 29.13	-25.00 ± 52.86	14.58 ± 23.93
s	7.06 ± 1.19	-16.65 ± 1.93	10.60 ± 0.76	3.20 ± 3.82	-10.53 ± 6.21	8.28 ± 2.43
<i>Finger 4</i>						
θ_{MPJ}	8.30 ± 5.98	-18.57 ± 10.20	11.30 ± 4.32	6.65 ± 5.77	-16.17 ± 9.67	10.52 ± 4.09
θ_{PIJ}	8.74 ± 4.18	-19.51 ± 7.60	11.79 ± 3.52	14.11 ± 10.64	-29.03 ± 18.84	15.98 ± 8.35
θ_{DIJ}	4.62 ± 7.88	-11.73 ± 14.90	8.10 ± 7.17	-3.60 ± 9.39	3.61 ± 17.80	0.95 ± 8.56
s	8.11 ± 4.14	-18.45 ± 7.11	11.36 ± 3.01	5.79 ± 1.79	-14.80 ± 2.91	9.99 ± 1.17

Table 5.2: Fit of a fifth order polynomial to $\theta_{MPJ}(t), \theta_{PIJ}(t), \theta_{DIJ}(t)$ and the arc length s for Subjects 3 and 4. See Table 5.1 for a full explanation

Subject	Error measure	inertia cost	log spiral	minimum torque change	minimum angular jerk
1	$E_{xy}(\times 10^{-4})$	15.67(± 20.78)	2.04(± 1.98)	51.31(± 64.86)	9.08(± 18.68)
	$E_{vel}(\times 0.01)$	2.49(± 2.43)	3.04(± 2.23)	3.67(± 3.29)	2.44(± 2.56)
	$E_{\theta}(\times 0.1)$	20.12(± 11.65)	15.99(± 5.62)	49.29(± 25.36)	9.65(± 7.21)
2	$E_{xy}(\times 10^{-4})$	13.10(± 10.99)	4.08(± 3.25)	57.49(± 55.37)	8.07(± 8.13)
	$E_{vel}(\times 0.01)$	2.57(± 1.71)	3.52(± 2.16)	3.74(± 2.85)	2.61(± 1.78)
	$E_{\theta}(\times 0.1)$	14.60(± 6.16)	12.28(± 5.81)	47.72(± 21.47)	9.63(± 4.73)
3	$E_{xy}(\times 10^{-4})$	6.58(± 5.59)	1.95(± 1.73)	25.27(± 26.58)	3.46(± 3.94)
	$E_{vel}(\times 0.01)$	2.21(± 1.40)	2.55(± 1.36)	2.47(± 1.75)	2.27(± 1.41)
	$E_{\theta}(\times 0.1)$	7.76(± 4.13)	10.96(± 1.12)	20.02(± 5.59)	5.06(± 2.97)
4	$E_{xy}(\times 10^{-4})$	9.12(± 10.70)	1.80(± 3.84)	24.86(± 28.76)	5.53(± 10.51)
	$E_{vel}(\times 0.01)$	3.07(± 1.66)	2.98(± 1.08)	4.02(± 1.96)	2.89(± 1.87)
	$E_{\theta}(\times 0.1)$	11.99(± 5.20)	15.42(± 2.27)	24.60(± 11.07)	5.75(± 5.28)

Table 5.3: The goodness of the fit for the four models - (i) minimum kinetic energy (inertia cost), (ii) best fit logarithmic spiral, (iii) minimum torque-change model and (iv) minimum angular jerk model.

For θ_{MPJ} and θ_{DIJ} , there is a reasonable fit for only some of the fingers for some of the subjects, whereas for θ_{DIJ} , the fit is generally poor.

5.3.2 Fit of the path

The goodness of the fits of the four models to the experimentally recorded data, in terms of the error measures defined in Equation (5.18), are summarized in Table 5.3. Six examples of the fits for Subject 2 for the models described above are presented in Figure 5.5. This figure shows the fit to the path, and the three joint angles. Figure 5.6 presents the torque predictions for the three joints, where the torque was calculated using Equation (3.1).

From Figure 5.5, it can be observed that for the path, the minimum torque change model predicted a path with curvature opposite to that observed in the other models. In terms of the joint angles, it can be observed that the medial phalange moves more than the other phalanges of the finger. The shape of the joint angles trajectories were similar (although scaled) between the different movements and joints.

In Figure 5.6, where the torque is plotted for the different models, the

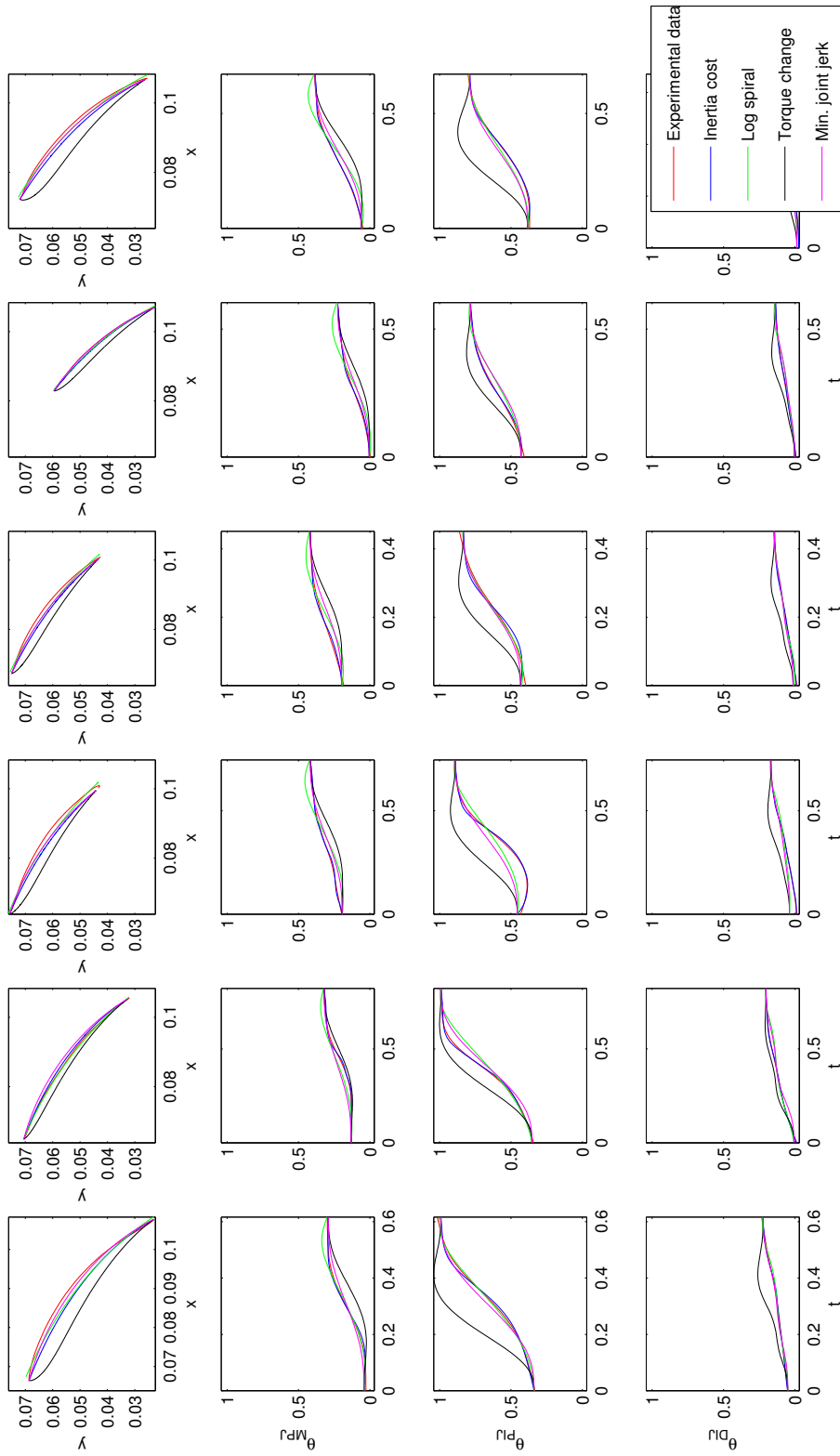


Figure 5.5: Fits of model and experimental data for the first six movements for Subject 2. The experimental data is shown in blue. The predictions are shown of the (i) minimum weighted squared joint derivatives (inertia cost) in red, (ii) best fit logarithmic spiral in green, (iii) minimum torque-change model in black and (iv) the minimum angular jerk model in magenta. The first row is in Cartesian space (x vs y), the next three are the joint angles plotted against time. Each column is a different movement.

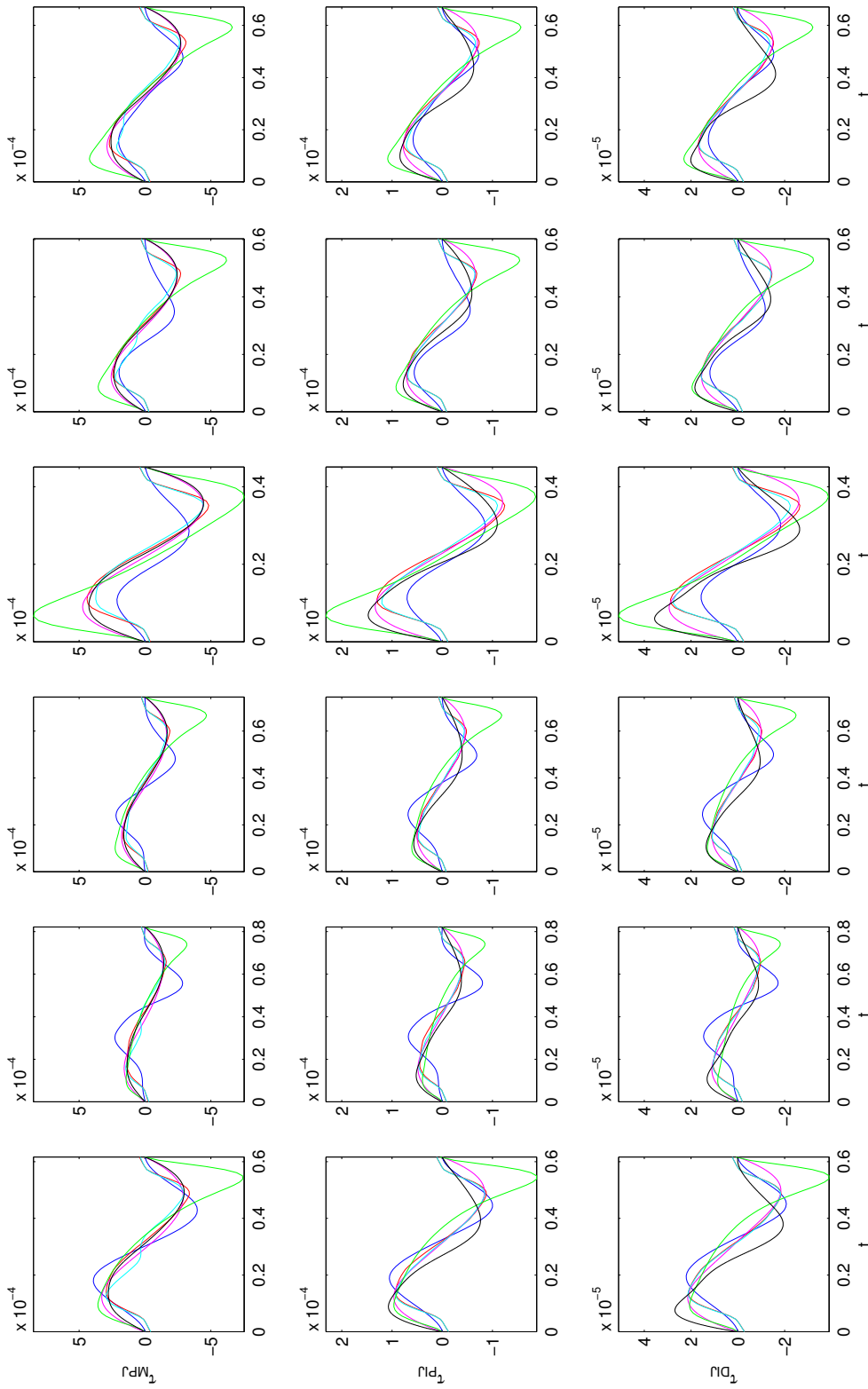


Figure 5.6: Fits of the model in terms of torque for the three joints for the first six movements for Subject 2. The models are as described in Figure 5.5. Each row is the torque at one joint, and each column is a different movement.

Subject	Error measure	inertia cost	log spiral	minimum torque change	minimum angular jerk
1	$E_{xy}(\times 10^{-4})$	17.91(± 23.03)	1.69(± 1.57)	70.00(± 76.65)	5.26(± 16.34)
	$E_{vel}(\times 0.01)$	4.85(± 4.89)	4.69(± 4.25)	6.04(± 3.95)	5.17(± 5.01)
	$E_{\theta}(\times 0.1)$	20.06(± 11.14)	17.83(± 2.76)	43.57(± 15.91)	8.77(± 8.82)
2	$E_{xy}(\times 10^{-4})$	14.58(± 11.48)	3.68(± 3.29)	116.14(± 73.42)	8.58(± 9.82)
	$E_{vel}(\times 0.01)$	2.64(± 1.31)	3.18(± 1.26)	6.09(± 2.79)	2.64(± 1.31)
	$E_{\theta}(\times 0.1)$	10.55(± 4.95)	7.44(± 2.30)	51.87(± 28.46)	6.45(± 3.31)
3	$E_{xy}(\times 10^{-4})$	4.04(± 2.67)	1.32(± 1.66)	26.63(± 30.21)	2.01(± 1.61)
	$E_{vel}(\times 0.01)$	1.81(± 0.84)	1.92(± 0.78)	2.58(± 1.59)	1.82(± 0.95)
	$E_{\theta}(\times 0.1)$	4.17(± 1.66)	4.67(± 0.54)	12.46(± 3.90)	2.44(± 1.86)
4	$E_{xy}(\times 10^{-4})$	6.06(± 11.58)	0.82(± 0.95)	13.41(± 15.64)	5.94(± 11.61)
	$E_{vel}(\times 0.01)$	1.85(± 1.14)	2.21(± 1.29)	2.22(± 1.22)	1.77(± 1.22)
	$E_{\theta}(\times 0.1)$	2.92(± 2.21)	5.01(± 0.73)	10.62(± 6.98)	2.57(± 2.08)

Table 5.4: The goodness of fit for the four models with the added 20g weight on the medial phalange, as described in Table 5.3.

models produce similar predictions, but these are sometimes slightly different from the experimentally recorded torque.

The following results refer to comparisons using multiple t-tests, after taking into account the Bonferroni correction. In terms of path, the logarithmic spiral model was significantly better than all the other models, followed by the minimum angular jerk, inertia cost and torque change. Each model in turn was significantly better than all the following models. In terms of joint angle, the minimum angular jerk showed the best fit, significantly better than the others. The logarithmic spiral and inertia cost models were not significantly different for joint angle error, but both were better than the minimum torque change model. In terms of xy velocity, the minimum angular jerk and the inertia cost are not significantly different, and both of them have a lower error than the logarithmic spiral and the minimum torque change model.

The fits of the model when a weight of 20g was added to the medial phalange are presented in Table 5.4. An example of the fit for Subject 2 is presented for the endpoint and joint angles in Figure 5.7 and the joint torques in Figure 5.8.

With the added weight, the multiple t-tests gave the same conclusions for

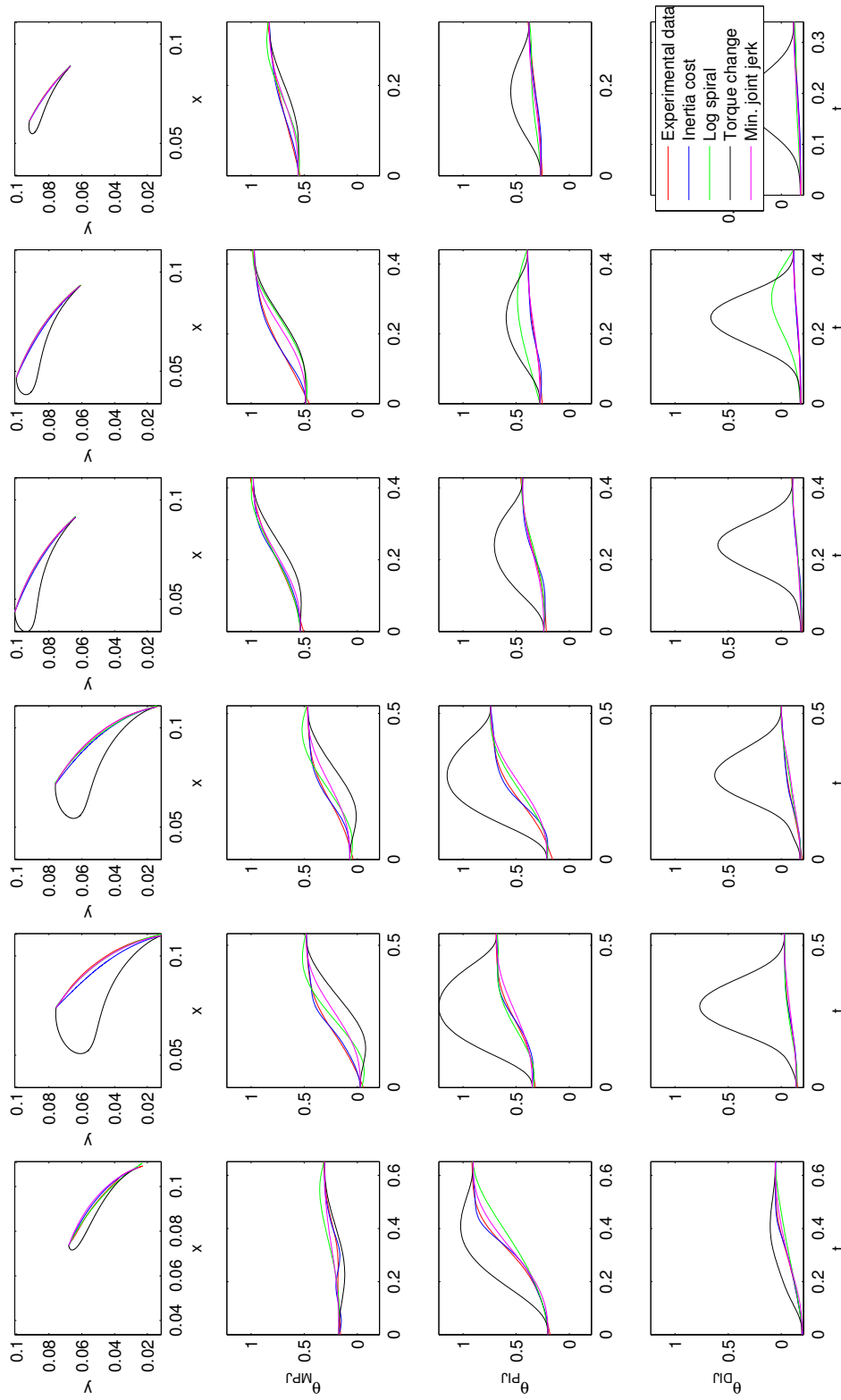


Figure 5.7: Fits of the model for the first six movements for subject 2, in terms of torque with the added 20g weight on the medial phalange. The graphs are as described in Figure 5.5.

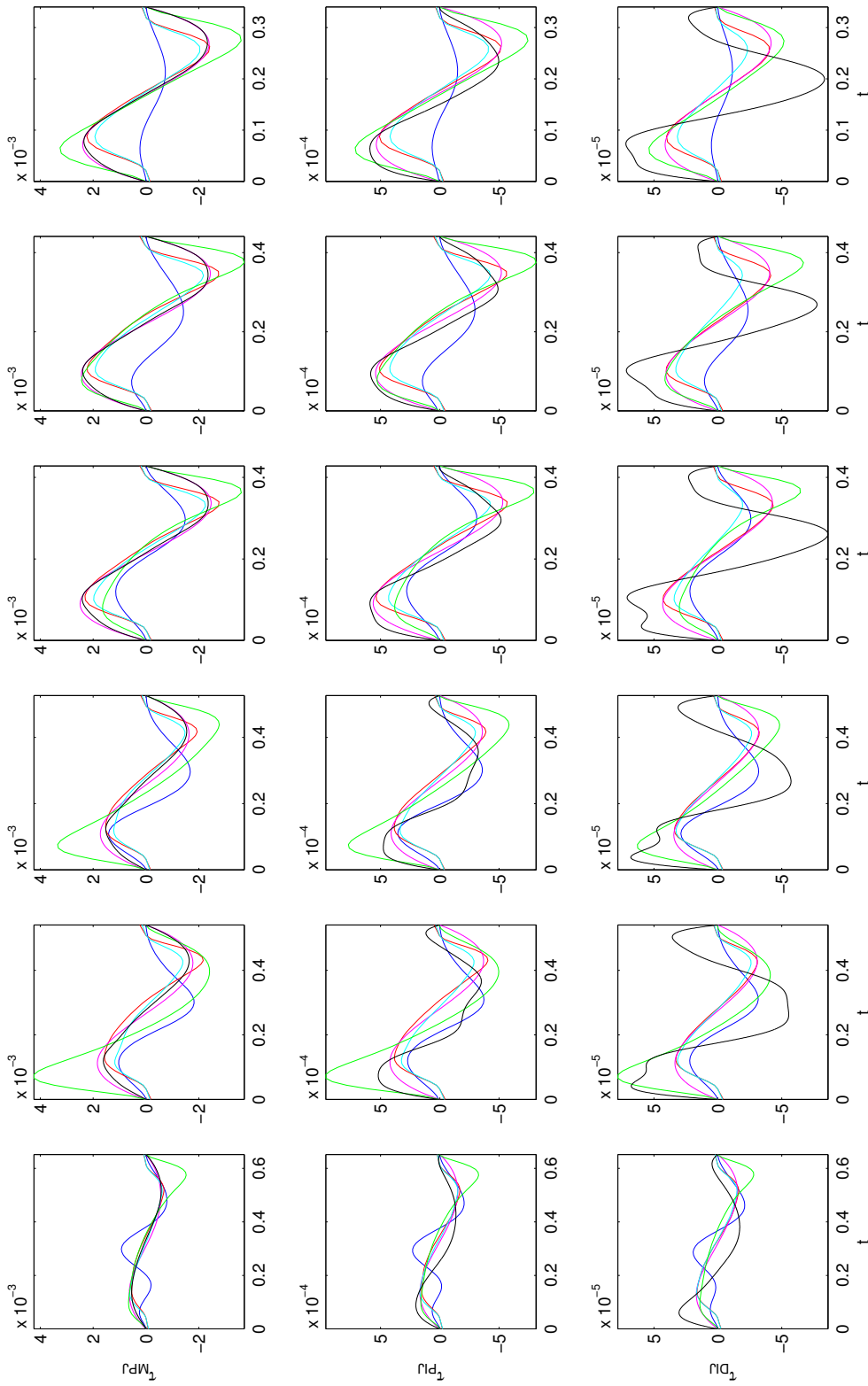


Figure 5.8: Fits of the model in terms of torque for the three joints for Subject 1. The graphs are as described in Figure 5.6.

the path and joint angle error. The xy velocity error measure in this case showed only that the logarithmic spiral model, the minimum angular jerk model and the inertia cost were all better than the minimum torque change model, but other differences were not statistically significant.

When comparing the predictions of the same model between the initial experiments and the experiments with the added weight, the prediction was significant worse with the added weight for only the minimum torque change model (for all 3 error measures).

As an additional comparison between the 3 best models, the error values E_{vel} and E_θ were plotted against the arc length, to see if the errors are constant with respect to increasing arc length. This comparison is plotted in Figure 5.9.

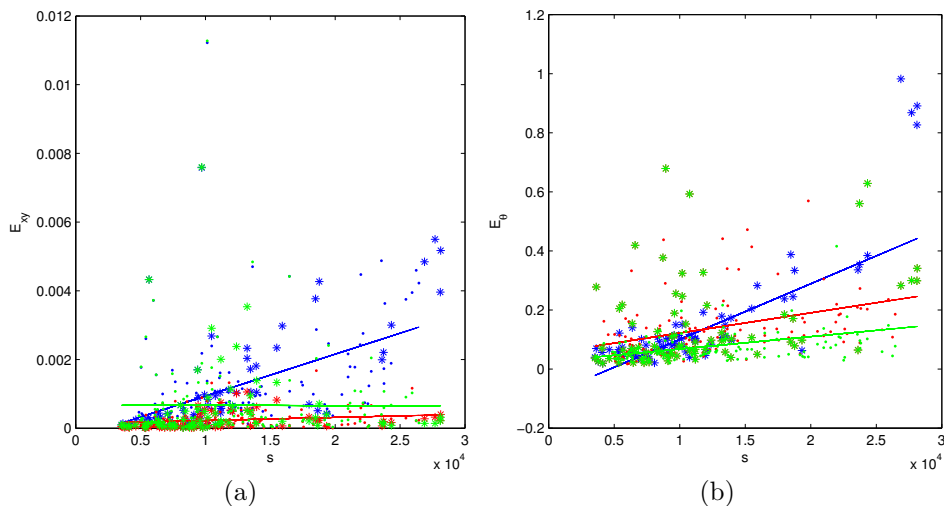


Figure 5.9: The error measures (a) E_{xy} and (b) E_θ , plotted against the arc length for the inertia cost model (blue), the log spiral model (red) and the minimum joint jerk model (green). The dots are the data from the condition without the weight, whereas the stars are from the condition with the weight. The lines are the regression lines for the appropriate model.

For the E_{xy} error measure, which measures only the path, the inertia cost model clearly produces worse predictions with larger arc length, while the other two models produce approximately constant errors across the range of arc lengths. For the E_θ measure, which also takes into account the velocity

profile, all the measures increase error with increasing arc length, although the inertia cost model increases at a higher rate.

5.4 Discussion

During grasping movements, the fingers have been observed to show stereotypical trajectories. The minimum arc length jerk trajectory was observed to predict reasonably well the arc length as a function of time, and hence define the velocity of the movement. This is similar to findings found in works for the arm (Biess et al., 2006a). The additional invariance observed in the path supports the notion that planning of the geometric aspects (i.e., the path), and the temporal aspects (i.e., the speed along this path) may be decoupled (Torres & Zipser, 2004).

The fingertip paths were well fitted by logarithmic spirals. While the a parameter, which determines the width of the spiral, was approximately constant across movements, significant variation was observed in the b parameter, which determines the rate of growth of the spiral. Additionally, the b parameter observed was not close to that found when the rate of growth is equal to the golden ratio, 1.618, as has been speculated but not tested in several papers (Littler, 1973; Park et al., 2003; Markley, 2003). Rather, the b parameter was generally found to be closer to zero, in which case the logarithmic spiral becomes a circle.

The joint trajectories observed showed that the medial phalange moved more than either the proximal or distal phalanges. This is consistent with the notion of reducing a kinetic energy related cost, as accelerating the lighter medial phalange requires less force than accelerating the proximal phalange (which also must rotate the other phalanges with it). The reason that the distal phalange, which weighs the least, and theoretically would not require rotating the other phalanges is not rotated more seems to be due to biomechanical constraints which prevent it from rotating independently.

The minimum torque change model was found, in general, to predict the path and trajectories significantly worse than the best 3 models. It predicted fingertip paths with a curvature opposite to that observed in the experimental

data. Furthermore, when the weight was added, changing the inertia of the finger and thus also the torque, the predictions became worse. Hence, there seems to be little support for this model in predicting index finger motion during grasping.

The other three models (the inertia cost, the minimum angular jerk and the logarithmic spiral path model) produced similar predictions for the path, velocity and angular trajectories, both with and without the weight. When considering only the path, the logarithmic spiral model performed the best, whereas when considering the joint angle trajectories with respect to time, the minimum angular jerk model performed best.

However, when the error in terms of the path were plotted against the arc length, the inertia cost model produced worse predictions with longer arc length, whereas the other two models produced approximately constant errors. This means that for longer movements, the performance of this model deteriorates. It needs to be remembered that the path of the logarithmic spiral model was determined by finding the best fit logarithmic spiral to the path, and hence it is not surprising that the path error is approximately constant across different values of the arc length. The other models were only provided with the boundary conditions.

An apparent contradiction is observed for the minimum angular jerk model. If each joint follows such a trajectory, this implies that the joint angles of the finger are linearly related, as was found in a recent work (Dejmal & Zacksenhouse, 2006) examining manipulative movements on objects. However, as was shown in Equation (5.8), this can not be the case if the path is a logarithmic spiral and θ_{PIJ} and θ_{DIJ} are linearly related. Although both assumptions cannot be true simultaneously, it seems that the difference between the observed trajectories and the model trajectories based on both these assumptions is small, and less than the statistical ability to differentiate between the two models using this data set. Additionally, in Tables 5.1 and 5.2, the 5th order polynomial fits to the joint angle trajectories are often not that close to the minimum jerk ones, as would be expected if minimum angular jerk is a good model for the movements. Analysis of additional movements may help determine which of these two models gives better predictions

for the behavior.

The different models have different numbers of free parameters. The logarithmic spiral model has two free parameters which are fitted from the observed path. Thus, this model will have a good fit for the path if the path is approximately a logarithmic spiral, which is the case for many short, slightly curved movements. However, this model does not give a motivation for why the CNS selects the observed logarithmic spiral path. The inertia-like cost model has three parameters (the weights of the Jacobi polynomials) for each of the two joint angles which are fitted according to the cost function. However, these are not free parameters, rather, they enable the approximate minimization of the cost function, and are selected based on the cost function and not from the observed trajectories. If analytic solutions to the minimization problem were possible, then no parameters would be required. A similar statement is true for the minimum torque-change model. Finally, the minimum angular jerk model does not have any parameters that need to be fitted since the analytic solution is known.

The assumption in the models that the distal interphalangeal joint angle is fully determined by the proximal interphalangeal joint was a necessary assumption in order to produce reasonable models. Otherwise, a model based on minimizing a kinetic energy related cost would prefer to move more the distal phalange, because moving this phalange alone involves moving less weight. This was indeed observed in preliminary versions of the model that were constructed. However, such movements appear to be biomechanically impossible. Furthermore, the use of this assumption allowed determination of the joint angles for the logarithmic spiral model (i.e., when given the path), otherwise, determining the joint angles for a given endpoint path has multiple solutions.

Finally, it should be noted that while logarithmic spirals approximate reasonably well the path of grasping movements, they cannot describe general finger movements. For example, a radial movement of the finger performed, cannot be approximated by any logarithmic spiral. In Cruz & Kamper (2006), where subjects were asked to make point-to-point finger movements in the plane, the observed trajectories can not be fitted well to logarithmic spi-

rals. Use of the models presented in this work for such trajectories would be a good test for their generalization to more general finger movements, rather than specifically finger movements involved in grasping, although more complex movements may involve the composition of multiple sub-movements. The examination of tasks requiring particular force and / or velocity demands, for example, playing the piano, tool use, or object manipulation, could also help determine the general applicability of such models.

The stereotypical trajectories observed in this work are based on more than biomechanical constraints. This can be observed from patients with problems controlling the movements of the fingers, who do not generate these stereotypical trajectories (Littler, 1973).

Chapter 6

Applications

In this section, two practical applications of the techniques presented in the thesis are described. The first is the construction of a telerobotics system, where a human operator in a virtual reality setup controls the movements and actions of a robot. The second is the use of grasp modelling to hypothetically predict the optimal grasps for use in some rehabilitation scenarios.

6.1 Grasp recognition for telerobotics

The experiments in Chapter 4 showed that different grasps are used on an object depending on the type of action or manipulation that will be performed. Based on this observation, we have designed and implemented a telerobotics system. Rather than a human operator providing low-level instructions to the robot (e.g., detailed trajectory and grasp points), our approach has been to transmit high-level task information (e.g., move to this location, grasp in order to unscrew), which we are able to abstract from recordings of the human operator's actions. In this way, the human operator, acting in a virtual reality setup, can naturally perform manipulations on objects, and the robot will perform these actions in a way that is suitable for the robot.

In a previous work (Berman et al., 2005), we showed that maintaining configurational similarity between a human demonstrator and the robot manipulator is in general not desirable. For example, a person would unscrew

the lid of a jar with the long axis of their forearm parallel to the horizontal plane, whereas for the robot we are considering here, the most efficient grasp is for the long axis of the last link to be parallel to the vertical axis. Maintaining configurational similarity in this case will cause suboptimal performance and for many tasks will not be able to succeed. Instead, we have taken the approach of devising a-priori a set of actions that can be performed by the robot on a set of objects. The selection of which task to perform is based on recognizing the intentions of the human operator.

System overview

The robot controller, running on a PC, maintains knowledge of the location, state and type of all objects in the scene. It communicates with the human interface using TCP/IP sockets over a network, using a specially defined XML protocol. The robot is an articulated robot with five degrees of freedom (ER-VII Scorobot, Intelitek), with an electrical parallel jaw gripper as an end effector. Initially, the robot controller sends the locations and orientations of all the objects in the scene. During use, the robot controller receives commands to move objects and perform actions on them. It performs these actions on the robot. When the given posture is unattainable (because the robot has only 5 degrees of freedom), the closest achievable posture is determined using an optimization procedure. It returns to the human interface the new state of the objects after the action is performed, or an error message if appropriate.

The human interface involves a virtual reality setup, displayed in Figure 6.1. The operator wears a CyberGlove and Fastrak, and the hand is rendered in real time on the display. The mirror setup shown prevents the operator from seeing their own hand and the rendered hand appears in approximately the location of their real hand, to make operation of the system more natural. The computer program, written in C++ using OpenGL, and running on a SGI Octane, also shows the objects that the robot has identified in the scene in their appropriate locations. The operator can grasp the objects and manipulate them. Feedback is provided via the colors of the objects.

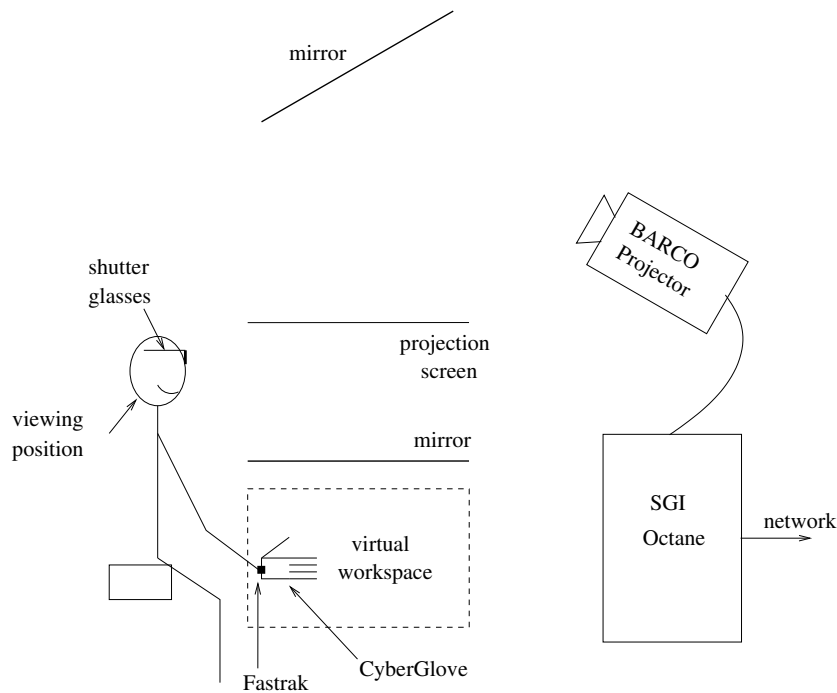


Figure 6.1: Virtual reality setup.

When the operator grasps an object, the type of grasp is recognized, from the possible grasps that can be performed on such an object (from a predefined set). Before using the simulation, the subjects undergo a short training session, where they perform a number of grasps 10 times each. A linear discriminant classifier is currently used, implemented in Matlab. The features for classification are the joint angles.

The program flow of the simulation is shown in Figure 6.2. The objects in the scene begin as being ungrasped. When three fingers including the thumb contact with an object, this is considered a potential grasp and object turns blue. If this grasp is held for two seconds, then the object is considered to have been grasped. The grasp at this point is recognized using the linear classifier, and the type of grasp and the object is sent to the robot. Once the operator starts moving the object, updates about its position are sent to the robot every 2 seconds if the current position is legal (if it is not intersecting with any other object). A further signal is sent to the robot when the operator ungrasps the object, along with its final position and

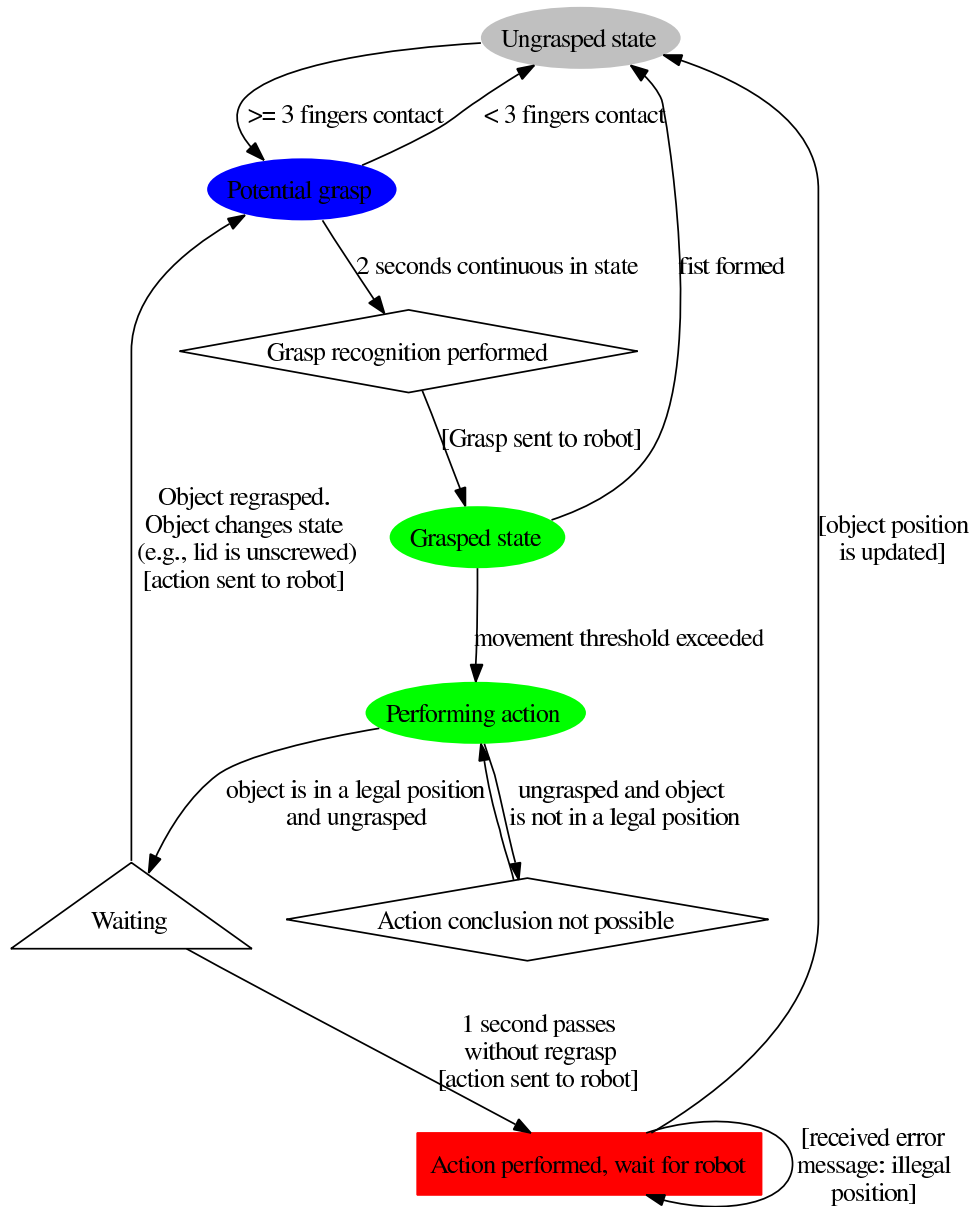


Figure 6.2: Program flow. The flow chart represents the different states of the program during execution. The program begins in the “ungrasped state”. The colors represent the current color of the object.

orientation. The ungrasped object turns red, and the simulation waits until a response is received from the robot (i.e., after the robot has completed the task) before allowing the human operator to continue to manipulate the scene.

Sample usage

Preliminary tests have been performed on the system, and it is possible to complete several tasks. For example, a set of toy blocks can be used to build a tower, or the jar can be opened, and the contents poured into a container. Screenshots of the human interface, and the robot performing one of the tasks, is shown in Figure 6.3. Further testing with untrained subjects is planned.

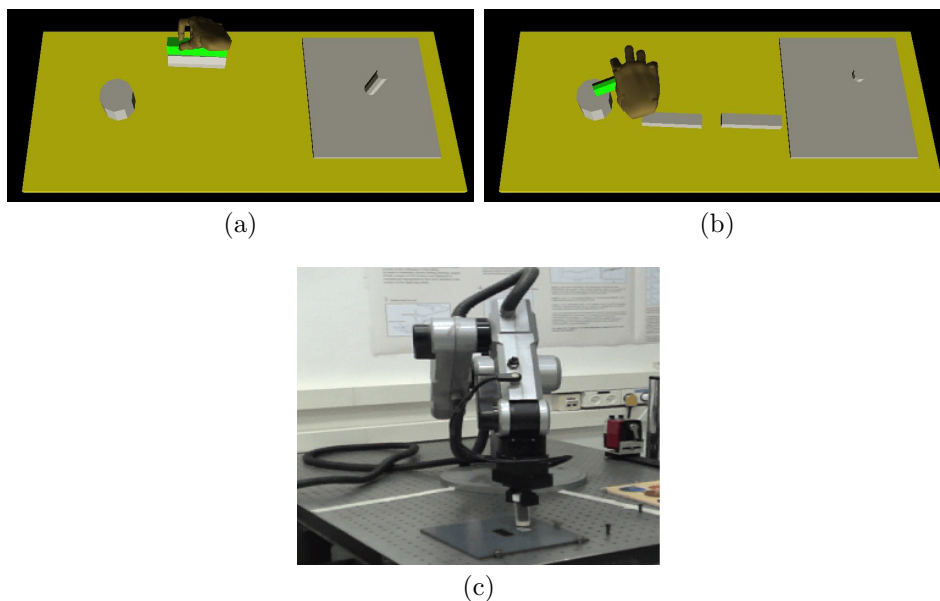


Figure 6.3: Screenshots of (a) building a tower and (b) pouring from the jar in the virtual reality human interface, and (c) a photo of the robot unscrewing the lid of the jar.

6.2 Optimal grasp prediction for use in rehabilitation

A potential application of the grasp modelling presented in Chapter 4 is to suggest the “optimal” grasps for patients to use when they have limited or impaired movement ability, perhaps after injury of some sort. While the analysis in the thesis has focused on movements of healthy individuals, the underlying principles can potentially be applied for grasping when full movement of the hand is not possible. A similar analysis could also be useful in studying grasping in infants and children, who also show limited ability to control their finger movements. This section is a hypothetical treatment of the issue, and has not been tested in real situations.

By applying the modeling presented in Section 4.4, the best grasps under particular constraints can be generated. Two examples are presented here, for lifting and unscrewing the lid of the jar. The first constraint considered is that only a small number of fingers, in this case two, can be used to perform the tasks. The second constraint used was that the hand has limited movement. This was modeled by fixing the interphalangeal joint of the thumb and the proximal and distal interphalangeal joints of the other fingers at zero.

The grasps for unscrewing and lifting the lid were selected by choosing the grasps that maximize the following measures, based on the results of Section 4.4

- Unscrewing - $1.5K_x + \tau_y$
- Lifting - $1.5K_x + (1 - F_x) + (1 - F_z)$

where K_x is the normalized stiffness compatibility along the x axis, τ_y is the torque production compatibility about the y axis, and F_x and F_z are the force production compatibilities along the x and z axes.

The five best grasps for lifting and unscrewing the lid with two fingers are shown in Figure 6.4.

For lifting the lid (Figure 6.4a), the two fingers are placed on opposite sides of the lid, with the phalanges of the thumb and the index finger approximately parallel. For unscrewing the lid, this is not the case - while the

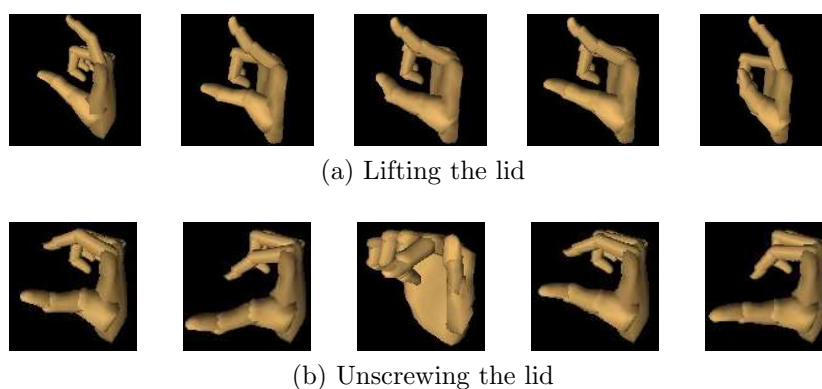


Figure 6.4: The five “best” two finger grasps for the two tasks on the lid.

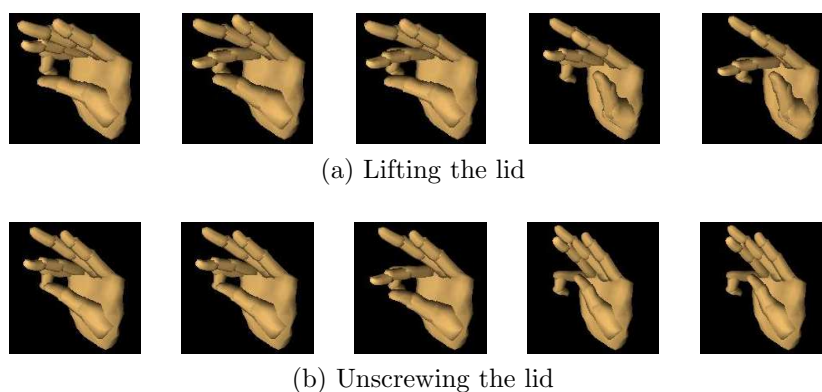


Figure 6.5: The five “best” grasps under the constraints that the interphalangeal joint of the thumb and the proximal and distal interphalangeal joints are zero for the two tasks on the lid.

thumb grasps the lid in a similar way, the index finger grasps the lid from a different angle. The third example grasps the lid with the side of the index finger.

The five best grasps for lifting and unscrewing the lid with four fingers, under the constraint that the interphalangeal joint of the thumb and the proximal and distal interphalangeal joints at zero are shown in Figure 6.5. For lifting the lid, the thumb is placed on one side, and either the other three fingers are placed opposite, or two fingers are placed at one location, and the fourth finger at another location. In order to unscrew the lid, two strategies were observed. Either the object is grasped with the side of the fourth finger

(the first three grasps) with the thumb parallel to the index finger, or the index, middle and ring fingers are parallel, and the thumb is rotated. This second strategy was not observed in the experiments.

These two examples indicate the potential of such a technique for use in rehabilitation. For use in a real situation, the model should take into account the geometry of the patient's hand, the size of the objects and the accuracy with which they are able to perform movements.

Chapter 7

Summary and conclusions

The field of human grasping presents many questions that require further research. The aim of this research has been to model the human fingers and hand using the tools of robotics, and to use these models to obtain insights into the invariant properties of our behavior during grasping. Despite the large amount of variance observed in finger movements and during grasping, we aim to extract the common features across movements and subjects and to interpret them. In particular, this thesis has focused on several areas. The impedance properties of the hand have been modeled, grasp choice for a selection of different tasks have been compared, and the finger trajectories used during grasping have been described.

The impedance properties of the index finger were estimated through a series of experiments with a novel protocol, described in Section 3.1.3. While maintaining a posture, the index finger was repeatedly perturbed using artificial tendons attached to an exoskeleton, and the resulting motion was recorded. Using an optimization approach with several constraints, the inertia of the finger was derived, and the values found were similar to those predicted by a geometric model. While the force required to accelerate the finger (measured by the inertia) is much smaller than the forces required to displace the finger (measured by the stiffness), the inclusion of the inertia term is important for accurately modeling the finger, particularly at high accelerations. It was shown in Section 3.1.4 that using a full dynamic model

sampled at many time points predicts significantly better the force than using only a first order model (i.e., just stiffness) calculated from the total magnitude of force and displacement.

Two main problems were found with this technique - the first was that there is a non-negligible amount of variation in the force profiles generated by the CyberGrasp exoskeleton (see Figure 3.3). The second is that the directions of force application were all very similar, which makes robust estimation of the impedance terms difficult (see Figure 3.11). Ideally, this procedure would be repeated with a different device that produces more accurate force profiles, and in many directions.

A technique was also presented for interpolating the stiffness between stiffness values recorded at different postures (in Section 3.2). This technique involved estimating the joint stiffness as a function of the joint angle, and from this determining the endpoint stiffness. This method was used in modeling the stiffness of the grasp at unmeasured postures.

The use of a tool or manipulation of an object requires that certain movements and forces be applied to the object or tool. The redundancy of the kinematic degrees of freedom within the hand means that in general, many grasps can be selected that satisfy the basic need for grasp stability. The grasp can be selected such that applying the desired motion or force can be performed in an efficient and accurate manner. In addition, the impedance properties of the grasp will affect the stability of the grasp, and how it handles errors. This work has attempted to describe how the selected grasp posture and stiffness affect the ability to manipulate objects and the suitability of the grasp for different manipulation tasks.

The grasps used during a series of manipulation tasks were examined. Based on measurements of the posture of the hand using the CyberGlove, described in Section 4.2, the grasp Jacobian was constructed. This allows the calculation of force and velocity transmission ellipses, which define the force or velocity that can be produced in a particular direction when the squared sum of the joint torques / velocities is 1. Additionally, all grasping fingers were simultaneously perturbed using the CyberGrasp, while grasping the object as if to manipulate it, in order to estimate the stiffness of the fingers.

By making an assumption about the unmeasured abduction stiffness, the grasp stiffness was also estimated.

While a large amount of variation was observed among different subjects in the number of fingers used, and the finger placement on the objects, some common patterns were observed, as described in Section 4.3. By examining the relative force and velocity production and stiffness properties between different types of manipulation on the same object, it was possible to observe patterns that were sometimes related to the requirements of the task.

This approach was extended using an optimization technique in Section 4.4, where a large number of legal grasps were computer generated. The grasps were generated such that they used the same number of fingers as the subject used during the experiments, and had the same joint ranges. Only grasps that were “legal” were considered, that is, if the posture of the hand could be feasibly used to grasp the object. The properties of the computer generated grasps were compared with the grasps selected by the subjects, in terms of their stiffness, and force and velocity production capabilities. This approach was used rather than standard optimization (where the parameters are varied in some way) because making small changes to a feasible grasp generally results in an unfeasible grasp, thus, it is difficult to vary the parameters in order to improve on some cost measure.

The normalized compatibility scores for the grasps for velocity or force production, and for stiffness, were calculated along the x , y and z axes, by determining for the proportion of computer generated grasps with a lower compatibility score. When the normalized compatibility scores across subjects and repetitions were significantly different from 0.5, it was assumed that this may signify that this parameter may have been optimized (minimized or maximized), as summarized in Tables 4.4 and 4.5. Several of the values that appear to have been optimized were related to the task requirements.

Evidence for task-based grasp planning has been provided by neural recording studies. Neurons in behaving monkeys in area F5 (in the rostral part of inferior area 6) have been observed to show selectivity for different types of grasping, namely precision grip, finger prehension and whole-hand prehension (Rizzolatti et al., 1988) and for the type of object (Raos et al.,

2006). The selectivity for grasp type, and not only for object type or size, suggests that there is a representation across objects used for the type of interaction, which may be based on the requirements or goals of the task. Area F5 is believed to be the monkey homologue of Broca's area in humans (Rizzolatti & Arbib, 1998). In area F2, in the caudal part of area 6, neurons were also observed that were selective for the type of grasp (Raos et al., 2004). These authors have suggested that these areas (F2 and F5) collaborate in the control of grasping. Neurons in the anterior intraparietal area (area AIP) in monkeys have also been found to be selective for visual responses to the shape, size and orientation of objects for grasping (Murata et al., 2000). Raos et al. (2006) suggested that the network of F5, F2 and AIP play complementary roles in the planning and execution of grasping movements.

While the present work has described some of the features of several types of manipulation, much further work needs to be done to fully understand how humans select grasps in order to manipulate objects. First, the number of fingers selected for manipulation requires further investigation. Theoretical work in robotics has characterized the minimum number of fingers necessary for properties such as force closure (for example, Mishra et al. (1987)). It is not clear how these results are reflected in the number of fingers selected by humans.

A source of uncertainty in the grasp model was introduced by the lack of measurements of the abduction stiffness. Measurements of the applied fingertip abduction forces would allow better modeling of the three dimensional fingertip stiffness and hence grasp stiffness. This may be possible using instrumented objects. Use of a full impedance model (including damping and inertia) for grasping could also contribute to the accuracy of the model, but would require a more accurate measurement device.

The translational and rotational stiffness ellipsoids plotted provided visualizations of the upper left and lower right quadrants, respectively, of the grasp stiffness matrix. The upper right quadrant of the grasp stiffness matrix represents the relationship between angular motion and translational forces, while the lower left quadrant represents the relationship between transla-

tional motion and torques. Further analysis needs to be performed to examine the patterns observed in these quadrants and their relationship to the selected tasks being performed.

Features of a grasp, in addition to the velocity and force transmission and stiffness characteristics, such as the available joint movements and distances from singularities can be defined (Shimoga, 1996). Additional invariant properties of the grasps which are selected may be revealed by further investigation of such features.

The finger trajectories used to perform these grasps were also examined. Invariant velocity profiles were observed on the Cartesian arc length along the path, and the velocity profiles minimized a cost consisting of the integral of the squared arc length jerk (Section 5.3.1). Based on this finding, it seems that the path and speed are planned separately. Three models were found to model well these trajectories, namely, minimizing a cost function that is the integral of the weighted squared joint derivatives along the path, following a logarithmic spiral, and minimizing angular jerk, as detailed in Section 5.3.2. The predictions of these models were significantly better than the predictions when using the minimum torque change model. When adding a weight to medial phalange of the finger, thus changing its inertia, the three best models produced errors that were not statistically significantly different, although for the minimum torque change model, the errors increased.

The separation of the planning of path, and the dynamics and velocity profile, as is suggested by the results of the modeling of the finger trajectories, is an attractive notion (Torres & Zipser, 2002; Biess et al., 2006a). This would allow different types of information to be involved in the planning of each feature, and would easily allow the scaling of the movement in time or in space.

7.1 Potential directions for future research

Several potential directions can be suggested as a result of the work described here. While the grasping model presented described the theoretical force and velocity transmission capabilities, these predictions have not been tested.

Such testing would be a useful confirmation of the power of the model, and could be performed by measuring the force production when subjects grasped objects in different ways and comparing these to the model predictions. Similarly, in order to confirm the stiffness predictions of the model, the subject can grasp a manipulandum, while the arm is braced. By applying small forces to the grasped object and measuring the resultant displacement, the grasp stiffness can be estimated, and compared to the stiffness predicted by the model.

It has been observed that the direction of the major axis of the arm stiffness ellipse is approximately aligned with a radial line joining the shoulder to the hand (Mussa-Ivaldi et al., 1985; Flash & Mussa-Ivaldi, 1990). Milner & Franklin (1998) noted that the orientation of the fingertip stiffness ellipse maintained a relatively fixed direction for each (of two) measured postures, approximately parallel to the axis of the proximal phalanx of the finger (i.e., it never varied by more than 20°). This rule was not in general observed from the data collected in these experiments. It would be instructive to collect stiffness data from a large number of postures, under different force conditions, to see if this, or an alternative rule can be found.

Currently, the velocity and force transmission properties were only examined at the start of manipulation. The time development of the velocity and force ellipsoids throughout grasping and manipulation should also be studied, in particular by examining the ellipsoids during grasp “gait” (i.e., performance of rhythmic tasks), and their relation to the changing demands of the manipulation with time.

Finally, although the observed features of grasping show a connection between the task and the kinematic and stiffness properties, it is unclear how such grasps could be efficiently constructed. Further research could focus on the form of candidate primitives for grasping, and how the observed grasps may be constructed from them. While kinematic synergies have been observed in generating hand postures during grasping (Santello et al., 1998; Mason et al., 2001; Santello et al., 2002), and in this work, stereotypical finger trajectories have been observed and described, primitives need to be also related to the manipulation and dynamic properties of the grasp. Pre-

liminary work was carried out on describing the movements of the fingers during grasping using non-negative matrix factorization of the joint angles trajectories. By using such representations, it might be possible to define a low-dimensional, continuous space under which optimization for desired properties could be performed, and eventually the optimal combinations of these synergies determined for performing grasping and manipulation.

One step in this direction would be the construction of a grasp taxonomy for objects of many shapes and sizes, for a variety of different tasks (defined by their stiffness and force production demands). The selected postures used, and their optimality in terms of the compatibility measures described here may provide further insights into the mechanisms used by the CNS for planning grasping movements.

Appendix A

Glove Calibration

Nomenclature

ϕ_j	Joint angle of joint j .
σ_j	Raw data from sensor j .
θ_j	Offset of sensor j .
g_j	Gain of sensor j .
g_j^k	Cross gain (effect of sensor k on j).
L_j	Length of link j .
ABD	Abduction / adduction of metacarpophalangeal joint.
MPJ	Extension / flexion of metacarpophalangeal joint.
PIJ	Extension / flexion of proximal interphalangeal joint.
DIJ	Extension / flexion of distal interphalangeal joint.
PA	Palm arch.
IJ	Thumb interphalangeal joint.
T_2^1	Homogenous transformation (4×4) matrix from frame 1 to frame 2.

Introduction

The CyberGlove (Immersion) contains 22 sensors that measure the joint angles of the hand. The sensors are located over or near the joints of the hand and wrist, and each sensor is designed to produce an output which has a linear relationship to the appropriate joint angle. The CyberGlove produces

a raw output as an integer between 0 and 255, which can be converted into joint angles by the relationship:

$$\phi_j = \theta_j + g_j \sigma_j$$

The values of θ_j and σ_j will be different for each subject, as they are dependent on how the glove sits on the joints. Hence a calibration technique is necessary to determine these values. Additionally, some sensors are affected by more than one joint. Cross gains g_j^k were used to take this into account:

$$\phi_j = \theta_j + g_j \sigma_j + \sum_{k=1}^{22} g_j^k \sigma_j \quad (\text{A.1})$$

where g_j^k is the effect of sensor k on joint j . In the calibration procedure used, most of the cross gains were assumed to be zero.

The calibration routine provided with the CyberGlove does not calibrate for finger lengths and provides only a very basic calibration of the joint angles (the calibration is only performed on the thumb and index finger). Hence when looking at the visualization of the hand based on this model, the positions of the fingertips often do not correspond well with the actual fingertip locations. Hence an alternative calibration technique was needed.

Previous works

Several calibration techniques have been proposed in the literature. Open-loop kinematic calibration (Rohling & Hollerbach, 1993, 1994; Fischer et al., 1998) involves using an external measuring device, which measures the 3D location of the fingertips while simultaneous recordings are made from the glove. The fingertip location is estimated based on an open-loop kinematic chain from the glove recordings and model parameters. The error between this estimation and the value recorded from the external measuring device is minimized by altering the model parameters, usually in an iterative process.

Calibration can also be performed by placing the joints at specified an-

gles while measuring from the glove (Kessler et al., 1995; Kamper et al., 2003). Regression is then used to determine the relationship between the sensor readings and the joint angles. Similarly, computer vision techniques can be used by placing colored stickers on the joints (Chou et al., 2000), allowing estimation of the relative joint lengths and the other model parameters. However, it is impossible to place the stickers exactly on the joints (because the joint is inside the finger) and the distance of the marker from the joint will also vary with the posture as the skin moves.

Another class of calibration techniques are known as zero-hardware techniques, in that they do not require any external device to perform the calibration. Menon et al. (2003) recorded the hand in a variety of known postures, and then performed linear regression between the actual joint angles and the glove recordings to determine the calibration parameters. In Griffin et al. (2000); Turner (2001), measurements were made from the CyberGlove while subjects made movements where they were required to ensure that the tip of the thumb and the tip of a specified finger were always touching. It is possible to then construct a kinematic chain of the two touching fingers, and use as the error the distance between the two fingertips in an iterative optimization procedure.

Implementation

The calibration technique that was used here is based on the technique proposed by Griffin et al. (2000); Turner (2001). This technique is an example of a zero-hardware solution.

The basis of the algorithm is to record data where the subject holds two fingertips (the thumb and one of the other fingers) together in a range of postures. The location of the relevant fingertips can be written as a function of the joint angles and the calibration parameters. The error in the current calibration parameters is defined as the distance between the appropriate fingers. This distance would be zero with a perfect calibration. The error is minimized simultaneously over the fingers used in the particular task (up to 4 finger/thumb combinations). Constraints were placed on the allowable values

Finger	Offset	Gain
Thumb	$\theta_{T_{TR}} \theta_{T_{MPJ}} \theta_{T_{ABD}} \theta_{T_{MCtwist}}$	$g_{T_{TR}} g_{T_{MPJ}} g_{T_{IJ}} g_{T_{ABD}}$
Index	$\theta_{I_{MPJ}} \theta_{I_{PIJ}} \theta_{I_{DIJ}} \theta_{I_{ABD}}$	$g_{I_{MPJ}} g_{I_{PIJ}} g_{I_{DIJ}} g_{I_{ABD}}$
Middle	$\theta_{M_{MPJ}} \theta_{M_{PIJ}} \theta_{M_{DIJ}} \theta_{M_{ABD}} \theta_{M_{TWI}}$	$g_{M_{MPJ}} g_{M_{PIJ}} g_{M_{DIJ}} g_{M_{ABD}}$
Ring	$\theta_{R_{MPJ}} \theta_{R_{PIJ}} \theta_{R_{DIJ}} \theta_{R_{ABD}}$	$g_{R_{MPJ}} g_{R_{PIJ}} g_{R_{DIJ}} g_{R_{ABD}}$
Pinky	$\theta_{P_{MPJ}} \theta_{P_{PIJ}} \theta_{P_{DIJ}} \theta_{P_{ABD}} \theta_{P_{PA}}$	$g_{P_{MPJ}} g_{P_{PIJ}} g_{P_{DIJ}} g_{P_{PA}}$
Palm	$\theta_{PITCH} \theta_{YAW}$	$g_{PITCH} g_{YAW}$

Finger	Lengths	Cross gains
Thumb	$L_{T1} L_{T2} L_{T3} L_{T4}$	$g_{T_{TR}}^{T_{ABD}} g_{T_{ABD}}^{T_{TR}} g_{T_{MCtw}}^{T_{TR}} g_{T_{MCtw}}^{T_{ABD}}$
Index	$L_{I1} L_{I2} L_{I3} L_{I4} L_{I5}$	$g_{I_{ABD}}^{M_{ABD}} g_{I_{ABD}}^{R_{ABD}}$
Middle	$L_{M1} L_{M2} L_{M3} L_{M4} L_{M5}$	$g_{M_{ABD}}^{I_{ABD}} g_{M_{ABD}}^{R_{ABD}} g_{M_{PIJ}}^{M_{MPJ}}$
Ring	$L_{R1} L_{R2} L_{R3} L_{R4} L_{R5}$	$g_{R_{ABD}}^{I_{ABD}} g_{R_{ABD}}^{M_{ABD}} g_{R_{PIJ}}^{R_{MPJ}}$
Pinky	$L_{P1} L_{P2} L_{P3} L_{P4} L_{P5}$	$g_{P_{ABD}}^{I_{ABD}} g_{P_{ABD}}^{M_{ABD}} g_{P_{ABD}}^{R_{ABD}} g_{P_{PIJ}}^{P_{MPJ}}$

Table A.1: The 87 parameters used in the calibration. Novel parameters not found in other models include the palm arch, twist of the middle finger $\theta_{M_{TWI}}$ and many of the cross gains.

for the calibration parameters to prevent trivial solutions. If no constraints were applied, an optimal solution would be to set all the gains to zero and to adjust the offsets so that the fingers always touch. The constraints were defined such that no parameter was allowed to change too much from the starting guess.

The calibration was performed over 87 parameters, listed in Table A.1. These parameters consist of the offsets, gains and cross gains (in Equation (A.1)). The fingertip locations were calculated using the model shown in Figure A.1.

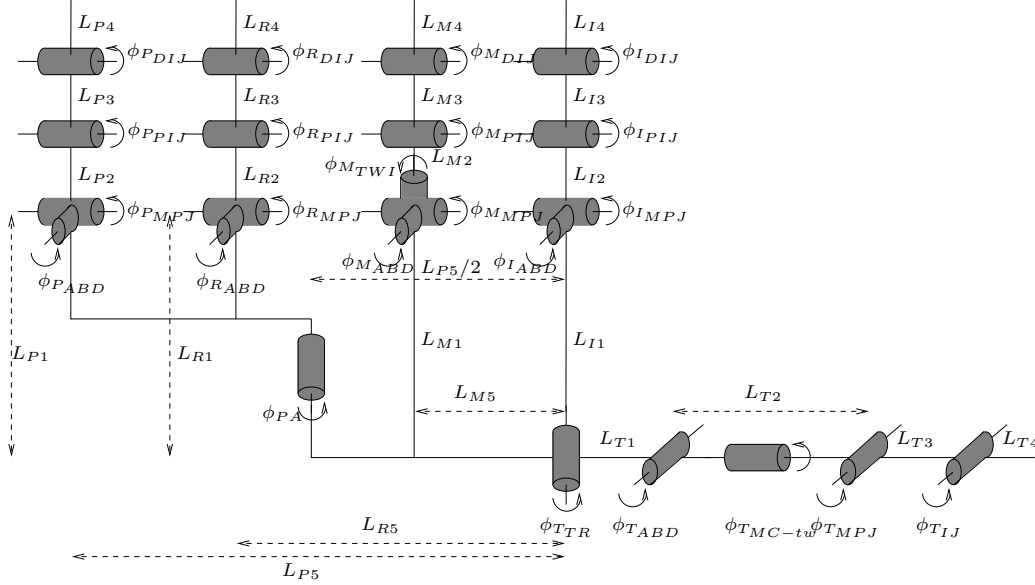


Figure A.1: The hand model used for calculating the grasp Jacobian, fingertip positions and in the calibration. All joints are modeled as revolute joints, visualized using cylinders. The abduction (ABD) and metacarpophalangeal joint (MPJ) axes pass through the same point. L_{Ti} , L_{Ii} , L_{Mi} , L_{Ri} and L_{Pi} represent the lengths of the i th metacarpal or phalange of the thumb, index, middle, ring and pinky finger respectively. The lengths were determined from the calibration procedure. The joint angles ϕ of the distal interphalangeal joints (DIJ), proximal interphalangeal joints (PIJ), metacarpophalangeal joints (MPJ), abduction joints (ABD), palm arch (PA), thumb rotation (TR) and thumb interphalangeal joint (IJ) were assumed to be linearly related to the raw CyberGlove data measured. The parameters of these relationships were determined for each subject in the calibration procedure. This model incorporates the measured palm arch, and the fixed (in the calibration sequence) twist of the middle finger, which are not included in other published models of the hand, but were found to be required to model well grasping movements of the hand.

The forward kinematics were calculated using the appropriate equations.
For the thumb:

$$\begin{aligned}
T_{TR}^0 &= \begin{bmatrix} 0 & 0 & -1 & 0 \\ \sin \phi_{TTR} & \cos \phi_{TTR} & 0 & 0 \\ \cos \phi_{TTR} & -\sin \phi_{TTR} & 0 & 0 \\ 0 & 0 & 0 & 1 \end{bmatrix} \\
T_{ABD}^{TR} &= \begin{bmatrix} \cos \phi_{TABD} & -\sin \phi_{TABD} & 0 & L_{T1} \\ 0 & 0 & 1 & 0 \\ -\sin \phi_{TABD} & -\cos \phi_{TABD} & 0 & 0 \\ 0 & 0 & 0 & 1 \end{bmatrix} \\
T_{MPJ}^{ABD} &= \begin{bmatrix} \cos \phi_{TMPJ} & -\sin \phi_{TMPJ} & 0 & L_{T2} \\ \sin \phi_{TMPJ} \cos \phi_{TMctwist} & \cos \phi_{TMPJ} \cos \phi_{TMctwist} & -\sin \phi_{TMctwist} & 0 \\ \sin \phi_{TMPJ} \sin \phi_{TMctwist} & \cos \phi_{TMPJ} \sin \phi_{TMctwist} & \cos \phi_{TMctwist} & 0 \\ 0 & 0 & 0 & 1 \end{bmatrix} \\
T_{IJ}^{MPJ} &= \begin{bmatrix} \cos \phi_{TIJ} & -\sin \phi_{TIJ} & 0 & L_{T3} \\ \sin \phi_{TIJ} & \cos \phi_{TIJ} & 0 & 0 \\ 0 & 0 & 1 & 0 \\ 0 & 0 & 0 & 1 \end{bmatrix} \\
T_{tip}^{IJ} &= \begin{bmatrix} 1 & 0 & 0 & L_{T4} \\ 0 & 1 & 0 & 0 \\ 0 & 0 & 1 & 0 \\ 0 & 0 & 0 & 1 \end{bmatrix} \\
T_{tip}^0 &= T_{TR}^0 T_{ABD}^{TR} T_{MPJ}^{ABD} T_{IJ}^{MPJ} T_{tip}^{IJ}
\end{aligned}$$

where T_2^1 is the homogeneous transformation from frame 1 to frame 2 for the thumb, the joint angles ϕ and lengths L are as shown in Figure A.1.

For the index finger:

$$F_{ABD}^0 = \begin{bmatrix} \cos \phi_{F_{ABD}} & 0 & \sin \phi_{F_{ABD}} & L_{F1} \\ 0 & 1 & 0 & 0 \\ -\sin \phi_{F_{ABD}} & 0 & \cos \phi_{F_{ABD}} & -L_{F5} \\ 0 & 0 & 0 & 1 \end{bmatrix}$$

$$F_{MPJ}^{ABD} = \begin{bmatrix} \cos \phi_{F_{MPJ}} & -\sin \phi_{F_{MPJ}} & 0 & 0 \\ \sin \phi_{F_{MPJ}} & \cos \phi_{F_{MPJ}} & 0 & 0 \\ 0 & 0 & 1 & 0 \\ 0 & 0 & 0 & 1 \end{bmatrix}$$

$$F_{PIJ}^{MPJ} = \begin{bmatrix} \cos \phi_{F_{PIJ}} & -\sin \phi_{F_{PIJ}} & 0 & L_{F2} \\ \sin \phi_{F_{PIJ}} & \cos \phi_{F_{PIJ}} & 0 & 0 \\ 0 & 0 & 1 & 0 \\ 0 & 0 & 0 & 1 \end{bmatrix}$$

$$F_{DIJ}^{PIJ} = \begin{bmatrix} \cos \phi_{F_{DIJ}} & -\sin \phi_{F_{DIJ}} & 0 & L_{F3} \\ \sin \phi_{F_{DIJ}} & \cos \phi_{F_{DIJ}} & 0 & 0 \\ 0 & 0 & 1 & 0 \\ 0 & 0 & 0 & 1 \end{bmatrix}$$

$$F_{tip}^{DIJ} = \begin{bmatrix} 1 & 0 & 0 & L_{F4} \\ 0 & 1 & 0 & 0 \\ 0 & 0 & 1 & 0 \\ 0 & 0 & 0 & 1 \end{bmatrix}$$

$$F_{tip}^0 = F_{ABD}^0 F_{MPJ}^{ABD} F_{PIJ}^{MPJ} F_{DIJ}^{PIJ} F_{tip}^{DIJ}$$

The matrices for the middle finger are identical, except for the addition of the twist term, which changes one matrix:

$$M_{MPJ}^{ABD} = \begin{bmatrix} \cos \phi_{M_{MPJ}} & -\sin \phi_{M_{MPJ}} \cos \phi_{M_{TWI}} & \sin \phi_{M_{MPJ}} \sin \phi_{M_{TWI}} & 0 \\ \sin \phi_{M_{MPJ}} & \cos \phi_{M_{MPJ}} \cos \phi_{M_{TWI}} & -\cos \phi_{M_{MPJ}} \sin \phi_{M_{TWI}} & 0 \\ 0 & \sin \phi_{M_{TWI}} & \cos \phi_{M_{TWI}} & 0 \\ 0 & 0 & 0 & 1 \end{bmatrix}$$

The ring finger is the same as the index finger, apart from the introduction of the “palm arch”. This models the way that the palm can close to allow opposition between the thumb and the ring and pinky fingertips (which is otherwise impossible). The matrices that take this into account are:

$$R_{PA}^0 = \begin{bmatrix} 1 & 0 & 0 & 0.5L_{R1} \\ 0 & \cos \phi_{PPA} & -\sin \phi_{PPA} & 0 \\ 0 & \sin \phi_{PPA} & \cos \phi_{PPA} & -0.5L_{P5} \\ 0 & 0 & 0 & 1 \end{bmatrix}$$

$$R_{ABD}^{PA} = \begin{bmatrix} \cos \phi_{RABD} & 0 & \sin \phi_{RABD} & 0.5L_{R1} \\ 0 & 1 & 0 & 0 \\ -\sin \phi_{RABD} & 0 & \cos \phi_{RABD} & -L_{R5} + 0.5L_{P5} \\ 0 & 0 & 0 & 1 \end{bmatrix}$$

The transformations for the pinky are analogous to those of the ring finger.

The optimization was performed using the non-linear least squares optimization in Matlab.

Results

As an example of the performance of the algorithm, a data set consisting of the static finger spelling alphabet of American Sign Language was collected. The postures of the hand using the calibration that is provided with the glove (the “default” calibration) were compared to the results of the algorithm described here. The images were rendered on a Silicon Graphics machine using a program written using OpenGL and the “Virtual Hand” API provided by Immersion, and compared to a frame taken from a simultaneously recorded video. The rendered images were manually rotated to match the video frame. The results are shown in Figure A.2.

The two techniques produced similar results for many of the postures, although there are several where they differ. In particular, the letter “O” performs badly with the “default” calibration, a posture that is particularly



Figure A.2: Rendering of the hand using the “default” calibration (provided with the CyberGlove) and the calibration presented in this section, for the static fingerspelling alphabet of American Sign Language. The letters that require movement (J and Z) are not shown.

important for grasping. Some postures, for example, “R” appear bad using both methods - this is a limitation of the glove capabilities (because only relative abduction/adduction between the fingers is measured, rather than absolute abduction of each finger).

This algorithm has been implemented and used successfully in the measurements throughout the thesis. It should be noted that this technique is strongly dependent on the starting point, and as a result, the solutions found may be local rather than global minima.

Appendix B

Derivation of the grasp Jacobian

Nomenclature

R	Rotation (3×3).	V^b	Body velocity.
p	Translation (3×1).	Ad_g	Adjoint transformation.
\bar{g}	Rigid motion (4×4).	J_h	Hand Jacobian.
ξ	Twist (6×1).	τ	Joint torques.
ν	Translational part of twist.	F_o	Force applied to the object.
ω	Axis of rotation (3×1).	R_{oc_i}	Contact i to object rotation.
q	A point on axis of rotation.	p_{oc_i}	Contact i to object translation.
J_f	Finger Jacobian.	G_i	Contact map for finger i .
F_{ci}	Force on object from contact i .	G	Grasp map.
f_{ci}	Force applied by finger i .	G_h	Grasp Jacobian.
B_{ci}	Soft finger constraint.	θ	Joint angles of the finger.
μ	Coefficient of friction.	\dot{x}_o	Object velocity.
γ	Coefficient of torsional friction.	ω_o	Object angular velocity.
FC_{ci}	Friction cone of finger i .	F_o	Force applied on the object.
\dot{x}_c	Velocities at the contacts.	τ_o	Torque applied on the object.

Introduction

A brief mathematical background of the relevant concepts is presented, while a more thorough exposition of part of the material presented here can be found in Murray et al. (1994). Here we have integrated analysis referring to different aspects of the grasping and manipulation derived from several earlier publications (Mason & Salisbury, 1985; Zatsiorsky, 2002). The derivation of the grasp Jacobian, which is the transformation from finger joint velocities to the velocity of the object is described.

Representation of rigid motions

Rigid motions of a body can be expressed by a homogeneous matrix:

$$\bar{g} = \begin{bmatrix} R & p \\ 0 & 1 \end{bmatrix} \quad (\text{B.1})$$

where R is a 3×3 matrix representing the rotation, and p is a 3×1 vector representing translation.

This motion can be compactly represented as a 6-dimensional *twist* $\xi = (\nu, \omega)$. For a pure rotation, this is given by

$$\xi = \begin{bmatrix} -\omega \times q \\ \omega \end{bmatrix} \quad (\text{B.2})$$

where ω is the axis of rotation, q is a point on that axis, and θ is the magnitude of the twist, and for a pure translation by

$$\xi = \begin{bmatrix} \nu \\ 0 \end{bmatrix} \theta \quad (\text{B.3})$$

The twist is related to the homogeneous transformation g by

$$\bar{g} = e^{\hat{\xi}\theta} \quad (\text{B.4})$$

where

$$\hat{\xi} = \begin{bmatrix} \hat{\omega} & \nu \\ 0 & 0 \end{bmatrix} \quad (\text{B.5})$$

Finger Jacobian

For each finger, the finger Jacobian J_f maps joint velocities $\dot{\theta}$ into the spatial velocity V_f of the finger tip:

$$\boxed{V_f = J_f(\theta)\dot{\theta}} \quad (\text{B.6})$$

It is given by

$$J_f(\theta) = \begin{bmatrix} \xi_1 & \xi'_2 & \cdots & \xi'_n \end{bmatrix} \quad (\text{B.7})$$

where ξ_1 represents the transformation from the first joint to the base coordinate frame, and ξ'_i is the combined transformation from the i th joint to the base coordinate frame.

Example of the Finger Jacobian for the index finger To calculate the Jacobian, we need to know the joint twists as a function of the joint angles. This is based on the model of the hand shown in Figure A.1. The first joint (abduction) is a rotation about the y axis, so $\omega_1 = \begin{bmatrix} 0 & 1 & 0 \end{bmatrix}'$. A point on the axis is given by $q_1 = \begin{bmatrix} l_1 & 0 & -l_5 \end{bmatrix}'$

The movement of the metacarpophalangeal joint (MPJ), whose axis passes through the same point as the first joint, is a rotation about the z axis. It must be first rotated into the base frame. i.e.

$$\omega'_2 = R_y(\theta_{ABD}) \begin{bmatrix} 0 \\ 0 \\ 1 \end{bmatrix} = \begin{bmatrix} \sin \theta_{ABD} \\ 0 \\ \cos \theta_{ABD} \end{bmatrix} \quad (\text{B.8})$$

where θ_{ABD} is the rotation of the abduction joint, and $R_y(\theta)$ is a rotation about the y axis of magnitude θ .

The movement of the third and fourth joints, the proximal interphalangeal

joint (PIJ) and the distal interphalangeal joint (DIJ) are also rotations about the z axis, and hence are in the same direction as the MPJ axis in base coordinates (i.e., $\omega'_4 = \omega'_3 = \omega'_2$). The points on the axis (q'_3 and q'_4) can be computed by combining the transformations:

$$\begin{aligned}
q'_3 &= q_1 + R_y(\theta_{ABD})R_z(\theta_{MPJ}) \begin{bmatrix} l_2 \\ 0 \\ 0 \end{bmatrix} = \begin{bmatrix} \cos \theta_{ABD} \cos \theta_{MPJ} l_2 + l_1 \\ \sin \theta_{MPJ} l_2 \\ -\sin \theta_{ABD} \cos \theta_{MPJ} l_2 - l_5 \end{bmatrix} \\
q'_4 &= q'_3 + R_y(\theta_{ABD})R_z(\theta_{MPJ})R_z(\theta_{PIJ}) \begin{bmatrix} l_3 \\ 0 \\ 0 \end{bmatrix} \\
&= q'_3 + \begin{bmatrix} (\cos \theta_{ABD} \cos \theta_{MPJ} \cos \theta_{PIJ} - \cos \theta_{ABD} \sin \theta_{MPJ} \sin \theta_{PIJ})l_3 \\ \sin \theta_{MPJ} \cos \theta_{PIJ} + \cos \theta_{MPJ} \sin \theta_{PIJ} l_3 \\ (-\sin \theta_{ABD} \cos \theta_{MPJ} \cos \theta_{PIJ} + \sin \theta_{ABD} \sin \theta_{MPJ} \sin \theta_{PIJ})l_3 \end{bmatrix}
\end{aligned} \tag{B.9}$$

where θ_{MPJ} is the rotation of the metacarpophalangeal joint, θ_{DIJ} the rotation of the distal interphalangeal joint, and θ_{PIJ} the rotation of the proximal interphalangeal joint.

The Jacobian can then be constructed and expressed as:

$$J_f = \begin{bmatrix} -\omega_1 \times q_1 & -\omega'_2 \times q'_2 & -\omega'_3 \times q'_3 & -\omega'_4 \times q'_4 \\ \omega_1 & \omega'_2 & \omega'_3 & \omega'_4 \end{bmatrix} \tag{B.10}$$

Grasping contact model

A contact model specifies the directions and orientations of forces that can be applied by a finger on an object, and the constraints on these forces due to friction. The constraints determine how much force can be applied before the finger will slip. As the fingertip and the object are not rigidly connected, it is not possible for the fingers to apply arbitrary forces and moments on an object. The model used here is known as the soft-finger model (Mason & Salisbury, 1985). The finger can apply forces in three directions, as well as torque about the axis of the finger. The forces applied

are subject to friction constraints. The contact model is represented by a matrix B_{c_i} , which transforms the fingertip forces to the forces applied to the object, and a friction cone, which describes the constraints on forces dictated by friction. Hence the forces F_{c_i} felt by the object due to the applied finger forces f_{c_i} under soft-finger constraint B_{c_i} (with a friction cone FC_{c_i}) will be

$$F_{c_i} = B_{c_i} f_{c_i}, \quad f_{c_i} \in FC_{c_i} \quad (\text{B.11})$$

where

$$B_{c_i} = \begin{bmatrix} 1 & 0 & 0 & 0 \\ 0 & 1 & 0 & 0 \\ 0 & 0 & 1 & 0 \\ 0 & 0 & 0 & 0 \\ 0 & 0 & 0 & 0 \\ 0 & 0 & 0 & 1 \end{bmatrix} \quad (\text{B.12})$$

and the friction cone FC_{c_i} is given by

$$\sqrt{f_1^2 + f_2^2} \leq \mu f_3, f_3 \geq 0, |f_4| \leq \gamma \quad (\text{B.13})$$

where μ is the coefficient of static friction and γ is the coefficient of torsional friction. The friction cone requires that the normal force (f_3) be positive, and that the magnitude of the other translational forces be less than the normal force multiplied by the coefficient of friction, otherwise the finger would slip. The friction constraints also require that the moment applied about the z axis be smaller than the coefficient of torsional friction multiplied by the normal force, in order to avoid slipping.

Hand Jacobian

The fingers can only apply forces and velocities on the object in certain directions, due to the contact constraints. A coordinate system can be defined at the contacts of the object and the fingers, parallel to the directions along which the force can be applied. There will be 4 dimensions for each finger (translation in three directions, and rotation about the z axis). The hand

Jacobian J_h is then defined as expressing the relationship between the vector of 21 joint velocities $\dot{\theta}$ of the hand, and the vector of 20 velocities in the contact coordinate system \dot{x}_c :

$$\boxed{J_h(\theta, x_0)\dot{\theta} = \dot{x}_c} \quad (\text{B.14})$$

This is derived by requiring that at each contact, the motion is constrained by the contact model described in the previous section:

$$B_{c_i}^T V_{f_i c_i}^b = 0 \quad (\text{B.15})$$

where $V_{f_i c_i}^b$ is the fingertip velocity in the contact frame. This velocity can be expressed in terms of the velocity of the i th fingertip ($V_{p f_i}^b$) and contact frame ($V_{p c_i}^b$) relative to the finger base frame, using adjoint transformations

$$Ad_g = \begin{bmatrix} R & \hat{p}R \\ 0 & R \end{bmatrix}, \quad Ad_g^{-1} = \begin{bmatrix} R^T & -R^T \hat{p} \\ 0 & R^T \end{bmatrix} \quad (\text{B.16})$$

which transform the velocity between coordinate systems. The contact frame is assumed to be fixed relative to the object frame and therefore the fingertip velocity in the contact frame consists of the object velocity \dot{x}_o transformed into the contact frame by $Ad_{g_{oci}}^{-1}$ added to the fingertip velocity in the base frame $V_{s_i f_i}$ transformed to the object frame by $-Ad_{g_{pc_i}}^{-1} Ad_{g_{pf_i}}$:

$$V_{f_i c_i}^b = -Ad_{g_{pc_i}}^{-1} Ad_{g_{pf_i}} V_{s_i f_i}^b + Ad_{g_{oci}}^{-1} \dot{x}_o \quad (\text{B.17})$$

This can then be substituted into the constraint equation (B.15) to give

$$\begin{aligned} B_{c_i}^T \left(-Ad_{g_{pc_i}}^{-1} Ad_{g_{pf_i}} V_{s_i f_i}^b + Ad_{g_{oci}}^{-1} \dot{x}_o \right) &= 0 \\ \Rightarrow B_{c_i}^T Ad_{g_{s_i c_i}}^{-1} J_{s_i f_i}^s \dot{\theta}_{f_i} &= G_i^T \dot{x}_o = \dot{x}_{c_i} \end{aligned} \quad (\text{B.18})$$

This is the equation for the i th finger. The hand Jacobian is composed by stacking the Jacobians for each finger together:

$$J_h(\theta, x_0) = \begin{bmatrix} B_{c_1}^T Ad_{g_{s_1 c_1}}^{-1} J_{s_1 f_1}^s(\theta_{f_1}) & 0 & 0 \\ 0 & \ddots & 0 \\ 0 & 0 & B_{c_k}^T Ad_{g_{s_k c_k}}^{-1} J_{s_k f_k}^s(\theta_{f_k}) \end{bmatrix} \quad (\text{B.19})$$

Note that the contact forces f_c can be related to the joint torques τ using the transpose of the hand Jacobian:

$$\boxed{\tau = J_h^T f_c} \quad (\text{B.20})$$

Grasp Map

The grasp map determines the effect of the contact forces on the object. The contact forces need to be transformed to the coordinate system of the object. For contact i , the force applied to the object F_{o_i} will be the contact forces transformed into the frame of reference of the object:

$$F_{o_i} = \begin{bmatrix} R_{oc_i} & 0 \\ \hat{p}_{oc_i} R_{oc_i} & R_{oc_i} \end{bmatrix} B_{c_i} f_{c_i} = G_i f_{c_i}, \quad f_{c_i} \in FC_{c_i} \quad (\text{B.21})$$

where R_{oc_i} is the rotation and \hat{p}_{oc_i} the translation from the object coordinates to the contact coordinates of finger i . G_i is known as the contact map, and maps the contact forces to object wrenches. If there are multiple fingers grasping an object, the total wrench (the generalized force, consisting of a linear and angular component) on the object will be the sum of the object

wrenches from each finger:

$$F_o = \left[\begin{bmatrix} R_{oc_1} & 0 \\ \hat{p}_{oc_1} R_{oc_1} & R_{oc_1} \end{bmatrix} B_{c_1} \cdots \begin{bmatrix} R_{oc_k} & 0 \\ \hat{p}_{oc_k} R_{oc_k} & R_{oc_k} \end{bmatrix} B_{c_k} \right] \begin{bmatrix} f_{c_1} \\ \vdots \\ f_{c_k} \end{bmatrix} \quad (\text{B.22})$$

$$= \begin{bmatrix} G_1 & \cdots & G_k \end{bmatrix} \begin{bmatrix} f_{c_1} \\ \vdots \\ f_{c_k} \end{bmatrix} = G f_c \quad (\text{B.23})$$

where G is known as the grasp map, defined as

$$G = \begin{bmatrix} G_1 & \cdots & G_k \end{bmatrix} = \left[\begin{bmatrix} R_{oc_1} & 0 \\ \hat{p}_{oc_1} R_{oc_1} & R_{oc_1} \end{bmatrix} B_{c_1} \cdots \begin{bmatrix} R_{oc_k} & 0 \\ \hat{p}_{oc_k} R_{oc_k} & R_{oc_k} \end{bmatrix} B_{c_k} \right] \quad (\text{B.24})$$

Grasp Jacobian

The grasp Jacobian G_h maps the joint velocities $\dot{\theta}$ to the velocity of the object \dot{x}_o :

$$\boxed{\dot{x}_o = G_h \dot{\theta}} \quad (\text{B.25})$$

It is defined as:

$$\boxed{G_h = G^{+T} J_h} \quad (\text{B.26})$$

where G^{+T} is the transpose of the generalized inverse of the grasp map. The grasp Jacobian for a multiple fingered grasp is analogous to the manipulator Jacobian for a single finger.

Velocity and Force Ellipsoids

The grasping hand may be considered as a mechanical transformer, that transforms joint velocities and torques from the fingers to velocities and forces in task space (Chiu, 1988). To determine the properties of this transformation, the magnitude of the joint velocity vector (i.e. its Euclidean norm) is fixed to be 1:

$$\dot{\theta}^T \dot{\theta} = 1 \quad (\text{B.27})$$

Using the grasp Jacobian (B.25), $\dot{\theta}^T$ and $\dot{\theta}$ can be written as

$$\begin{aligned}\dot{\theta} &= G_h^{-1} \dot{x}_o \\ \dot{\theta}^T &= \dot{x}_o^T (G_h^T)^{-1}\end{aligned}$$

Substituting these into Equation (B.27) gives

$$\dot{\theta}^T \dot{\theta} = \dot{x}_o^T (G_h^T)^{-1} G_h^{-1} \dot{x}_o = \dot{x}_o^T (G_h G_h^T)^{-1} \dot{x}_o = 1 \quad (\text{B.28})$$

The values of \dot{x}_o that satisfy this relationship are the possible object velocities that can be produced when the norm of the joint velocity vector is 1. These values can be visualized by an ellipsoid. The translational velocity ellipsoid is defined by

$$\dot{x}_o^T (G_{h(\text{trans})} G_{h(\text{trans})}^T)^{-1} \dot{x}_o \leq 1 \quad (\text{B.29})$$

where $G_{h(\text{trans})}$ is the translational component of the grasp Jacobian (i.e., the first 3 rows). The translational component of the grasp map can be considered independently of the rotational component because the translational velocity of the object is a function only of these three rows (as well as the joint velocities). The velocity transmission ellipsoid represents the velocity transmission ratio between the fingers' joint velocities and the object velocity. Velocity is optimally produced along the major axis of the ellipsoid. This means that for joint velocities with a constant norm, the maximum velocity is produced in this direction (Zatsiorsky, 2002). Similarly, the angular velocity ellipsoid is defined by

$$\omega_o^T (G_{h(\text{angular})} G_{h(\text{angular})}^T)^{-1} \omega_o \leq 1 \quad (\text{B.30})$$

where $G_{h(\text{angular})}$ is the angular component of the grasp Jacobian.

Force ellipsoids can also be defined in terms of the grasp Jacobian because the inverse of the grasp Jacobian relates joint torques to the forces applied by the grasp on the object. The translational and rotational force ellipsoids are analogously defined by

$$F_o^T (G_{h(\text{trans})} G_{h(\text{trans})}^T) F_o \leq 1 \quad (\text{B.31})$$

and

$$\tau_o^T (G_{h(\text{angular})} G_{h(\text{angular})}^T) \tau_o \leq 1 \quad (\text{B.32})$$

respectively.

Bibliography

Ansuini C., Santello M., Massaccesi S. & Castiello U. (2006). Effect of end-goal on hand shaping. *Journal of Neurophysiology*, 95(4):2456–2465. [Cited on page 11]

Arbib M., Iberall T. & Lyons D. (1985). Schemas that integrate vision and touch for hand control. In M. Arbib & A. Hansen, eds., *Vision, Brain & Cooperative Communication*, pages 489–510. MIT Press, Cambridge. [Cited on page 11]

Archibald R.C. (1918). The logarithmic spiral. *The American Mathematical Monthly*, 25(4):185–193. [Cited on page 84]

Berman S., Friedman J. & Flash T. (2005). Object-action abstraction for teleoperation. In *IEEE International Conference on Systems, Man and Cybernetics (SMC)*. Hawaii. [Cited on page 111]

Bernstein N. (1967). *The Co-ordination and Regulation of Movements*. Pergamon Press, London. [Cited on page 5]

Biess A., Liebermann D. & Flash T. (2006a). A spatiotemporal motor integration model for three-dimensional point-to-point arm movements based on temporal and geometric planning constraint. In preparation. [Cited on pages 87, 88, 106, and 123]

Biess A., Nagurka M. & Flash T. (2006b). Simulating discrete and rhythmic multi-joint human arm movements by optimization of nonlinear performance indices. *Biological Cybernetics*, 95(1):31–53. [Cited on page 91, 91, and 91]

Brook N., Mizrahi J., Shoham M. & Dayan J. (1995). A biomechanical model of index finger dynamics. *Medical Engineering & Physics*, 17(1):54–63. [Cited on pages 15, 15, and 20]

Brook N., Shoham M. & Dayan J. (1998). Controllability of grasps and manipulations in multi-fingered hands. *IEEE Transactions on Robotics and Automation*, 14(1):185–192. [Cited on page 44]

Burdet E., Osu R., Franklin D., Yoshioka T., Milner T. & Kawato M. (2000). A method for measuring endpoint stiffness during multi-joint arm movements. *Journal of Biomechanics*, 33(12):1705–1709. [Cited on page 18]

Burdet E., Tee K., Mareels I., Milner T., Chew C., Franklin D., Osu R. & Kawato M. (2006). Stability and motor adaptation in human arm movements. *Biological Cybernetics*, 94(1):20–32. [Cited on page 19]

Buttolo P. (1996). *Characterization of Human Pen Grasp with Haptic Displays*. Ph.D. thesis, University of Washington. [Cited on pages 20, 20, and 67]

Buxbaum L.J., Kyle K.M., Kathy T. & Detre J.A. (2006). Neural substrates of knowledge of hand postures for object grasping and functional object use: Evidence from fMRI. *Brain Research*, 1117(1):175–185. [Cited on page 2]

Chiu S. (1988). Task compatibility of manipulator postures. *International Journal of Robotics Research*, 7(5):13–21. [Cited on pages 12, 54, 67, and 144]

Chou T.S., Gadd A. & Knott D. (2000). Hand-eye: A vision-based approach to data glove calibration. In *Human Interface Technologies*, pages 47–54. [Cited on page 129]

Coelho J. Jr. & Grupen R. (1997). A control basis for learning multifingered grasps. *Journal of Robotic Systems*, 14(7):545–557. [Cited on page 44]

Comaish S. & Bottoms E. (1971). The skin and friction: Deviations from Amonton's laws, and the effects of hydration and lubrication. *British Journal of Dermatology*, 84(1):37–43. [Cited on page 53]

Cruz E. & Kamper D. (2006). Kinematics of point-to-point finger movements. *Experimental Brain Research*, 174(1):29–34. [Cited on page 108]

Cutkosky M. (1985). *Robotic Grasping and Fine Manipulation*. Kluwer, MA. [Cited on page 68]

Cutkosky M. (1989). On grasp choice, grasp models, and the design of hands for manufacturing tasks. *IEEE Transactions on Robotics and Automation*, 5(3):269–279. [Cited on pages 6, 7, and 44]

Danion F., Schöner G., Latash M., Li S., Scholz J. & Zatsiorsky V. (2003). A mode hypothesis for finger interaction during multi-finger force-production tasks. *Biological Cybernetics*, 88(2):91–98. [Cited on pages 5, 13, and 13]

Darainy M., Malfait N., Gribble P., Towhidkhah F. & Ostry D. (2004). Learning to control arm stiffness under static conditions. *Journal of Neurophysiology*, 92(6):3344–3350. [Cited on page 19]

de Schutter J. & van Brussel H. (1988). Compliant robot motion I. A formalism for specifying compliant motion tasks. *International Journal of Robotics Research*, 7(4):3–17. [Cited on pages 8, 67, and 76]

Dejmal I. & Zacksenhouse M. (2006). Coordinative structure of manipulative hand-movements facilitates their recognition. *IEEE Transactions on Biomedical Engineering*, 53(12):2455–2463. [Cited on page 107]

Dempster W. (1955). Space requirements of the seated operator. Technical Report WADC-TR-55-159, Aerospace Medical Research Laboratories, Wright-Patterson Air Force Base, OH. [Cited on page 89]

Dolan J., Friedman M. & Nagurka M. (1993). Dynamic and loaded impedance components in the maintenance of human arm posture. *IEEE Transactions on Systems, Man, and Cybernetics*, 23(3):698–709. [Cited on pages 18, 20, 24, and 31]

Elliott J. & Connolly K. (1984). A classification of manipulative hand movements. *Developmental Medicine & Child Neurology*, 26(3):283–296. [Cited on page 7]

Feldman A. (1966). Functional tuning of the nervous system with control of movement or maintenance of a steady posture, II: Controllable parameters of the muscles. *Biophysics*, 11(3):565–578. [Cited on page 11]

Fischer M., van der Smagt P. & Hirzinger G. (1998). Learning techniques in a dataglove based telemanipulation system for the DLR hand. In *IEEE International Conference on Robotics and Automation*, volume 2, pages 1603–1608. Leuven, Belgium. [Cited on page 128]

Flash T. & Hogan N. (1985). The coordination of arm movements: An experimentally confirmed mathematical model. *Journal of Neuroscience*, 5(7):1688–1703. [Cited on pages 88 and 90]

Flash T. & Mussa-Ivaldi F. (1990). Human arm stiffness characteristics during the maintenance of posture. *Experimental Brain Research*, 82(2):315–326. [Cited on pages 18 and 124]

Fod A., Matarić M. & Jenkins O. (2002). Automated derivation of primitives for movement classification. *Autonomous Robots*, 12(1):39–54. [Cited on page 7]

Friedman J. & Flash T. (2007). Task-dependent selection of grasp kinematics and stiffness in human object manipulation. *Cortex*, 43(3):444–460. [Cited on page 45]

Fuentes O. & Nelson R. (1998). Learning dextrous manipulation skills for multifingered robot hands using the evolution strategy. *Machine Learning*, 31:223–237. [Cited on page 8 and 8]

Gentilucci M. (2002). Object motor representation and reaching-grasping control. *Neuropsychologia*, 40(8):1139–1153. [Cited on pages 6 and 44]

Gibbons J. (1971). *Nonparametric Statistical Inference*. McGraw-Hill, New York. [Cited on page 56]

Gibson J. (1979). *The Ecological Approach to Visual Perception*. Lawrence Erlbaum, Hillsdale, NJ. [Cited on page 44]

Gomi H. & Kawato M. (1996). Equilibrium-point control hypothesis examined by measured arm stiffness during multijoint movement. *Science*, 272(5258):117–120. [Cited on page 18]

Gomi H. & Kawato M. (1997). Human arm stiffness and equilibrium-point trajectory during multi-joint movement. *Biological Cybernetics*, 76(3):163–171. [Cited on page 18]

Griffin W., Findley R., Turner M. & Cutkosky M. (2000). Calibration and mapping of a human hand for dextrous telemanipulation. In *ASME IMECE - Haptic Interfaces for Virtual Environments and Teleoperator Systems Symposium*. [Cited on page 129 and 129]

Grinyagin I.V., Biryukova E.V. & Maier M.A. (2005). Kinematic and dynamic synergies of human precision-grip movements. *Journal of Neurophysiology*, 94(4):2284–2294. [Cited on page 18]

Gu X. & Ballard D. (2006). An equilibrium point based unifying movement control in humanoids. In *Robotics: Science and Systems*. Philadelphia, PA. [Cited on page 11]

Gupta A., Rash G.S., Somia N.N., Wachowiak M.P., Jones J. & Desoky A. (1998). The motion path of the digits. *Journal of Hand Surgery*, 23A(6):1038–1042. [Cited on page 83]

Haggard P. (1994). Perturbation studies of coordinated prehension. In K. Bennett & U. Castiello, eds., *Insights into the Reach to Grasp Movement*, pages 151–170. Elsevier Science, Holland. [Cited on page 5]

Hahn P., Krimmer H., Hradetzky A. & Lanz U. (1995). Quantitative analysis of the linkage between the interphalangeal joints of the index finger. *Journal of Hand Surgery (British and European Volume)*, 20B(5):696–699. [Cited on pages 70, 87, 93, and 93]

Hajian A. & Howe R. (1997). Identification of the mechanical impedance at the human finger tip. *Journal of Biomechanical Engineering*, 119(1):109–114. [Cited on pages 19, 19, 39, and 52]

Hermens F. & Gielen S. (2004). Posture-based or trajectory-based movement planning: a comparison of direct and indirect pointing movements. *Experimental Brain Research*, 159(3):340–348. [Cited on page 93]

Hester R., Cetin M., Kapoor C. & Tesar D. (1999). Criteria-based approach to grasp synthesis. In *IEEE International Conference on Robotics and Automation*, volume 2, pages 1255–1260. Detroit, Michigan. [Cited on page 44]

Hogan N. (1985a). Impedance control: An approach to manipulation: Part I - Theory, Part II - Implementation, part III - Applications. *Journal of Dynamic Systems, Measurement, and Control*, 107(1):1–24. [Cited on page 12]

Hogan N. (1985b). The mechanics of multi-joint posture and movement control. *Biological Cybernetics*, 52:315–331. [Cited on pages 20 and 41]

Iberall T. (1997). Human prehension and dexterous robot hands. *International Journal of Robotics Research*, 16(3):285–299. [Cited on pages 6 and 44]

Ilg W. & Giese M. (2002). Modeling of movements sequences based on hierarchical spatial-temporal correspondence of movement primitives. In *2nd Workshop on Biologically Motivated Computer Vision, Tübingen*. [Cited on page 8]

Jakobson L. & Goodale M. (1991). Factors affecting higher-order movement planning: a kinematic analysis of human prehension. *Experimental Brain Research*, 86(1):199–208. [Cited on page 6]

Jeannerod M. (1981). Intersegmental coordination during reaching at natural visual objects. In J. Long & A. Baddeley, eds., *Attention and Perfor-*

mance IX, pages 153–169. Lawrence Erlbaum Associates, USA. [Cited on pages 5, 82, and 89]

Jerde T., Soechting J. & Flanders M. (2003). Biological constraints simplify the recognition of hand shapes. *IEEE Transactions on Biomedical Engineering*, 50(2):265–269. [Cited on page 9]

Jindrich D., Balakrishnan A. & Dennerlein J. (2004). Finger joint impedance during tapping on a computer keyboard. *Journal of Biomechanics*, 37(10):1589–1596. [Cited on page 19]

Kamper D., Cruz E. & Siegel M. (2003). Stereotypical fingertip trajectories during grasp. *Journal of Neurophysiology*, 90(6):3702–3710. [Cited on pages 5, 83, 88, 88, and 129]

Kamper D., Hornby G. & Rymer W. (2002). Extrinsic flexor muscles generate concurrent flexion of all three finger joints. *Journal of Biomechanics*, 35(12):1581–1589. [Cited on pages 18 and 41]

Kao I., Cutkosky M. & Johansson R. (1997). Robotic stiffness control and calibration as applied to human grasping tasks. *IEEE Transactions on Robotics and Automation*, 13(4):557–566. [Cited on pages 12, 19, 40, 52, and 56]

Kessler G., Hodges L. & Walker N. (1995). Evaluation of the CyberGlove as a whole-hand input device. *ACM Transactions on Computer-Human Interaction*, 2(4):263–283. [Cited on page 129]

Kim B.H., Yi B.J., Oh S.R. & Suh I. (2004). Non-dimensionalized performance indices based optimal grasping for multi-fingered hands. *Mechatronics*, 14(3):255–280. [Cited on page 12]

Kowadlo G., Friedman J. & Flash T. (2005). Predicting grasp inertia with a geometric model. In *Australasian Conference on Robotics and Automation*. Sydney, Australia. [Cited on pages 18, 18, and 40]

Leijnse J. (1997). Measuring force transfers in the deep flexors of the musician's hand: Theoretical analysis, clinical examples. *Journal of Biomechanics*, 30(9):873–882. [Cited on page 69]

Li Z. & Sastry S. (1988). Task-oriented optimal grasping by multifingered robot hands. *IEEE Transactions on Robotics and Automation*, 4(1):32–44. [Cited on page 12]

Li Z., Zatsiorsky V., Latash M. & Bose N. (2002). Anatomically and experimentally based neural networks modeling force coordination in static multi-finger tasks. *Neurocomputing*, 47:259–272. [Cited on page 69]

Lin Q., Burdick J. & Rimon E. (2000). A stiffness-based quality measure for compliant grasps and fixtures. *IEEE Transactions on Robotics and Automation*, 16(6):675–688. [Cited on page 19]

Littler J.W. (1973). On the adaptability of man's hand (with reference to the equiangular curve). *Hand*, 5(3):187–191. [Cited on pages 83, 85, 106, and 109]

Markley J. Jr (2003). The Fibonacci sequence: Relationship to the human hand. *Journal of Hand Surgery*, 28A(4):704–706. Letter to the editor. [Cited on pages 85 and 106]

Marteniuk R., MacKenzie C., Jeannerod M., Athenes S. & Dugas C. (1987). Constraints on human arm movement trajectories. *Canadian Journal of Psychology*, 41(3):365–378. [Cited on page 6]

Mason C., Gomez J. & Ebner T. (2001). Hand synergies during reach-to-grasp. *Journal of Neurophysiology*, 86(6):2896–2910. [Cited on pages 5, 9, 10, 83, and 124]

Mason M. (1981). Compliance and force control for computer controlled manipulators. *IEEE Transactions on Systems, Man, and Cybernetics*, 11(6):418–432. [Cited on pages 8, 67, and 76]

Mason M. (2001). *Mechanics of Robotic Manipulation*. MIT Press, Cambridge, MA. [Cited on page 44]

Mason M. & Salisbury J. (1985). *Robot Hands and the Mechanics of Manipulation*. MIT Press, MA. [Cited on pages 49, 50, 138, and 140]

Menon A., Barnes B., Mills R., Bruyns C., Twombly A., Smith J., Montgomery K. & Boyle R. (2003). Using registration, calibration, and robotics to build a more accurate virtual reality simulation for astronaut training and telemedicine. In *The 11th International Conference in Central Europe on Computer Graphics, Visualization and Computer Vision (WSCG)*. Plzen - Bory, Czech Republic. [Cited on page 129]

Meulenbroek R., Rosenbaum D., Jansen C., Vaughan J. & Vogt S. (2001). Multijoint grasping movements: Simulated and observed effects of object location, object size, and initial aperture. *Experimental Brain Research*, 138(2):219–234. [Cited on page 8]

Miller A., Knoop S., Christensen H. & Allen P. (2003). Automatic grasp planning using shape primitives. In *IEEE International Conference on Robotics and Automation*. Taipei, Taiwan. [Cited on page 11]

Milner T. & Franklin D. (1998). Characterization of multijoint finger stiffness: Dependence on finger posture and force direction. *IEEE Transactions on Biomedical Engineering*, 45(11):1363–1375. [Cited on pages 19, 52, 56, and 124]

Mishra B., Schwartz J. & Sharir M. (1987). On the existence and synthesis of multifinger positive grips. *Algorithmica*, 2(4):541–558. [Cited on page 122]

Murata A., Gallese V., Luppino G., Kaseda M. & Sakata H. (2000). Selectivity for the shape, size, and orientation of objects for grasping in neurons of monkey parietal area aip. *Journal of Neurophysiology*, 83(5):2580–2601. [Cited on page 122]

Murray R., Li Z. & Sastry S. (1994). *A Mathematical Introduction to Robotic Manipulation*. CRC Press, Boca Raton, FL. [Cited on pages 22, 23, 24, 88, and 138]

Mussa-Ivaldi F., Hogan N. & Bizzi E. (1985). Neural, mechanical, and geometric factors subserving arm posture in humans. *Journal of Neuroscience*, 5(10):2732–2743. [Cited on pages 18, 18, 18, 41, 54, and 124]

Nakano E., Imamizu H., Osu R., Uno Y., Gomi H., Yoshioka T. & Kawato M. (1999). Quantitative examinations of internal representations for arm trajectory planning: Minimum commanded torque change model. *Journal of Neurophysiology*, 81(5):2140–2155. [Cited on page 92]

Napier J. (1993). *Hands*. Princeton University Press, Princeton, NJ. Revised by Tuttle, R.H. [Cited on pages 6, 13, 14, and 14]

Nölker C. & Ritter H. (2000). Parameterized SOMs for hand posture reconstruction. In S.I. Amari, C. Giles, M. Gori & V. Piuri, eds., *Proceedings of the International Joint Conference on Neural Networks (IJCNN)*, Como, Italy.. [Cited on page 11]

Norkin C. & White D. (1985). *Measurement of Joint Motion: A Guide to Goniometry*. F. A. Davis Company, Philadelphia. [Cited on page 70]

Okadome T. & Honda M. (1999). Kinematic construction of the trajectory of sequential arm movements. *Biological Cybernetics*, 80(3):157–169. [Cited on page 93]

Park A.E., Fernandez J.J., Schmedders K. & Cohen M.S. (2003). The Fibonacci sequence: Relationship to the human hand. *Journal of Hand Surgery*, 28A(1):157–160. [Cited on pages 85 and 106]

Pollick F., Chizk C., Häger-Ross C. & Hayhoe M. (2000). Implicit accuracy constraints in two-fingered grasps of virtual objects with haptic feedback. In *Haptic Human-Computer Interaction Workshop*. University of Glasgow. [Cited on page 6]

Raos V., Umiltá M.A., Gallese V. & Fogassi L. (2004). Functional properties of grasping-related neurons in the dorsal premotor area F2 of the macaque monkey. *Journal of Neurophysiology*, 92(4):1990–2002. [Cited on pages 2 and 122]

Raos V., Umiltà M.A., Murata A., Fogassi L. & Gallese V. (2006). Functional properties of grasping-related neurons in the ventral premotor area F5 of the macaque monkey. *Journal of Neurophysiology*, 95(2):709–729. [Cited on pages 2, 121, and 122]

Riley M. & Atkeson C. (2002). Robot catching: Towards engaging human-humanoid interaction. *Autonomous Robots*, 12(1):119–128. [Cited on page 8]

Rizzolatti G. & Arbib M. (1998). Language within our grasp. *Trends in Neurosciences*, 21(5):188–194. [Cited on page 122]

Rizzolatti G., Camarda R., Fogassi L., Gentilucci M., Luppino G. & Matelli M. (1988). Functional organization of inferior area 6 in the macaque monkey. II. Area F5 and the control of distal movements. *Experimental Brain Research*, 71(3):491–507. [Cited on page 121]

Rohling R. & Hollerbach J. (1993). Calibrating the human hand for haptic interfaces. *Presence*, 2(4):281–296. [Cited on page 128]

Rohling R. & Hollerbach J. (1994). Modeling and parameter estimation of the human index finger. In *IEEE International Conference on Robotics and Automation*, volume 1, pages 223–230. San Diego, CA. [Cited on page 128]

Rosenbaum D., Cohen R., Meulenbroek R. & Vaughan J. (2006). Plans for grasping objects. In M. Latash & F. Lestienne, eds., *Motor Control and Learning*, pages 9–25. Springer, New York, NY. [Cited on page 44]

Rosenbaum D., Loukopoulos L., Meulenbroek R., Vaughan J. & Engelbrecht S. (1995). Planning reaches by evaluating stored postures. *Psychological Review*, 102(1):28–67. [Cited on page 8]

Rosenbaum D., Meulenbroek R., Vaughan J. & Jansen C. (2001). Posture-based motion planning: Applications to grasping. *Psychological Review*, 108(4):709–734. [Cited on pages 2, 8, 8, 82, and 90]

- Sancho-Bru J., Perez-Gonzalez A., Vergara-Monedero M. & Giurintano D. (2001). A 3-D dynamic model of human finger for studying free movements. *Journal of Biomechanics*, 34(11):1491–1500. [Cited on page 20]
- Santello M., Flanders M. & Soechting J. (1998). Postural hand synergies for tool use. *Journal of Neuroscience*, 18(23):10105–10115. [Cited on pages 9, 9, and 124]
- Santello M., Flanders M. & Soechting J. (2002). Patterns of hand motion during grasping and the influence of sensory guidance. *Journal of Neuroscience*, 22(4):1426–1435. [Cited on pages 5, 9, 9, 83, and 124]
- Shimoga K. (1996). Robot grasp synthesis algorithms: A survey. *International Journal of Robotics Research*, 15(3):230–266. [Cited on pages 5, 11, 44, and 123]
- Smeets J. & Brenner E. (1999). A new view on grasping. *Motor Control*, 3(3):237–271. [Cited on pages 6, 8, and 82]
- Smeets J. & Brenner E. (2002). Does a complex model help to understand grasping? *Experimental Brain Research*, 144(1):132–135. [Cited on page 8]
- Soechting J. & Flanders M. (1993). Parallel, interdependent channels for location and orientation in sensorimotor transformations for reaching and grasping. *Journal of Neurophysiology*, 70(3):1137–1150. [Cited on page 5]
- Soechting J. & Flanders M. (1997). Flexibility and repeatability of finger movements during typing: Analysis of multiple degrees of freedom. *Journal of Computational Neuroscience*, 4(1):29–67. [Cited on page 9]
- Speeter T. (1991). Primitive based control of the Utah/MIT dextrous hand. In *IEEE International Conference on Robotics and Automation*, pages 866–877. Sacramento, CA. [Cited on page 8 and 8]
- Tee K., Burdet E., Chew C. & Milner T. (2004). A model of force and impedance in human arm movements. *Biological Cybernetics*, 90(5):368–375. [Cited on page 18]

- Thompson D.W. (1992). *On Growth and Form: The Complete Revised Edition*. Dover. Reprint of 1942 edition. [Cited on page 84, 84, 84, and 84]
- Torres E. & Zipser D. (2002). Reaching to grasp with a multi-jointed arm. I. Computational model. *Journal of Neurophysiology*, 88(5):2355–2367. [Cited on page 123]
- Torres E. & Zipser D. (2004). Simultaneous control of hand displacements and rotations in orientation-matching experiments. *Journal of Applied Physiology*, 96(5):1978–1987. [Cited on page 106]
- Tsuji T., Morasso P., Goto K. & Ito K. (1995). Human hand impedance characteristics during maintained posture. *Biological Cybernetics*, 72(6):475–485. [Cited on page 18, 18, and 18]
- Tsuji T., Yakeda Y. & Tanaka Y. (2004). Analysis of mechanical impedance in human arm movements using a virtual tennis system. *Biological Cybernetics*, 91:295–305. [Cited on page 19]
- Turner M. (2001). *Programming Dexterous Manipulation by Demonstration*. Ph.D. thesis, Stanford University. [Cited on page 129 and 129]
- Uno Y., Kawato M. & Suzuki R. (1989). Formation and control of optimal trajectory in human multijoint arm movement. minimum torque-change model. *Biological Cybernetics*, 61(2):89–101. [Cited on page 92]
- Van Doren C. (1998). Grasp stiffness as a function of grasp force and finger span. *Motor Control*, 2(4):352–378. [Cited on page 20 and 20]
- Wada Y., Kaneko Y., Nakano E., Osu R. & Kawato M. (2001). Quantitative examinations for multi joint arm trajectory planning—using a robust calculation algorithm of the minimum commanded torque change trajectory. *Neural Networks*, 14(4-5):381–393. [Cited on page 91 and 91]
- Wren D. & Fisher R. (1995). Dexterous hand grasping strategies using pre-shapes and digit trajectories. In *IEEE International Conference on Systems, Man and Cybernetics (SMC)*. Vancouver, BC, Canada. [Cited on page 11]

Yoshikawa T. (1985). Manipulability of robotic mechanisms. *International Journal of Robotics Research*, 4(2):3–9. [Cited on page 12]

Zacksenhouse M. & Marcovici P. (2001). Interactive recognition of simultaneous manipulative hand movements. *Mechatronics*, 11(4):389–407. [Cited on page 9]

Zatsiorsky V. (2002). *Kinetics of Human Motion*. Human Kinetics, Champaign, IL. [Cited on pages 138 and 145]

Zatsiorsky V., Li Z. & Latash M. (1998). Coordinated force production in multi-finger tasks: Finger interaction and neural network modeling. *Biological Cybernetics*, 79(2):139–150. [Cited on pages 5 and 13]

Publications based on Ph.D. research

Journal articles

- Friedman J. & Flash T. (2007). Task-dependent selection of grasp kinematics and stiffness in human object manipulation. *Cortex*. 43(3):444–460.

Refereed conference proceedings

- Kowadlo G., Friedman J. & Flash T. (2005). Predicting grasp inertia with a geometric model. In *Australasian Conference on Robotics and Automation*. Sydney, Australia.
- Berman S., Friedman J. & Flash T. (2005). Object-action abstraction for teleoperation. In *IEEE International Conference on Systems, Man and Cybernetics (SMC)*. Hawaii.

Independent collaboration

I declare that all the work in the thesis is a result of my independent efforts, with the following exceptions:

Measurement of index finger inertia The initial concept and preliminary experiments for measuring index finger inertia (Section 3.1) were conducted together with Gideon Kowadlo (a visiting PhD student from Monash University, Australia). I performed the derivation of the inertia included here, as well as the experiments and data analysis.

Trajectories of the fingertips The use of Jacobi polynomials (page 91) with the inertia-based cost function was performed with the assistance of Dr. Armin Biess. I used his code for generating the basis functions and performing this optimization, whereas the other models and the other work in this chapter were my own.

Telerobotics The telerobotics project (Section 6.1) was performed together with Dr. Sigal Berman. We worked together on the concepts underlying the system. She built the robot interface, and I built the human interface.

Glove calibration The glove calibration technique (Appendix A) was performed together with Lior Noy. We developed and tested together the algorithm, while I performed most of the software implementation.